

Ingo Müller

**Influence of Cellulose Ethers
on the Kinetics of Early Portland
Cement Hydration**



Ingo Müller

**Influence of Cellulose Ethers on the Kinetics of
Early Portland Cement Hydration**

Karlsruher Mineralogische und Geochemische Hefte

Schriftenreihe des Instituts für Mineralogie und Geochemie,
Universität Karlsruhe (TH)

Band 32

Influence of Cellulose Ethers on the Kinetics of Early Portland Cement Hydration

von
Ingo Müller



universitätsverlag karlsruhe

Dissertation, Westfälische Wilhelms-Universität Münster
Mathematisch-Naturwissenschaftliche Fakultät, 2006

Anschrift des Autors:

Ingo Müller
Hercules GmbH
Paul-Thomas-Str. 56
D – 40599 Düsseldorf

Anschrift der Schriftleitung:

Karlsruher Mineralogische und Geochemische Hefte
Institut für Mineralogie und Geochemie
Universität Karlsruhe (TH)
D – 76128 Karlsruhe

Impressum

Universitätsverlag Karlsruhe
c/o Universitätsbibliothek
Straße am Forum 2
D-76131 Karlsruhe
www.uvka.de



Dieses Werk ist unter folgender Creative Commons-Lizenz
lizenziert: <http://creativecommons.org/licenses/by-nc-nd/2.0/de/>

Universitätsverlag Karlsruhe 2006
Print on Demand

ISSN: 1618-2677
ISBN-13: 978-3-86644-077-7
ISBN-10: 3-86644-077-4

Acknowledgement

I'd like to thank Prof. Dr. Andrew Putnis, Inst. f. Min., Westf. Wilhelms-Universitaet Muenster, and PD Dr. habil. Dirk Bosbach, Inst. f. Nukl. Ents. (INE), Forschungszentrum Karlsruhe, for giving me the great opportunity to graduate, for patiently reviewing this thesis and for their helpful advices and discussions.

My special thanks are dedicated to Dr. John Bard, Dr. Dieter Schweizer and Dr. Wilfried Hohn at Hercules Inc. for the kind permission to transform a Hercules research project into a public PhD thesis. Without their essential support and endless patience this project would not have been possible.

Many thanks to the very ambitious crews of the Swiss Light Source and the SINQ Neutron Source at the Paul Scherrer Institut in Villigen, Switzerland. Especially I'd like to thank Dr. Heinz Weyer, Dr. Bernd Schmitt and Dr. Bruce Patterson for their helpful company in many sleepless nights at the Material Research Beamline. I'm very grateful for the help of Dr. Peter Fischer and Dr. Denis Sheptyakov at the High Resolution Powder Diffractometry of Thermal Neutrons. Many thanks to Dr. Fabia Gozzo and Dr. van der Veen who promised to handcuff me to the heating system until I get the publications done.

I'd like to thank Angelika Breit and Dr. Ermrich for XRD analyses and software support and Dr. Klaus Lipus at the VDZ for ESEM-FEG-images.

Many thanks to my colleagues, especially to Dr. Michael Dittel, Alexander Kindler, Stefan Hucko and Wolfgang Hildebrandt for their help at the Hercules Construction Material Laboratory in Duesseldorf. I'm particularly grateful for the associated apprenticeship of Michael Zwanzig and his colleagues at the Heinrich-Hertz-Berufskolleg in Duesseldorf.

Last not least I'd like to thank my dear friends Annette Rolfes in Muenster and Susanne Herppich in Zurich for their kind support and friendly hospitality. I always enjoyed to take you out for dinner in times when I had to reconfigure my mental hard disc drive.

A Note on Notation

Mutated vowels and pronounced s in German names are written in international notation (ae, oe, ue, ss).

Content

1. Abstract	1
2. Introduction	2
2.1 Subject	2
2.2 Objectives	2
2.3 Nomenclature	3
2.4 Historical Background	5
2.4.1 The Development of Cement	5
2.4.2 The Development of Cellulose Ethers	7
2.5 Materials	7
2.5.1 Portland Cement	7
2.5.2 Clinker and Cement Phases	8
2.5.3 Hydration Processes of Portland Cement	12
2.5.4 Cellulose Ethers	13
2.5.5 Macroscopic Effects of Cellulose Ethers on Dry Mortars	17
2.5.6 Dry Mortar Applications and their Economic Relevance	18
2.6 State of Research	20
3. Methods	24
3.1 Standard Wet Paste Preparation	24
3.2 Etringite Pure Phase Synthesis	25
3.3 Particle Size Distribution (PSD)	25
3.4 Specific Surface Area	26
3.5 Helium Pycnometry	27
3.6 Ultrasonic Measurements	27
3.7 Heat Flux Calorimetry	28
3.8 Adsorption Tests and Size Exclusion Chromatography (SEC)	29
3.9 Powder Diffraction	33
3.9.1 Laboratory X-Ray Powder Diffraction	33
3.9.2 Synchrotron X-Ray Powder Diffraction	34
3.9.3 Thermal Neutron Powder Diffraction	37
3.10 Environmental Scanning Electron Microscopy - Field Emission Gun (ESEM-FEG)	39

4. Material Characterization	40
4.1 Defined Portland Cement	40
4.2 Pure Mineral Phases	42
4.3 Cellulose Ethers	43
4.4 Cement and Pure Phase Admixtures	44
5. Results	46
5.1 The Adsorption of Cellulose Ethers on Cement Phases	46
5.2 The Retarding Effect of Cellulose Ethers on Early Portland Cement Hydration	53
5.2.1 Ultrasonic Measurements	53
5.2.2 Heat Flux Calorimetry	55
5.2.3 Laboratory XRD	59
5.2.4 Synchrotron XRD	66
5.2.5 Synchrotron XRD with Liquid Injection	73
5.2.6 Thermal Neutron Powder Diffraction	81
5.2.7 ESEM-FEG	83
6. Summary	89
6.1 Portland Cement Hydration without Cellulose Ether	89
6.2 CE-caused Retardation	91
6.3 CE-Adsorption	93
7. Discussion	95
7.1 Stepwise Ettringite Formation	95
7.2 Interactions of Cellulose Ethers with Cement	96
8. Outlook	98
Appendix	99
A.1 Figures	99
A.2 Abbreviations	104
A.3 References	106
A.4 Technical Equipment	109
A.5 Co-operations	110

1. Abstract

The present study is focused on the effects of cellulose ethers (CEs) on the kinetics of early Portland cement hydration. The retarding effects of cellulose ethers on the development of single cement phases could be traced to the adsorption behaviour of the polymers. A method was developed to quantify the amount of cellulose ether adsorbed on the surfaces of cement phases. The specific surface area of some hydrated phases was analysed by determination of nitrogen gas adsorption isotherms. The amount of adsorbed cellulose ether was determined by analysing the residual free water of a cement paste by size exclusion chromatography. It could be demonstrated that the adsorption behaviour of the polysaccharide depends on the mineral phase and on the degree of substitution (DS), a key parameter of cellulose ether characterization.

Beside other methods, the hydration processes were monitored in-situ by the means of ultrasonic measurements, synchrotron X-ray and neutron powder diffraction and environmental scanning electron microscopy using a field emission gun. The results of all independent methods showed a good correlation. The following phase reactions could be observed within the first 24 hours of Portland cement hydration:

1. tri-calcium aluminate + bassanite + water \rightarrow ettringite (1st generation)
2. bassanite + water \rightarrow gypsum
3. anhydrite + water \rightarrow gypsum
4. tri-calcium aluminate + gypsum + water \rightarrow ettringite (2nd generation)
5. tri-calcium silicate + water \rightarrow calcium silicate hydrates + portlandite

It turned out that cellulose ethers had a strong direct effect on the hydration of the silicate components of cement. Tri-calcium silicate and its hydration products showed the highest values of polymer adsorption. The adsorption led to a surface intoxication and therefore to delayed hydration reaction. The effects of cellulose ethers on the aluminates were less specific. No CE adsorbed on the surface of ettringite, a hydration product of tri-calcium aluminate and calcium sulphates. Nevertheless the ettringite crystallization after 4 hours was strongly retarded by cellulose ethers depending on their DS. This retardation was an indirect phenomenon caused by delayed development of ion-concentration in the pore water. This delay again was a consequence of the retardation of the silicate hydration caused by cellulose ethers. In general it can be said that the lower the degree of substitution of the cellulose ethers, the larger the amount of adsorbed polymers and the stronger the retarding effect.

2 Introduction

2.1 Subject

Cement is the most important construction material used today. It is used as a binder in many mineral-based building material formulations all over the world. Its importance is not only due to its binding function in concrete but also in dry mortars. In comparison to concrete, dry mortars are more specialized and therefore more sophisticated. Except for masonry mortar they do not have load-carrying functions in civil engineering. Dry mortars in general consist of mineral binders such as cement, lime or gypsum, fillers such as silica sand or carbonates and various organic and inorganic auxiliary agents. Dry mortar is the term for an industrial product offered by cement producers to the workers and craftsmen on construction sites as a complete formulation that only needs water to be applied. The most important applications are plasters and renders, tile cements and self-levelling compounds, masonry mortars and thermal insulation compounds, joint fillers and grout. The dry mortar comes as powder in bags or silos and has to be mixed with water at the construction site.

Cellulose ethers (CEs) are the most important rheological regulators for aqueous systems. Their primary function is that of a thickener and control agent for the water balance. CEs dissolved in aqueous solution increase the viscosity of the liquid as a function of molecular weight and addition level. They are used in construction materials as well as in paints, food, pharmaceuticals, body care and household cleaners. Due to their film-forming property they are also used as glue in paper and tobacco industries and for the application of wallpapers. The common field of cement and cellulose ether is the dry mortar application. Concrete as a load carrier usually does not contain cellulose ethers because of their strength weakening effect. In contrast to concrete there is almost no dry mortar formulation without cellulose ether as the most important rheological regulator.

2.2 Objective

Due to the complexity and great variety of mineral-based construction materials the work is focused on the organic-inorganic interaction between cement phases and cellulose ethers in ordinary Portland cement (OPC), pure cement phases and admixtures thereof. Other materials should only be mentioned as examples where it appears to be reasonable.

Experiences in product development showed that cellulose ether retards the hardening of cement. The retardation times vary with variations of the chemistry of the polymer. The CE-caused increase of viscosity of the pore solution may hinder the ion transport. But the retarding effect does not correlate with the viscosities of CE-solutions. This is evidence that

the pore solution is not the only hydration-controlling factor influenced by CE. A direct interaction between dissolved polymer and solid phase is assumed. Classic retarders for gypsum such as phosphonic acid derivatives adsorb on the faces of gypsum crystals. The surface intoxication leads to retarded crystal growth and a change of the crystal morphology^[Bos1]. Following this idea, the study focused on the question whether CE-adsorption on cement phases controls the hydration kinetics. This leads to the following questions:

What is the polymer's key parameter controlling retardation if viscosity plays a minor role?

Is the retarding effect of CE phase-specific?

If yes, can the retarding effect be correlated with phase-specific adsorption?

In order to answer those questions methods were developed that allow to quantify CE-adsorption and to monitor hydration processes phase- and time-resolved. Two ways seemed to be practicable: 1. Phase-resolved investigations on phase development in cement. X-ray powder diffraction (XRD), in particular synchrotron-XRD as in-situ method, should be suitable. 2. Macroscopic integral methods to determine sum parameters can also give phase-resolved results if experiments are performed on pure phases. Batch-type experiments with subsequent residual free water analysis were performed in order to quantify the CE-adsorption per phase.

2.3 Nomenclature

Material research is an interdisciplinary science. Contributions come from physics, chemistry, mineralogy, ceramic research and last not least from handcraft. The big advantage is that the manifold input creates a fertile environment for development. A disadvantage is that any discipline cultivates its own language. To avoid confusion it is indispensable to define a strict nomenclature. Craftsmen for example call powdered construction materials "gypsum" if they are based on calcium sulphates of any kind. Mineralogists give trivial names to natural mineral phases. These names may derive from old common names (gypsum), from their chemical composition (anhydrite), a location where a natural form has been found for the first time (ettringite), the name of a person to be honoured (brownmillerite) or a word composition of ancient Greek or Latin that describes physical properties (chlorite, from *chloros* = green). Cement research scientists of the 19th century adopted the trivial name system of mineralogy and invented names for artificial phases that sound similar to mineral names (alite, belite, celite). Chemists prefer descriptions of chemical compositions (tri-calcium silicate) on the basis of the international IUPAC-standard and use the chemical formula (Ca_3SiO_5). Ceramic

engineers divide the chemical formula into its oxide components ($3\text{CaO}\cdot\text{SiO}_2$). In ceramics it is usual to abbreviate those components with single letters (C_3S). Tables 2.1 and 2.2 give term definitions of the most important oxide components and cement phases.

oxide component	ceramic short formula	oxide component	ceramic short formula
Al_2O_3	A	H_2O	H
CaO	C	SiO_2	S
Fe_2O_3	F	SO_3	$\bar{\text{S}}$
MgO	M	K_2O	K

Table 2.1: Oxide components and their ceramic symbols (examples)

Full expression, trivial name	Ceramic short formula / abbreviation ¹⁾	Phase composition
Ca-sulphate, anhydrite	$\text{C}\bar{\text{S}}$	CaSO_4
Ca-sulphate hemi-hydrate, bassanite	$\text{C}\bar{\text{S}}\text{H}_{0.5}$	$\text{CaSO}_4\cdot 0.5\text{H}_2\text{O}$
Ca-sulphate di-hydrate, gypsum	$\text{C}\bar{\text{S}}\text{H}_2$	$\text{CaSO}_4\cdot 2\text{H}_2\text{O}$
tri-Ca-aluminate	C_3A	$\text{Ca}_3\text{Al}_2\text{O}_6$
di-Ca-aluminate ferrite, celite	$\text{C}_2(\text{A},\text{F}), \text{C}_4\text{AF}^{1)}$	$\text{Ca}_2(\text{Al},\text{Fe})_2\text{O}_5$
di-Ca-silicate, belite	C_2S	Ca_2SiO_4
tri-Ca-silicate, alite	C_3S	Ca_3SiO_5
Ca-aluminate hydrates	CAH	various ¹⁾
Ca-silicate hydrate	CSH	stoichiometrically not determined ¹⁾
Ca-hydroxide, portlandite	CH	$\text{Ca}(\text{OH})_2$
Ca-aluminate tri-sulphate hydrate, ettringite	$\text{AFt}^{1)}$	$\text{Ca}_3\text{Al}_2\text{O}_6\cdot 3\text{CaSO}_4\cdot 32\text{H}_2\text{O}$
Ca-aluminate mono-sulphate hydrate	$\text{AFm}^{1)}$	$\text{C}_3\text{Al}_2\text{O}_6\cdot \text{CaSO}_4\cdot 12\text{H}_2\text{O}$

Table 2.2: Expressions of cement phases and their formulas as used in this thesis.

¹⁾ for detailed explanation see chapter 2.5.2.

2.4 Historical Background

Men have used building materials since the middle stone age. The basic material was certainly wood and fur. In the first permanent settlements of the late stone age clay, respectively loam, was used. Further development in early antiquity led to loam brick or quarrystone masonry with clay, lime or gypsum as masonry mortar. First cements with pozzolan as hydraulic binder are known from ancient Greeks, Phoenicians and Romans. The knowledge of making cement was not lost with the decline of the Roman Empire but its application became very rare. In the Middle Ages half-timbered buildings were European standard. The gaps of wooden frame works were filled with straw and clay with a lime render finishing. Sacred buildings and constructions with strategic importance or representative character such as castles and town halls were erected with quarrystone masonry. Ceramic brick masonry was used in prospering cities and trade centres since the 15th century. Masonry for residential homes spread even over remote places with improved general living standard in the 18th and 19th century. Cement was reinvented in the 18th century in England. In the 19th century steel and glass completed the list of modern construction materials.

Organic components in combination with mineral binders have been used since the antiquity. Soaps, resins and proteins in their natural form were added to the binders to improve their workability. Lime for example was mixed with cottage cheese, which contains casein. Casein is a retarder for lime and retards the carbonization. In the 19th century cellulose was etherified with nitric acid for military use. Other derivatives were used as thickeners in dry mortars for roughly forty years.

2.4.1 The Development of Cement

Greek, Phoenician and Roman civil engineers found out that a mixture of lime, clay and pozzolan, a powdered volcanic ash, is a hydraulically setting binder ^[VDZ1]. Hydraulic means that the material hardens under water as opposed to pure lime or gypsum. One of the oldest written witnesses of ancient construction material development is ascribed to Vitruv ^[Vit1]. He described binders made of stone debris, lime, sand, pozzolan and milled bricks as "opus caementitium" (= work made of stone debris) from the 3rd century B.C. Later the hydraulic components made of pozzolan and milled bricks were shortly named "caementum". The hydraulic powders were dry-mixed with lime. The Roman concrete achieved compressive strengths up to 40 N/mm² and last in Roman architecture until today.

In the 18th century the Englishman John Smeaton discovered that limestone, naturally contaminated with clay minerals, could be fired to a hydraulic binder without pozzolan. The

further development took place in England. In 1796 James Parker held a patent for hydraulic binder fired from natural clay-rich lime-sandstone that he called "Roman cement". The name "cement" was transferred to hydraulic binders in general. Edgar Dobs held a patent for hydraulic lime that has been burned from an artificial mixture of limestone and clay in 1810. Later Joseph Aspdin improved the limestone-clay-mixture and called the product "Portland cement". Even this early Portland cement was rather more like Roman cement since clinker conditions at 1450 °C had not been reached yet. The name was chosen for two reasons: first the colour of the cement was similar to those of natural limestone found in the region of Portland, second the Portland limestone was a well-established high quality quarrystone in the construction material market. With the name the cement should be associated with high quality. Joseph's son William Aspdin reached clinker conditions in his cement factory in 1843 for the first time. Higher burning temperatures led to this important improvement. The further development improved the cement in respect of strength by increasing the content of clinker phases in the burned product. In Germany and France Portland cement was manufactured for the first time in 1850 and in the USA in 1870.

The first national standard concerning cement quality was introduced in Prussia in 1878. The hydraulic properties of granulated alkaline cinder, a waste product of steel production, was discovered in 1862 by Emil Langen in Germany. The resulting smelter cement was the first cement made of artificial raw materials. The German cement industries introduced a national standard in 1882 that defined that a Portland cement must be burned to clinker condition from at least 98 molar-% of natural raw materials. Other national standards were introduced in France in 1885 and England in 1905. The development in the 20th century led to further cement types like the iron-free white cement or the fast setting aluminate cement. For concrete and most dry mortars Portland cement is still the most important. Further work was focused on standardization on a national basis in the thirties and forties. The specification on cement quality was summarized in Germany in 1932 in the national standard DIN 1164. Later, since the eighties, national standards were transformed to common European standards in the European Union.

It was not a coincidence that modern cement production started in England. In the Middle Ages wood was nearly the only fuel. Its energy content was too poor to produce Roman cement. The little charcoal that could be made by men was urgently needed for steel production. Even the Romans had no better fuel than wood, but pozzolan is a volcanic rock. The firing energy to produce this hydraulic material came from the upper mantle of the earth.

With the invention of lignite firing during the industrial revolution in England there was plenty of energy available for burning cement.

2.4.2 The Development of Cellulose Ethers

The history of cellulose ether started with military application. Gunpowder had been used by Chinese for centuries before it was brought to Europe. While the Chinese used it for fireworks only, gunpowder became an explosive and a propellant for military use in Europe in the 15th century. It was the only explosive, respectively propellant, known until the sixties of the 19th century. The handling of gunpowder is very dangerous since this unstable material reacts unpredictable, especially when moist. The invention of nitro-glycerine in the 19th century replaced gunpowder as an explosive. The further development of nitro-explosives led to dynamite and nitro-cellulose ^[Dye1]. Both explosives are relatively safe in handling and are more effective than gunpowder. Partly nitrated cellulose was used as explosive by the Saracens during the era of crusades since the 11th century. Brushwood was soaked with nitric acid and placed in tunnels beneath castle walls to destroy Christian strongholds. Completely nitrated cellulose was the first water-soluble cellulose derivative used as propellant since the second half of the 19th century. Other derivatives like Carboxy-methylcellulose (CMC) and methylcellulose (MC) were developed as glue for cardboard and paper in the early 20th century ^[Sch1]. The further development of cellulose ethers led to a wide range of derivatives used mainly as thickeners, soluble in hot and/or cold water and organic solutants. The first application of cellulose ethers in construction materials appeared with the development of dry mortars in about 1960.

2.5 Materials

This chapter will give a brief overview of Portland cement, its primary and hydrated mineral phases, cellulose ethers and dry mortars. Material properties, phase development during hydration and the task of cellulose ethers will be briefly described.

2.5.1 Portland Cement

Cement is a fine mineral powder with hydraulic properties, i.e. the ability to harden under water. The most important mineral phases of ordinary Portland cements belong to the system CaO-Al₂O₃-SiO₂-SO₃-H₂O. The Association of German Cement producers (Verein Deutscher Cement-Fabrikanten) defined that the name "Portland cement" must not be used for any cements others than those produced of at least 98 molar percent of natural raw materials.

These raw materials are limestone, clay and silica sand. Limestone is a rock consisting mainly of calcite, a calcium carbonate. Clay is rich in aluminium-bearing phyllosilicates. Silica sand (quartz) is the main source for silicon oxide. A mixture of these three components is burned at temperatures above 1400 °C. First the calcite decarbonizes at approx. 600 °C. The calcium oxide reacts with the Al₂O₃- and Fe₂O₃- components of clay minerals above 700 °C. Reaching clinker conditions at 1450 °C, CaO reacts with the silicon oxide. The products of this process are mainly tri-calcium aluminate (C₃A), di-calcium aluminate ferrite (C₂(A,F), celite), tri-calcium silicate (C₃S, alite) and di-calcium silicate (C₂S, belite). These are the primary clinker phases of Portland cement. "Clinker" describes the clinking noise when cement granules fall out of the furnace onto the floor. The granules are milled down together with calcium sulphate. The sulphate is added as retarder for C₃A-hydration. Usually gypsum (calcium sulphate di-hydrate, C₂S̄H₂) is used. Since the granules are still hot and the milling process also produces heat, the primary sulphate dehydrates partly to calcium sulphate hemi-hydrate (C₂S̄H_{0.5}) and partly to water-free calcium sulphate (anhydrite, C₂S̄). A certain ratio of hemi-hydrate and anhydrite can also be added on purpose to control the C₃A hydration kinetics.

2.5.2 Clinker and Cement Phases

Tri-calcium aluminate, C₃A, Ca₃Al₂O₆

Tri-calcium aluminate occurs in different polymorphs. Pure C₃A is cubic. In OPC an orthorhombic modification is formed by incorporation of alkalis especially potassium. Cubic and orthorhombic forms can coexist in OPC. A mixture of both polymorphs is hard to analyse by X-ray diffraction. Cubic C₃A is the most reactive phase in OPC closely followed by the orthorhombic form. Monoclinic modifications of C₃A are known but they are of no importance in OPC.

Celite, di-calcium aluminate ferrite, C₂(A,F), Ca₂(Al, Fe)₂O₅

C₂(A,F) is a solid solution of the binary system Ca₂Al₂O₅ - Ca₂Fe₂O₅. The term C₂(A,F) is an abbreviation for C₂A_xF_{1-x}. Without other oxide components the series of solid solutions is continuous i.e. all ratios of Al₂O₃ and Fe₂O₃ exist. In OPC C₂(A,F) exists usually with a component ratio around 0.5. The single point phase C₂A_{0.5}F_{0.5} may also be written as C₄AF. Brownmillerite is natural C₂(A,F) often associated with ettringite in contact-metamorphic limestone. C₂(A,F) binds Fe₂O₃, the most important colour-giving oxide component of Portland cement. The colour of OPC therefore depends on the amount of C₂(A,F) in cement and the Fe/Al-ratio in that phase. The colour of Portland cement ranges from brown over grey to greenish grey. A C₂(A,F)-free Portland cement is white.

Alite, tri-calcium silicate, C_3S , Ca_3SiO_5

C_3S is the main component of OPC with contents above 70 mol-%. C_3S exists in several modifications depending on the temperature. Below 980 °C two triclinic forms T1 and T2 are known. The pure compound at room temperature is T1 with a transition point to T2 at 620 °C. Above 980 °C three monoclinic polymorphs are known: M1, M2 and M3 in order of increasing temperatures with transition points at 990 °C and 1060 °C. A rhombohedral high-temperature-modification exists above 1070 °C. Due to impurities of substituent ions C_3S exist at room temperatures in OPC as metastable polymorphs close to M1 or M3 or a mixture of both. The hydration of C_3S has the largest contribution to strength development of OPC.

Belite, di-calcium silicate, C_2S , Ca_2SiO_4

Five different polymorphs are known from C_2S . The stability of pure components depends on the temperature. These modification in order of increasing temperature are: γ , β , α'_L , α'_H and α with transition points at 500, 690, 1160 and 1425 °C. Like C_3S , modifications stable at higher temperatures can be stabilized at lower temperature by impurities. In OPC impurities stabilizes the β -form at room temperature. The hydration of C_2S contributes to strength development but C_2S is less active than C_3S .

Anhydrite, calcium sulphate, $C\bar{S}$, $CaSO_4$

Anhydrite is the calcium sulphate end-member of the binary system $CaSO_4 - H_2O$. Three different polymorphs exist with different solubilities in water: cubic anhydrite I, orthorhombic anhydrite II and hexagonal anhydrite III ^[BGG1]. The firing of gypsum or bassanite at temperatures above 110 °C forms hexagonal anhydrite III which is soluble in water. Anhydrite III still contains little water, less than 0.05 per formula unit. Depending on the partial pressure of vapour during the firing process an α -form (wet) and β -form (dry) exists. In contradiction to the usual phase indices of mineralogy the Greek indices in this case do not represent different polymorph phases but different morphologies. The α -form is well crystalline with idiomorph crystals. The β -form is produced by rapid dehydration that does not allow the anhydrite to recrystallize well. It consists of cryptocrystalline particles with a rough surface. Due to the increased surface area the β -form dissolves much faster in water than the α -form. Higher burning temperatures lead to the formation of orthorhombic anhydrite II at temperatures above 350 °C. This phase exists only in one morphological form and is not soluble in water. Natural anhydrite is the orthorhombic form. Firing at temperatures above 800 °C causes anhydrite II to partly desulphurize. The incorporation of remaining CaO into the crystal leads to renewed activation of the anhydrite II to react with water ^[Kue1]. Cubic

anhydrite I only exists at temperatures above 1180°C and is therefore irrelevant for construction materials. Anhydrite is added to OPC as a retarder for C₃A-hydration. Usually the sulphate carrier is added to cement during grinding in the form of gypsum. The heat produced during the milling process dehydrates the gypsum to hemi-hydrate and β-anhydrite. A certain anhydrite to hemi-hydrate ratio can also be added on purpose to control the kinetics of ettringite formation in the early cement hydration process ^[Hae1, Win1]. The dissolution rates of the sulphates are critical.

Bassanite, calcium sulphate hemi-hydrate, $C\bar{s} H_{0.5}$, $CaSO_4 \cdot \frac{1}{2}H_2O$

Two forms exist with different water-contents. Besides the common monoclinic CaSO₄·0.5H₂O there is a trigonal CaSO₄·0.8H₂O. The dehydration process of gypsum above 50 °C forms CaSO₄·0.5H₂O. Its natural form is called bassanite. Hemi-hydrate is also divided into an α- and β-form. Also in the case of C \bar{s} H_{0.5} the Greek indices indicate no polymorphs with different crystal structure. The difference lies in the crystallinity and morphology of the hemi-hydrate. As with anhydrite III the formation of α- and β-C \bar{s} H_{0.5} depends on the partial vapour pressure during the dehydration of gypsum. β-hemi-hydrate is a phase with poor crystallinity and rough surfaces. α-hemi-hydrate occurs in idiomorphic crystals. Both forms can be easily detected by their BET-values. The typical specific surface area of β-calcium sulphate hemi-hydrate lies between 6 and 16 m²/g whereas that of the α-form is around 1 m²/g. Due to increased surface area β-hemi-hydrate dissolves much faster in water than α-hemi-hydrate. Like anhydrite and gypsum, hemi-hydrate is added to cement to control C₃A-hydration.

Gypsum, calcium sulphate di-hydrate, $C\bar{s} H_2$, $CaSO_4 \cdot 2H_2O$

Only one monoclinic modification exists. Gypsum is the raw material for most calcium sulphates used in construction materials. Its origin maybe from natural sources as well as from industrial by-products. Large amounts of gypsum come from desulphuration facilities of power plants and from phosphoric and citric acid production. Natural calcium sulphates occur as gypsum and anhydrite. Natural bassanite plays a negligibly small role. Like hemi-hydrate and anhydrite gypsum is added to cement to control C₃A-hydration.

Ettringite, calcium aluminate ferrite tri-sulphate hydrate, AFt, $Ca_6(Al,Fe)_2O_6(SO_4)_3 \cdot 32H_2O$

Ettringite is the first hydration product of OPC in presence of sulphates. It also exists in nature in contact-metamorphic limestone. It was first found near the village Ettringen in the Middle German Highlands from which the mineral got its name. Besides the pure phase from which only one modification exists, solid solutions with other components of OPC are known. Fe(III) for example can substitute Al. All polymorphs are hexagonal. The abbreviation AFt stands for calcium aluminate ferrite tri-sulphate hydrate. In Portland cement ettringite crystallizes rapidly within the first minutes of cement hydration. A second ettringite formation follows after hours. Both, first and second ettringite formation are sometimes summarized in the literature as primary ettringite formation to distinguish those hydration processes from the so-called secondary ettringite formation. The latter one is caused by sulphate-contaminated, meteoric water (acid rain) that intrudes into aged cement after years leading to fatal damage in constructions. The formation of ettringite and monosulphate in Portland cement hydration processes was studied in-situ using synchrotron XRD by Christensen et al. ^[Chr1]. Further details on ettringite formation as a nucleation and growth process out of pore solution is given by Amathieu and Estienne ^[Ama1].

Monosulphate, calcium aluminate ferrite monosulphate hydrate, AFm,

$Ca_4(Al,Fe)_2O_6SO_4 \cdot 12H_2O$

Monosulphate is a degradation product of ettringite that is formed when the sulphate is undersaturated in the pore solution of OPC. AFm stands for calcium aluminate ferrite monosulphate hydrate since this phase may also contain a ferrite component.

Calcium aluminate hydrates, CAH

CAH is a collective term for all calcium aluminate hydrates. The most important phases are C_4AH_{19} and the later dehydration product C_4AH_{13} . In OPC their formation is inhibited by the addition of sulphates. C_4AH_{19} first occurs when all sulphate and ettringite is consumed by monosulphate.

Portlandite, calcium hydroxide, CH, $Ca(OH)_2$

Portlandite is, besides CSH-phases, the main hydration product of C_3S and C_2S . Due to the lower Ca-content the C_2S -contribution to portlandite formation is smaller than that of C_3S . Portlandite reacts with atmospheric CO_2 to calcite, the trigonal Ca-carbonate. Williams et al. ^[Wil1] made quantitative determination of the CH-content in hydrating cement in-situ by means of synchrotron XRD.

Calcium silicate hydrates, CSH

In contrast to CAH, CSH is not a collective term for various well-defined calcium silicate hydrates. It describes an X-ray amorphous phase with uncertain stoichiometry. In older studies it is usually described as gel due to its amorphous appearance in XRD-measurements and its diffuse appearance in early scanning electron microscopy (SEM). In the early nineties Taylor^[Tay1] still describes CSH as gel although its structure is determined as similar to tobermorite. Improved techniques in SEM especially the field emission gun (FEG) and the environmental scanning electron microscopy (ESEM) led to higher resolution. Standard SEM requires carbon- or gold coating of the sample to provide a conductive layer on the sample surface. ESEM does not need such conductive coating. ESEM-FEG studies by Stark, Moeser and Eckart^[Sta1, Sta2] showed the crystalline nature of CSH. Still the determination of crystal structure and chemistry is difficult since the crystals appear as tiny needles only a few nm in size. The gel-like morphology in early SEM-studies is explained by the carbon layer whose thickness is larger than the CSH crystal sizes. CSH is the main hydration product in OPC and contributes mostly to strength formation. Whitfield and Mitchel^[Whi1] did quantitative phase analysis of amorphous phases in Portland cement based on the Rietveld method.

2.5.3 Hydration Processes of Portland Cement

The clinker phases of Portland cement usually do not exist as single-phase particles since the original clinker granules exist as more or less homogeneous breccias of all phases. Also the fine particles of powdered cement consists rather of all clinker phases randomly distributed. The most reactive clinker phase is C_3A . In sulphate-free cements C_3A would react with water immediately forming different calcium aluminate hydrates (CAH). First C_4AH_{19} crystallizes. During the drying process of cement the C_4AH_{19} dehydrates to C_4AH_{13} . The cement sets quickly with fast strength development. To avoid this fast reaction the C_3A -hydration in Portland cement is retarded by calcium sulphate. The reaction of C_3A with sulphates produces ettringite, a reaction that prevents CAH formation during early hydration. Taylor^[Tay1] describes cement hydration in three steps: 1. The early period (initial state), 2. the middle period (accelerated state) and 3. the late period with divisions after approx. three and 24 hours of hydration. Taylor's discussion is based on the studies of Scrivener^[Scr1]. C_3A as the most active phase reacts immediately with water and sulphate forming ettringite and a little CAH. Simultaneously some of the calcium silicate reacts with water. The polymineralic particle is covered by a thin colloidal Al- and Si-rich shell with significant amounts of calcium and sulphate. The component ratio of the shell varies with the underlying primary phase. Within

10 minutes ettringite crystallizes as short-prismatic hexagonal crystals on the outer side of the shell and in the pore spaces. The place of ettringite formation suggests that nucleus formation takes place out of solution as a dissolution-precipitation-process.

In the accelerated state CSH begins to grow rapidly at the outer side of the shell. It is assumed that CSH nucleates on the ettringite. The shell grows outwards and the dissolving primary phases leave a gap between grain and shell ^[Sta3] filled with highly concentrated solution. This is evidence that 1. CSH formation is also a dissolution-precipitation-process and 2. the shell is ion-permeable at this stage. The morphology of CSH depends on the free space available for crystallization. After 12 hours the outward growth of the shell has reached so far that shells of neighbored grains interconnect. This development coincides with maximum heat evolution and highest rate of strength formation. CH crystallizes in the pore rooms simultaneously with CSH formation. At the end of the accelerated stage ettringite growth takes place forming needle-like crystals. Scrivener ^[Scr1] sees the second ettringite crystallization related to C₃S hydration.

The late period is characterized by decreased permeability of the shell. CSH starts to grow inwards. Since CSH grows faster than C₃S retreats, the gap fills up and vanishes after 7 days. With ongoing reaction of C₃A the sulphate concentration drops rapidly inside the shell. This leads to monosulphate formation at the inner side whereas at the outside ettringite may persist. As the gap between shell and grain disappears the reaction rate decreases. Further CSH formation is assumed to be a topochemical reaction replacing C₃S in place. The hydration of C₂S and C₂(A,F) is hard to observe. Significant amounts of C₂S have been hydrated after 14 days but remaining C₂S may react slowly over years.

2.5.4 Cellulose Ethers

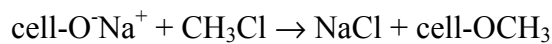
Cellulose ethers are derivatives of cellulose, a polysaccharide consisting of β-1,4-glycosidically bonded anhydroglucose units (fig. 2.01). The numbering of the carbon positions starts at the carbon [1] next to the ring oxygen with a link to the neighbored anhydroglucose ring. The numbering follows the direction to the next carbon linked to a hydroxyl group (away from the ring oxygen). The carbon at position [4] is linked by an oxygen to the [1]-position of the previous ring (1,4-bonding). The carbon position [6] does not belong to the ring but is situated in a side branch connected to position [5]. OH-groups are linked to carbons on positions [2], [3] and [6].

Cellulose consists of amorphous and mostly crystalline domains of parallel oriented polymer molecules, which are not soluble in water. They are bonded to each other by

intermolecular H-H bridging bonds at the hydroxyl groups of the anhydroglucose units. These bonds also exist within one molecule as intramolecular H-H bridging bonds. Besides lignin, cellulose is the main component of wood. The chain length of the polymer molecule depends on the raw material. The molecular weight increases with the raw material in the following order: grass and other lower plants, wood, cotton.

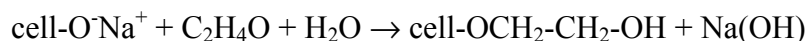
In order to etherify cellulose the polymer is first deprotonated in caustic soda solution. The H-H-bonds are broken and the remaining oxygen of the former OH-groups of the dissolved or swollen, negatively charged polymer molecules are associated with sodium cations (fig. 2.02). Sodium cellulose is water-soluble. The conversion with sodium hydroxide is necessary to make the active groups accessible for etherifying agents. In the next step the etherifying agent is added, e.g. methylchloride:

Na-cellulose + methylchloride \rightarrow NaCl + methylcellulose (MC, fig. 2.03):



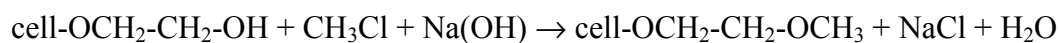
The surplus of sodium hydroxide solution is neutralized with hydrochloric acid. Finally the cellulose ether is washed, dried and milled. Common etherifying agents beside methyl chloride are ethylene oxide, propylene oxide and others. Combinations of etherifying agents are possible. Common cellulose ether types in dry mortar applications are methyl-hydroxy-ethylcellulose (MHEC, fig. 2.05) and methyl-hydroxy-propylcellulose (MHPC, fig. 2.06). Methylcellulose (MC) and hydroxy-ethylcellulose (HEC, fig. 2.04) play minor roles in dry mortar formulations. The substitution of the hydroxyl groups takes place in the following way ^[Han1] :

Na-cellulose + ethylene oxide + water \rightarrow hydroxy-ethylcellulose + Na-hydroxide:



Hydroxy-ethylcellulose + methylchloride + Na-hydroxide

\rightarrow methyl-hydroxy-ethylcellulose + Na-chloride + water:



Na-cellulose + propylene oxide + methylchloride

\rightarrow methyl-hydroxy-propylcellulose + Na-chloride:



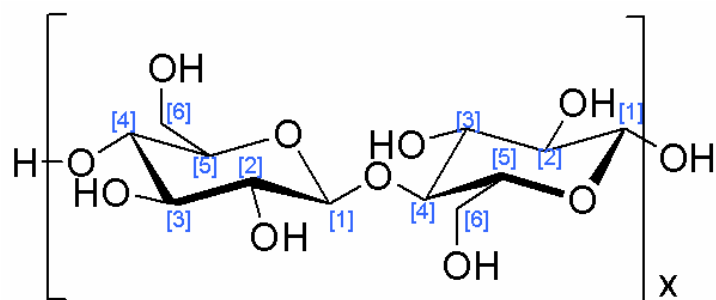


Fig. 2.01: Configuration of cellulose with carbon positions (blue characters).

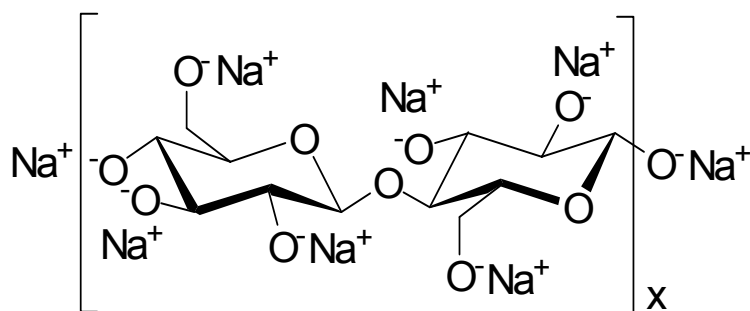


Fig. 2.02: Sodium cellulose, generally called alkali-cellulose

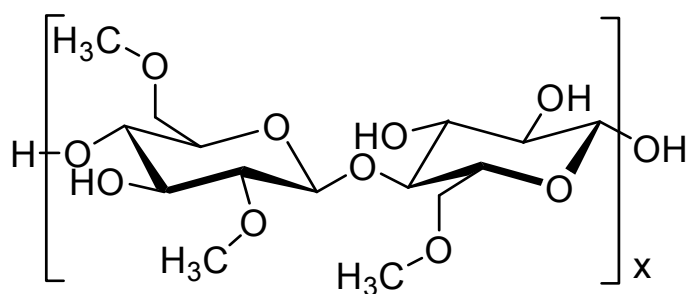


Fig. 2.03: Methylcellulose with DS = 1.5

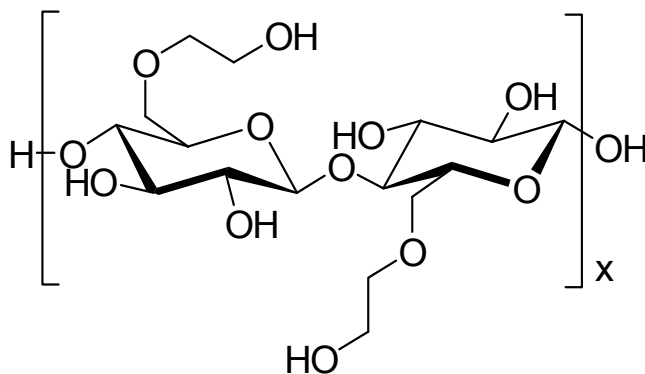


Fig. 2.04: Hydroxy-ethylcellulose, DS = 1.0

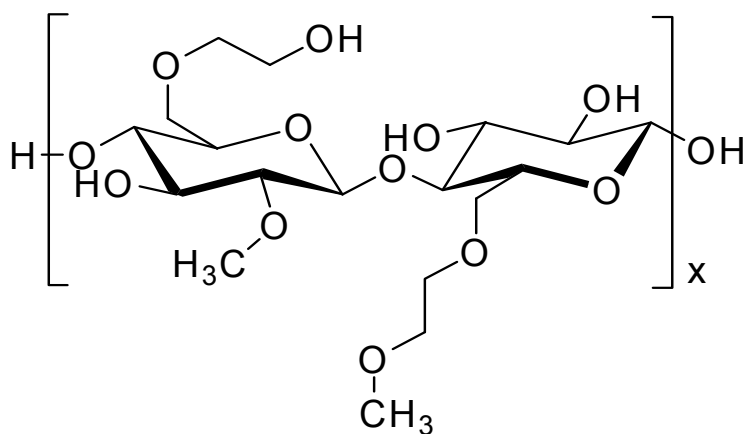


Fig. 2.05: Methyl-hydroxy-ethylcellulose, DS = 1.5

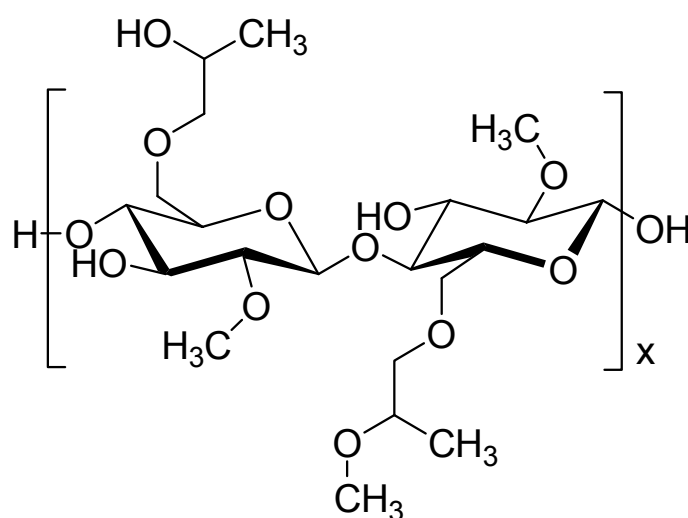


Fig. 2.06: Methyl-hydroxy-propylcellulose, DS = 2.0

The stoichiometric equations given above are simplified disengagements and do not reflect the actual production processes. The latter are not disclosed by the producers. The substitution of OH-groups of one ring with different substituents can take place either:

1. in one position successively, e.g. figure 2.05, right ring, position [6]: $-\text{OCH}_2\text{-CH}_2\text{-OCH}_3$; or
2. in different positions parallel, e.g. figure 2.05, left ring, position [6]: $-\text{OCH}_2\text{-CH}_2\text{-OH}$ and position [2]: $-\text{OCH}_3$.

On the construction material market MHEC, MHPC and MC are known under the collective name methylcellulose (MC). It has to be kept in mind that in this case the term methylcellulose does not reflect the actual chemistry of the cellulose ether.

Cellulose ethers are characterized by their chemistry as mentioned above, the conversion grade (MS and DS), molecular weight and milling grade. The degree of substitution (DS) is the average number of OH-groups per anhydroglucose ring substituted by etherifying groups. The substituents are usually statistically distributed over the whole polymer. The hydroxyl

group on position [3] is sterically hindered so that less substituents are found on position [3]. The relative activities of the three positions in respect of substitution are given in table 2.3. Since there are three positions to be substituted the DS may vary from zero (cellulose) to three. For HEC the molar degree of substitution (MS) defines the molar fraction of substituents per anhydroglucose ring.

The degree of polymerization (DP) is the number of anhydroglucose units per polymer chain and determines the length of the polymer's backbone. The backbone length of the cellulose ether cannot be higher than that of the cellulose used as raw material. The viscosity of an aqueous solution at a given CE-concentration depends on the DP-value. The longer the molecules the higher the viscosity for a given CE-type. Instead of the DP-value the viscosity in 1%- or 2%-aqueous solution or the molecular weight can be given. The milling grade defines the fineness of CE powder. The finer the powder the higher the specific surface area and the higher the dissolution rate and the higher the risk of lumping.

Position	[2]	[3]	[6]
methylchloride	0.967	0.667	1.000
ethylenoxide	0.300	0.100	1.000

Table 2.3: Relative activities (position [6] = 1) of substitution positions

2.5.5 Macroscopic Effects of Cellulose Ethers on Dry Mortars

Cellulose ethers have significant effects on the physical properties of wet mortar pastes. In the first place cellulose ether is a thickener that increases the viscosity of the fluid phase to give higher consistency of the paste. This effect is a function of molecular weight and addition rate. The higher the degree of polymerization the higher the viscosity at a given addition level. The increased viscosity also inhibits the gravity-separation in thin fluid pastes, which is very important for self-levelling compounds. CE improves the adhesion of the wet mortar to a substrate. Good adhesion to the substrate improves the bonding of the mortar and increases the adhesion strength of the hardened material at the interface.

MC-types (MHEC and MHPC) stabilize air voids in the paste. MC is not a pronounced air entraining agent - surfactants are much more effective - but it stabilizes voids that have been entrained while stirring. This property is in most cases desired. The yield of dry mortars depends on the maximum possible water ratio and on the total air void volume. A big air void volume also increases the heat and sonic isolation ability, important properties of thermal insulation systems and indoor plasters or renders. Air void stabilization is also important for good workability. If air voids collapse during shape-giving processes proper application is

hampered (e.g. combing of tile cements or smoothing of render). On the other hand air voids deteriorates the cohesive strength of the hardened mortar. Strength (cohesive, flexile and compressive) is an exponential function of bulk density.

Cellulose ether and water molecules have a strong affinity. A hydrate shell surrounds each CE molecule. This immobilizes the fluid phase and gives water retention ability to the mortar. Without water retention ability the water will be sucked into a porous substrate by capillary forces and is no longer available for the hydration process. The hardening of the mortar is disturbed. To provide water-retention ability is the most important property of cellulose ethers.

All properties of cellulose ethers mentioned above are desired for good performance. In some cases CE alone is not sufficient. Further additives are needed to improve the rheology and consistency, to achieve mechanical flexibility, better cohesion and adhesion. But water retention capacity makes CE indispensable. No other polymer provides water retention values (WRV) as does CE and no other polymer provides so many improvements in respect of workability. This makes CE an universal rheological regulator not only for construction materials. Wherever an aqueous system has to be adjusted to defined rheology cellulose ether is the first choice in food, pharmacy, body care, household cleaners and ceramic extrusion. An overview of the physical properties of cellulose ether in various applications is given by Croessmann and Klaus (1975) ^[Cro1].

2.5.6 Dry Mortar Applications and their Economic Relevance

Mortar is a construction material consisting of three major components: binder, filler and additives. Binders maybe cements, calcium sulphates, lime or organics such as latex or combinations thereof. Silica sand, carbonates or light materials (polystyrene, perlite) can work as fillers. Until the fifties of the last century the mortar was mixed at the construction site by the craftsmen (job-site mixing). This method did not enable workmen to compose mixtures with well-defined component ratios. Cement producers started to offer complete application-specific formulations and delivered them as dry powder ("dry mortar") in bags or silos in contrast to concrete, which comes as wet mixture. The industrial mortar production allows to develop highly specialized products with optimized well-defined addition ratios of all components based on laboratory test results and to apply plasters on large wall areas with the help of spraying pumps ^[Irs1]. In the sixties cellulose ether was added for the first time. Job site mixed materials had to be applied in thick layers of several centimetres to counterbalance the

water loss on porous substrates. Due to the water retention ability of CE it was now possible to apply thin layers (approx. 1 cm for plaster and render).

Gypsum-based dry mortars are mainly indoor plasters and joint fillers. The binder is usually calcium sulphate hemi-hydrate in some cases with addition of anhydrite. Sulphate-based floor screeds contain anhydrite as binder for higher strength. Fillers are quartz sand, carbonates or coarse anhydrite.

Cement-based systems are used for render (in- and out-door), tile cements, thermal insulation systems, self-levelling compounds and masonry mortars. Render is the most undemanding application of cement-based mortars since the demand on strength is not very high. Therefore it has the broadest variety of components. Render equalizes uneven walls and protect the substrate. Indoor application is in most cases to prepare walls for painting or wallpapers. Their advantage against gypsum-based plasters is their high alkalinity that prevents mustiness in humid rooms. Other applications are decorative renders. Outdoor renders have to be chemically resistant against meteoric influences. Renders can be applied by hand or with help of spraying machines.

Tile cement is the glue between tiles and substrate. Tile cements are highly sophisticated due to the high requirements on strength and flexibility, open and correction time. Open time is the time after application on the wall in which the attachment of tiles is possible. Correction time is the time in which a tile can be slightly moved for correction without losing adhesion.

Masonry mortars bind the bricks or stones in masonry and equalize uneven sizes. The mortar has to be softer than the bricks. Thus mechanical stress causes cracks or adhesion loss in the joint instead breaking the brick. It is easier to repair damages of the mortar layer than to replace broken bricks.

Self-levelling compounds are the most demanding formulations. They are designed to equalize uneven floors unaided. The consistency must be thin enough to flow but segregation must be avoided. Cementitious systems shrink during hydration. Since self-levelling compounds are spread in thin layers over large floor spaces shrinkage would cause cracks. To counterbalance cement shrinkage calcium sulphates are added. The sulphates react with the alumina component of the cement to form strongly expanding ettringite. Cement shrinkage and ettringite expansion must be synchronized by well-defined ratios of cement and sulphates as well as retarders and accelerators.

Thermal insulation systems are thick polystyrene boards covered on the outside by a thin render layer that is enforced by an integrated plastic lattice. Instead of render, tile cement can be applied to fix tiles or brick blenders.

The global market shows regional differences. While masonry combined with render or plaster is the traditional way to build in Europe, the North American region has little masonry. Private residential homes are erected as light constructions from wood and plasterboards. Bigger constructions are made of concrete. Instead of render, walls are covered with gypsum plasterboards on which wallpapers can be applied directly. Ready-to-use formulations based on organics are used for joint fillers. They already contain water and setting is caused by drying. Tile cements are more common in the U.S. than other mortars. The most important market for dry mortars is Europe traditionally.

2.6 State of Research

The development of construction materials in the times before John Smeaton was mostly based on handcraft experiences that have been made for generations of masons. Inventions were mostly made by coincidence and non-systematic trial and error experiments. Systematic research based on well-aimed experimental work is known from Roman civil engineers. The English historian R. Rank-Graves^[Ran1] mentioned the development of a hydraulic cement for the enlargement and reinforcement of the harbour of Ostia in the 1st century A.D. The Roman scholar Vitruv^[Vit1] described pozzolan-based cements and concrete and referred to mortars of the 3rd century B.C. Modern cement research started almost contemporaneously with cement production at the end of the 18th century. At the same time the scientific analytic methods developed rapidly. Much work has been invested in the determination of the chemistry and crystal structures of cement phases. Efforts have been made to understand the phase transition processes during hydration. The development of XRD and SEM methods and their application for decades led to an huge amount of publications difficult to survey. A summary of the state of research in the nineties is given by Taylor^[Tay1] and Verein Deutscher Zementwerke^[VDZ1]. Stark et al.^[Sta1, Sta2] gave new aspects of Portland cement hydration based on ESEM-FEG studies. Synchrotron XRD was used for in-situ monitoring of phase developments during hydration by Christensen (2003)^[Chr1] and Williams (2003)^[Wil1].

Also using ESEM-FEG Eckart and Stark^[Eck1] (1997) studied the hydration of C₃A in presence of sulphates in pure phase admixtures. They describe the morphology of ettringite and its dependence on the pH-value of the pore solution. At a pH over 12 a very fine crystalline or X-ray amorphous form of ettringite was found. This correlates with the results from studies by T. Cerulli^[CER1] (2005) from Mapei, Milan, who found a correlation between ettringite morphology and sample preparation. Thereafter the first ettringite formed within the first minutes of hydration of OPC is always poorly crystalline or is an X-ray amorphous form.

Therefore only weak ettringite peaks occurs in in-situ X-ray diffraction patterns. This changes significantly if the paste is quenched with acetone. X-ray diffraction patterns of samples where the hydration process is stopped in this way, show strong peaks of well crystalline ettringite. Cerulli also confirmed those results with ESEM-FEG images of gel-like phases formed in the very early hydration. The poorly crystalline ettringite recrystallizes to well-crystalline ettringite in the undisturbed cement paste after a few hours. Cerulli estimated the amount of ettringite generated in the first formation to be about 80 masspercent of all ettringite formed during the whole hydration process. Moeser ^[Moe1] (2003) gave an explanation why some cement phases occasionally appear as poorly crystalline in ESEM-FEG images. He found that the tiny crystals can be destroyed by the electron beam resulting in a change of chemistry and a loss of crystallinity.

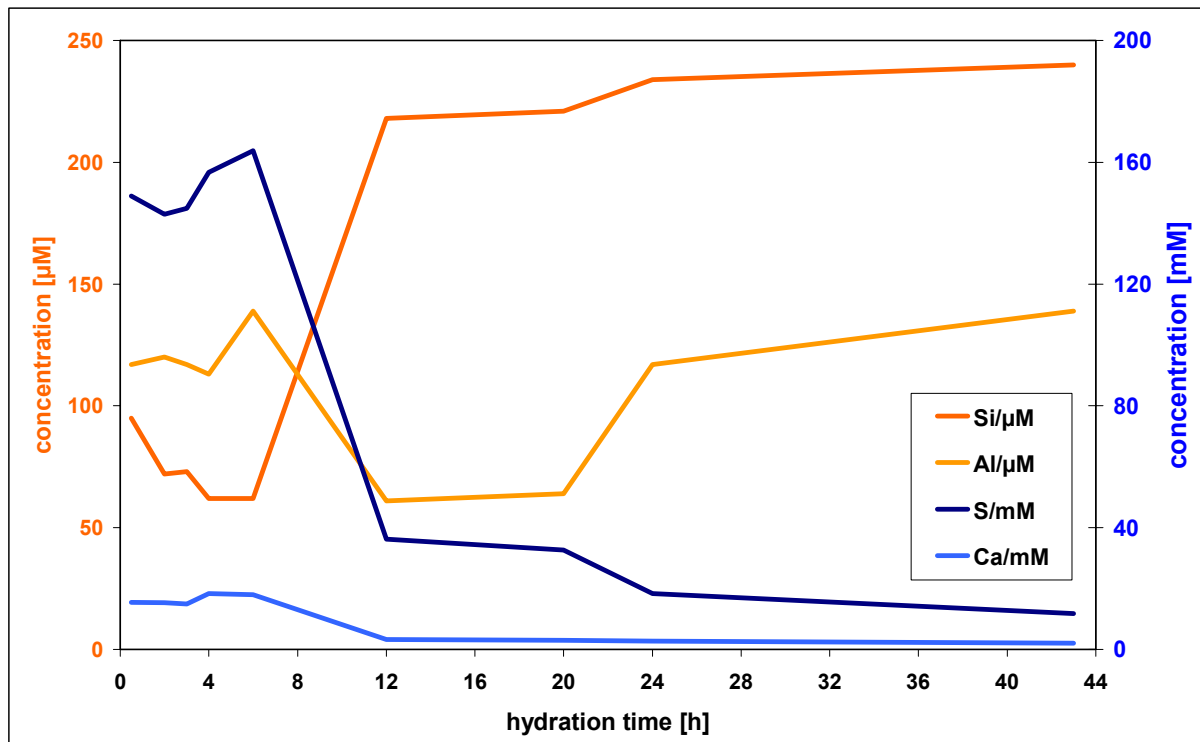


Fig. 2.07: Temporal development of ion concentrations in the pore solution of Portland cement. Data from D. Rothstein et al. ^[Rot1]

Rothstein et al. ^[Rot1] (2002) studied the ion-content of pore solutions in wet cement pastes as a function of hydration time. The authors determined beside others the elemental concentrations of S, Si, Al and Ca dissolved in the pore water of Portland cement and monitored the development during hydration. They found a sharp decline of S, Al and Ca-concentrations accompanied with a steep increase of Si in a time between 6 and 12 hours of hydration (fig. 2.07). They divided the hydration process into stage A (before the changes) and stage B

(after the changes). From elemental concentrations they calculated the saturation indices (SI) of gypsum, portlandite, ettringite and monosulphate based on thermodynamic models. Ettringite turned out to be a very stable phase with supersaturation throughout the observed time of 28 days. The SI of portlandite increased from undersaturation in stage A to supersaturation in B. For gypsum the SI decreased from saturation to undersaturation. Monosulphate was supersaturated all the time but significantly less than ettringite.

Little work has been done in public on the effects of cellulose ether on cement hydration. Only few papers on this subject have been published. Bayer and Lutz ^[Bay1] summarize the effect of CE in dry mortars in aspect of workability. A. Janni ^[Jan1] studied the interaction of cellulose ethers with other film-forming polymers and their migration. The influence of polysaccharides on cement hydration was recently studied by Peschard et al. ^[Pes1]. The authors recognized the degree of substitution and the molecular weight as the key parameter of the polymer. They came to the conclusion that CE has no effects on ettringite crystallization and only a weak retarding effect on portlandite formation compared to those of starch ether and dextrin. They found that the polymer degradation in alkaline solution depends on the molecular weight and that sugar acid as a degradation product causes the retardation of portlandite formation. Dextrin degrades to sugar acids whereas no degradation products of CE could be detected.

Coarna ^[Coa1] et al. studied the effects of a methyl-hydroxy-propylcellulose (MHPC) with a DS of 1.8 on the strength development of Portland cement. They found a delayed evolution of flexural strength due to the retarding effect of CE on Portland cement. After long-time storage (>100 days) they found increased flexural strength of samples containing 3 mass-% CE. Based on Electron Spectroscopy for Chemical Analysis they assume a chemical reaction between CE and mineral phases. Thereafter C-O bonds of the CE break and the oxygen reacts with calcium on the mineral surface.

The influence of methyl-hydroxy-ethylcellulose (MHEC) with a DS of 1.75 on the hydration of Portland cement extrusion pastes was studied by Ridi et. al. ^[Rid1]. In pure phase experiments they found a significant retardation of C₃S and C₂S hydration in the presence of MHEC. The retarding effect of CE on the hydration processes of C₃A and C₄AF was studied in absence of sulphates. A significant inhibition of the crystallization of the cubic stable phases C₃AH₆ respectively C₃(A,F)H₆ was detected.

Brandt ^[Bra2] investigated the calcium sulphate hydration in diluted systems in the presence of CE. The dissolution of calcium sulphate hemi-hydrate is non-specifically retarded as a function of viscosity. The crystallization of calcium sulphate di-hydrate is slightly

DS-specifically retarded independently of viscosity. At low DS the morphology of crystal surface step growth changes from prismatic to needle-like crystals.

The effects of cellulose ethers on early cement hydration has been recently studied by J. Pourchez ^[Pou1] at the Ecole des Mines de St. Etienne, France, and C.-J. Haecker ^[Hae1] from Shin-Etsu. Their results were discussed at the annual CEReM meeting in February 2005 in Paris. Both agree that CE has a DS-dependent retarding effect on early cement hydration. The lower the DS the stronger the retardation. In contrast to Pourchez, Haecker found also a DS-specific adsorption behaviour of CE on cement particles. But Haecker doubts a causal relation between CE-adsorption and CE-caused retardation. Because his studies came to the result that the increase of CE-addition level in excess of adsorption saturation still amplifies the CE-caused, DS-specific retardation ^[Hae2]. In their latest investigations Pourchez et al. ^[Pou2] also discussed the effects of degradation products of cellulose ethers in an alkaline environment. The results showed that CE is very stable in alkaline media. Nevertheless they identified and quantified hydroxy carboxylic acids generated during alkaline degradation but found that their effect on cement hydration is rather small. Furthermore the authors determined, that the capacity of CE to complex calcium ions is negligibly small.

Earlier works at Hercules Inc. investigated the influence of cellulose ethers on the hydration behaviour of OPC and gypsum based machine plasters. Results were given in internal reports that were not published. As far as the author of this thesis was involved results achieved in these studies are used in this work. Especially an investigation on the hydration processes of Portland cement using the same materials as used in this work gave fertile inputs to this thesis. The hydration processes were studied by the means of ultra sonic measurements, heat flux calorimetry and laboratory X-ray powder diffraction.

Other organic polymers have been subjects of research. Yoshiaka et al. ^[Yos1] determined the phase-specific adsorption of superplasticizers on cement particles. The adsorption of those ionic polymers depends on the ζ -potential of the mineral phase. Plank et al. ^[Pla1] found out that poly-carboxylates were mostly adsorbed on ettringite whereas almost no polymers of that type adsorbed on gypsum and portlandite. The effect of superplasticizers on hydration processes of cement was investigated by Roessler and Stark ^[Roe1]. The physical influence of superplasticizers on wet cement pastes was studied by Al-Wakee et al. ^[Alw1].

3. Methods

The investigation methods described in this chapter can be divided into the following subgroups: 1. methods to produce and to characterize the used raw materials and 2. investigation methods to describe the nature and consequences of CE-cement interaction during early hydration, which is the original purpose of this work. X-ray powder diffraction was used for both aims. Not all methods are described in detail if standard methods are state of the art of science and are described in the literature. Some analytical devices were not operated by the author himself. In those cases the operator involved in these investigations is mentioned.

The sample preparation methods vary in detail with the different experimental set-ups. In some cases it was even necessary to change the sample formulation but in general it was tried to keep a standard formulation. Detailed information on sample formulations will be given in chapter 4.4. The sample preparation will be described with the corresponding investigation methods. All experiments except ESEM-FEG were performed at room temperature. Due to the limited sample volume in all experiments it can be assumed that hydration heat did not lead to a significant increase of temperature within the sample since the thermal energy could be easily conducted into the environment. This correlates with dry mortar applications because those construction materials are usually applied in thin layers of mostly less than two centimetres over a large area of several square metres. In both cases (experiment and application) the material can easily dissipate the hydration heat into the environment. The largest sample volume was 3 cm by 2.5 cm by 3.5 cm (= 26.25 cm³) for ultrasonic measurements, the smallest one was about 8 mm³ for synchrotron X-ray powder diffraction.

3.1 Standard Wet Paste Preparation

A standard preparation procedure for wet slurries was introduced for all experiments except those demanding a special preparation due to their experimental set-up. Cellulose ethers were dry blended with OPC prior to water addition. After adding tap water the mixture was allowed to suck for 15 seconds. Afterwards the slurry was stirred with a Braun multimix 350 W electric kitchen stirrer in lowest gear for another 15 seconds. The slurry was then immediately applied on the sample carrier. If not mentioned otherwise, the addition level of cellulose ether was 0.5 masspercent on dry cement. The water/solid ratio (w/s) was usually 0.5. The preparation of a reference sample was similar with the difference that no CE was added to the cement. For these standard formulations tap water was used. Perhaps the ion-concentration of the tap water affects the hydration process. But all tests were done in comparison to the

reference sample without cellulose ether. In this comparative approach the ion concentration of the tap water does not matter as long as the same water was used within one test series. Comparative investigations are standard methods in construction material laboratories and therefore tap water is mostly used. The tap water used in this investigation was rich in Ca-carbonate corresponding with a degree of approx. 16° German hardness.

3.2 Ettringite Pure Phase Synthesis

Ettringite is the only pure mineral phase that has not been purchased but was synthesized by the author in the Hercules laboratory. The synthesis recipe was given by S. Barnett^[Bar1] from the University of Leeds, referring to L.J. Struble^[Str1]. The raw materials for the synthesis were calcium oxide from Aldrich and aluminium sulphate 16-hydrate ($\text{Al}_2(\text{SO}_4)_3 \cdot 16\text{H}_2\text{O}$) from Fluka (table 4.4). As an auxiliary agent sucrose was added (Sigma-Aldrich, catalogue no. 17,994-9).

Since the process is sensitive to atmospheric carbon dioxide, measures had to be taken to avoid carbonization. The calcium oxide was fired for 24 hours at 1000 °C to decarbonize. An adequate volume of deionized water was boiled to remove dissolved CO_2 . Water and CaO cooled down under a nitrogen-atmosphere. A slurry of 13.4 g CaO in 890 cm³ of a 10 mass-% aqueous sucrose solution was prepared in a glove box under a nitrogen atmosphere. Another slurry of 25.11 g of Al-sulphate hydrate in 40 cm³ of water was added. The sucrose was to inhibit CAH-precipitation. The mixture was stirred for 5 minutes and then filtered by nitrogen pressure filtration using a micropore filter with 12 µm pore size. The sludge was washed several times with decarbonized water during filtration to remove the water-soluble sucrose. The sludge was finally dried under nitrogen gas stream at 35 °C for one week in a Micromeritics SmartPrep sample station. The purity was verified by standard laboratory X-ray powder diffraction (chapter 4.2).

3.3 Particle Size Distribution (PSD)

The PSD measurements were done by W. Hildebrandt at Hercules Inc. using a Sympatec Gradis PFS granulometer. A highly diluted particle-air-stream was blown perpendicular to a laser beam. The beam was diffracted in a specific circular pattern depending on the grain sizes. Concentric arranged detectors analyse the diffraction pattern perpendicular to the primary beam with the beam focus in the centre. The finer the particles the stronger the aberration of the diffracted beam from the original direction. Assuming that all particles are spheres a particle size distribution can be calculated based on a mathematical model.

3.4 Specific Surface Area

Blaine

The Blaine value is a rough measure of the geometric surface area of a powder and is related to the air stream resistance when a gas floats through a powder sample in a defined cylinder. Based on the assumption that all grains are spheres of the same size the particle size can be calculated from the air stream resistance. Since all grains are supposed to be equally sized, the geometric surface area can be derived as area size per volume. This value divided by the pure density of the sample returns a geometric surface area as area size per mass and is usually given as cm^2/g . Since this method is not suitable to describe the surface of a powder correctly it is not used in the Hercules laboratory. The Blaine value is rather more related to the mean of grain size distribution and can be used as a quality parameter for milled materials. Therefore it is often used in cement factories to determine the milling grades of cements. The Blaine value was not considered in this work with the following exceptions: the Blaine values of the Portland cement, the tri-calcium aluminate and the tri-calcium silicate pure phases that were used in this study were determined by the suppliers to check the milling grade. The Blaine measurements were performed by HeidelbergCement AG and at the University of Aachen.

S_V-value

A geometric surface area can be calculated from the particle size distribution received from laser-granulometry based on the assumption that all particles are spheres. This surface area, the so-called S_V-value, is given as area per volume (m^2/cm^3). This value divided by the sample pure density returns the specific geometric surface area as area per mass (m^2/g). This value usually correlates with the Blaine-value in a linear way but the absolute figure is usually higher than the Blaine-value. The difference derives from the different assumptions of both methods. Both assume that all particles are spheres. Blaine assumes spheres of equal size whereas the S_V-value is received from size data with a certain size distribution. Also the S_V-value, respectively the calculated geometric specific surface area, does not describe real surfaces correctly. S_V-values were calculated by W. Hildebrandt at Hercules Inc.

BET

The only direct measurement method to determine the reactive surface area is to measure the amount of adsorbed gas molecules at gas-fluid-equilibrium temperature when the space demand of a single adsorbed molecule is known. This method goes back to Brunauer, Emmet and Teller ^[Bru1] and is therefore called the BET-method. As adsorbent nitrogen is usually used. For specific surface areas below 0.5 m²/g Krypton shows more accurate results.

The specific surface areas of all raw materials used in this work were determined with nitrogen by using a Micromeritics Gemini adsorption analyser. All samples were dried before measurements under dry nitrogen air stream at 35°C for three days in a Micromeritics SmartPrep sample station. The careful drying of the sample is essential since very small amount of adsorbed moisture decreases the surface accessible for nitrogen significantly. All measurements were done at -197 °C, the condensation point of nitrogen. At this temperature the dynamic equilibrium between adsorbed and gas phase becomes static. The BET measurements were done using a Micromeritics Gemini sorption analyzer.

3.5 Helium Pycnometry

To determine the pure densities of powders a Micromeritics helium pycnometer of the AccuPyc series was used. The sample preparation for pycnometry is not as critical as for BET-measurements since adsorbed humidity has only small effects on the total sample volume. Nevertheless for accurate measurements the samples were dried under the same conditions as described for BET-measurements.

3.6 Ultrasonic Measurements

Ultrasonic measurements replace Vicat needle tests in many laboratories of the construction material industries since the 1990's. The Vicat needle penetration test is a rough mechanical method to determine the strength of a hydrating mortar according to national/European standard DIN/EN 196-3. A pin loaded with a certain weight is dropped from a certain height onto the mortar. The penetration depth of the pin is a measure for the strength of the mortar. Inhomogenities such as lumps and air voids often falsify the test results. The advantage of ultra sonic measurements is that inhomogenities cannot falsify the results and that the monitoring time and temporal resolution are unlimited. Vicat tests end when the sample has no more space for pinholes. Ultrasonic has been developed as a non-destructive method to investigate the strength and damages of any solid material. The sonic velocity within a solid is a function of the elastic modulus, the compressibility and the Poisson number, material

parameters that depend basically on the strength of a material. Detailed information on ultrasonic measurements with the basic physical background are given by A. T. Herb (2003) ^[Her1]. The strength development of a wet cement paste can be monitored by detecting the increase of sonic speed. A Steinkamp BP 7 ultrasonic tester ^[Ste1] with a 25 kHz transmitter was used for this work (Fig. A.01, appendix A.1). The polystyrene sample mould with an inner size of 3 cm by 6 cm by 3.5 cm has circle-shaped holes of 3 cm in diameter at both short sides to integrate sender and receiver. Polystyrene is a highly porous material and capillary forces would suck water from the cement paste although polystyrene is hydrophobic. Polystyrene takes water up to 100 masspercent. To prevent water suction the polystyrene moulds were stored in water for one day before measurements. The underwater storage saturated the polystyrene pores with water. It turned out that at the beginning of the experiments, when the wet cement paste was soft, the conduction of the sonic signal through the water-saturated polystyrene walls of the mould was much faster than through the sample. This falsified the results of early measurements. To overcome this problem the mould was cut into half between sender and receiver and both halves were mounted onto a dry polystyrene board with a gap of approx. 1 mm. The gap decouples the two halves of the mould acoustically. The cement paste was viscous enough not to leak through the gap. To protect the probes, to improve the acoustic coupling and to ease the dismounting after tests, sender and receiver were covered with vaseline. The distance between sender and receiver, variable within 0 and 6 cm, was fixed for the tests at 2.5 cm. For this method standard wet paste formulations as described in chapter 3.1 were used.

3.7 Heat Flux Calorimetry (HFC)

HFC measurements were performed by S. Hucko and M. Zwanzig at Hercules Inc. For the calorimetric measurements on OPC the standard formulations as described in chapter 3.1 were used. About 4 g of the paste was filled in the specimen container and covered tightly. The sample was inserted in the custom-made HFC and measurement started. Environmental temperature during the whole period of hydration was 23°C. A disadvantage is that the sample preparation between first water contact and first measurement takes several minutes. Therefore the first three minutes of hydration cannot be observed. Tests were done to insert dry powder into the HFC-measure cell and to start the measurement before water was injected. But in all these tests the water did not mix with the powder properly. The slurries were strongly inhomogeneous and the test results could not be reproduced. Pure phase

formulations were prepared similar to cement paste preparation. But due to the small sample amount no electric stirrer could be used and the slurry was stirred by hand.

3.8 Adsorption Tests and Size Exclusion Chromatography (SEC)

To determine the amount of cellulose ethers adsorbed on mineral phases the CE-concentration in the residual pore water was analysed by SEC in comparison to a CE-solution that has not been in contact to mineral particles. The measurements were done by M. Dittel and the author at Hercules Inc. using a HPLC Waters 2695 Separation Module in combination with a Waters 410 Differential Refractometer. The eluent was a 0.2 molar lithium acetate / acetic acid buffer with a pH of 4.8.

The refractive index of the eluent-polymer solution is linearly proportional to the polymer concentration. The advantage of the SEC is that it separates the CE from the inorganic ions, which affect the refractive index as well. Furthermore it can be taken into account that cellulose ethers have broad molecular weight distributions. The total CE-concentration in the eluent solution is calculated as an integral over the elution curve. The columns are filled with a macroporous gel. The penetration of the polymers into the gel pores depends on pore and molecule sizes^[Lec1]. The total volume of the gel package in the column is the sum of pure volume of the gel body, the inner volume V_i of the gel pores and the outer volume V_0 between the gel particles. The fluid flows through the accessible volume within the column with a constant flowrate $F = V_e/t$. The elution volume V_e of a material with a molecule size too big to intrude into the pores, equals the outer volume V_0 :

$$V_e = V_0 \text{ for large molecules}$$

The molecular size exceeds the exclusion limit and the molecules move through the column without retardation. Small molecules which have access to the whole pore volume pass the column with an elution volume of

$$V_e = V_0 + V_i \text{ for small molecules}$$

Molecules with sizes in-between have access only to a fraction K_D of the inner volume with $0 < K_D < 1$. Their elution volume is

$$V_e = V_0 + K_D V_i$$

The material parameter K_D is the apparent distribution ratio of a material distributed in solvent inside and outside of the gel pores. K_D depends on the molecule size, gel pore distribution, gel material, solvent, temperature and the configuration of the molecule. The

molecule leaves the column and reaches the detector after the time $t = F V_e = F (V_0 + K_D V_i)$ with K_D as a function of the molecule size if all other parameters are constant. The higher the molecular weight the shorter the migration time through the column.

The CE was predissolved in water respectively in saturated ion-solutions. The composition of the saturated solutions depended on the solid phase to be investigated. To mimic pH conditions similar to those in cement pore water, all experiments with pure phases were performed in $\text{Ca}(\text{OH})_2$ -saturated solution. Since this solution was sensitive to atmospheric carbon dioxide, measures had to be taken to avoid Ca-carbonate precipitation. Therefore the water used to prepare the solution was deionized and boiled to remove dissolved CO_2 . The Ca-oxide to be dissolved in the water was fired at temperatures above $1000\text{ }^\circ\text{C}$ to decarbonize. Water and CaO cooled down over-night under a nitrogen gas stream. The calcium oxide was dissolved in the prepared water with excess solid CaO respectively precipitated $\text{Ca}(\text{OH})_2$ to achieve saturation. The thin slurry was afterwards filtered under nitrogen overpressure to remove the solid and to produce a clear, saturated solution. The micropore filter had a pore size of $12\text{ }\mu\text{m}$. Other solid phases were added to this solution in order to achieve saturation with respect to the phase of interest. This suspension was stirred for 30 minutes. After each addition of solids the solution was filtered again as described before. Cellulose ethers were dissolved in the prepared solutions prior to experiments.

The CE-concentration and the water/solid ratio depended on the mineral phase to be investigated and its specific surface area. The amount of CE relative to the solid phase must exceed the maximum amount that could be adsorbed. Otherwise there would be no residual CE left in the pore water to be analysed. On the other hand the excess amount must be small enough so that the difference of CE-concentrations in the primary solution and the residual pore water was distinct enough to be quantified accurately. The water ratio depended on the water-demand of the slurry. The consistency of the slurry must be thin enough to enable a sharp separation between fluid and solid phase. The water demand was primarily a function of the specific surface area of the powder sample. The larger the specific surface area, the higher the water-demand. The adsorption experiments could be divided into two types:

1. stable conditions under which the mineral phase did not change and dissolution and crystallization effects did not play a role. These tests were done with the pure hydrated phases portlandite, ettringite and gypsum in saturated solutions under a nitrogen atmosphere. The solutions had to be ion-saturated with respect to the investigated phase to avoid dissolution of the solid. The cellulose ethers were dissolved in these solutions prior to adsorption experiments.

2. dynamic conditions under which hydration processes took place during the experiments. Those experiments were done with ordinary Portland cement, pure C_3S , pure C_3A and a mixture of 70 mass-% C_3A , 15 mass-% calcium sulphate hemi-hydrate and 15 mass-% calcium sulphate. For the dynamic experiments unprepared tap water was used. The cellulose ethers were dissolved in water prior to experiments. No efforts have been made to saturate the solution in aspect of the investigated phases in dynamic experiments because dissolution of the primary phases takes place during hydration anyway. Even no Ca-hydroxide was dissolved in the solution before the experiment started. In OPC and C_3S solutions $Ca(OH)_2$ -saturation is quickly achieved.

Dynamic conditions only allowed relative statements on CE-adsorption. It could only be said how much of the cellulose ether has been adsorbed in masspercent of the original CE dissolved in the solution. It allowed to compare the adsorption behaviour of different CE-types and to monitor the adsorption over time. But the amount of CE adsorbed per square meter of the mineral surface could not be quantified since the specific surface area changed during the hydration process. Inaccuracy was also caused by the amount of water consumed in the hydration process. This amount was not determined but it is assumed that it is approximately the same in all experiments with the same mineral phases but different CE-types. Furthermore in dynamic experiments it could not be differentiated between CE adsorbed on the mineral surfaces and CE that might have been incorporated as inclusion into growing crystals.

Under stable conditions the amount of cellulose ether adsorbed per square meter of the mineral phase could be quantified since the specific surface area of the mineral could be determined prior to experiment. The stable experiments have been performed with single pure phases only. The BET-value of the gypsum of $0.2 \text{ m}^2/\text{g}$ was too small for quantitative adsorption tests. The gypsum was therefore triturated until the specific surface area achieved a value of $1.7 \text{ m}^2/\text{g}$.

First the cellulose ether was dissolved in the particular solutions. A small part of the solutions was kept as reference sample. The rest was added to the mineral powder with a defined liquid/solid ratio. After certain time intervals a part of the slurry was taken and put into a centrifuge. Using a Heraeus BioFuge the slurries were centrifuged at 19,000 g for 30 minutes to divide the fluid from the solid phase. The reference CE-solution was also centrifuged for comparison. All solutions were passed through a $5\mu\text{m}$ -filter to remove micro-particles. The pore water and the original CE-solution were then analysed by SEC. The

CE-concentration in the pore water decreased by the amount of adsorbed CE. All experiments were made at room temperature.

The determination of the CE-adsorption shall be demonstrated with the following example: 0.5 mass.-% of HEC 1.1 was dissolved in $\text{Ca}(\text{OH})_2$ -saturated solution (formulation F27, tab. 5.1, p 45). A part of this solution was taken as reference sample A058 before the fluid was mixed with solid $\text{Ca}(\text{OH})_2$ (portlandite) for comparison. 20 g of the solution was then mixed with 10 g portlandite (w/s = 2.0, formulation F28). After one hour the slurry and the control sample were centrifuged for 30 minutes. The centrifugation separated solid and fluid phases in the slurry. The control sample A058 was only centrifuged to let it undergo the same treatment as the other sample. No gravity separation of CE from the liquid was found in the control sample. Both samples were passed through a 5μ -filter and analysed with SEC. The detection signals over the time are plotted in figure 3.01.

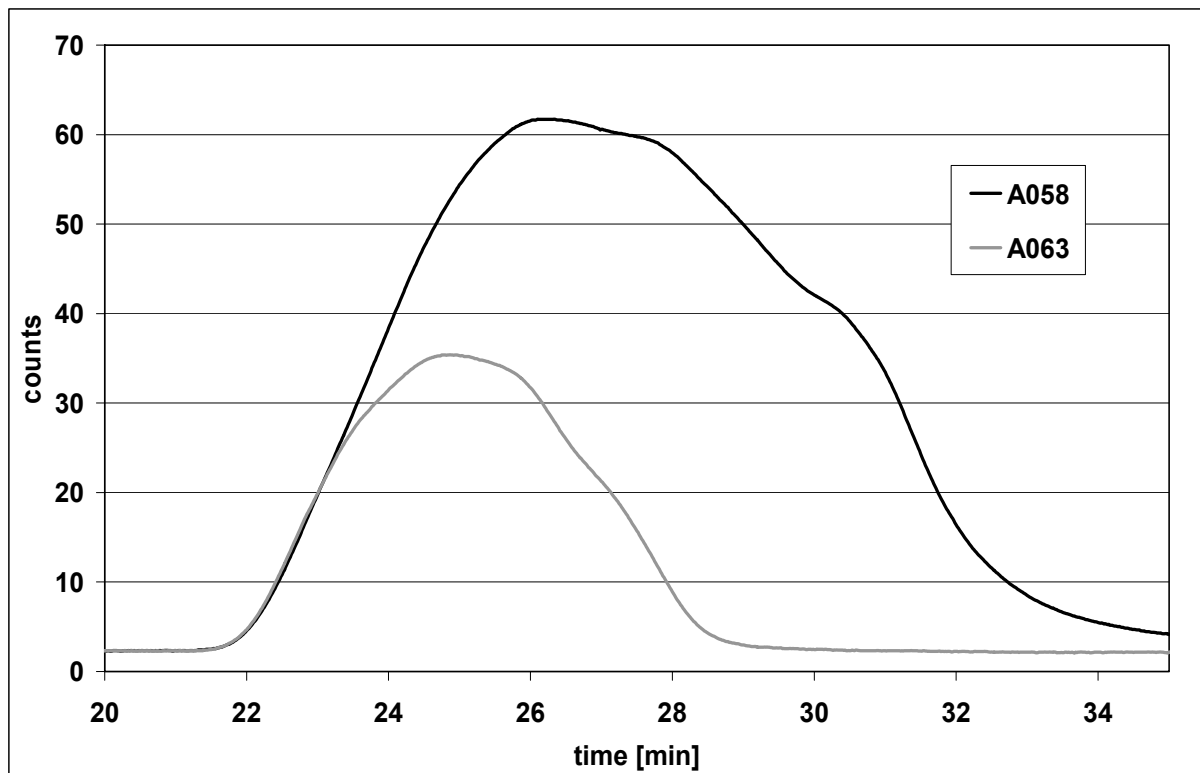


Fig. 3.01: Elution curve of HEC 1.1 in eluent solution determined by SEC. The molecular weight is reciprocal to the elution time. The total amount of CE in the solution is linear related to the integral beneath the elution curve. Analysis A058 was done on the primary solution that had no contact to solids. Analysis A063 was done on the residual solution after contact to solid portlandite for 1 h. The difference between both distribution curves is interpreted as the loss of HEC 1.1 in solution caused by CE-adsorption on the surfaces of the portlandite particles.

The integration of the distribution curve of A058 returned a value of 24 985 012 counts in total. This value corresponded with a CE-concentration of 0.5 mass-% in aqueous solution since that had been the original addition rate. The distribution curve of the residual solution A063 extracted from the portlandite slurry showed an integrated value of 8 287 581 counts in total. Since the detector signal is a linear function of the polymer concentration the residual CE-content of the pore solution of sample A063 was:

$$[\text{CE}] = 0.5 \text{ mass-\%} \times 8\,287\,581 / 24\,985\,012 = 0.166 \text{ mass-\%}$$

That means that approx. 67 % of the initial amount of CE was adsorbed on portlandite. 20 g of a 0.5%-solution of HEC 1.1 were added to 10 g of portlandite, i.e. 0.01 g HEC 1.1 per 1 g portlandite. 67 mass-% of HEC 1.1 was adsorbed, that equals 0.0067 g HEC 1.1 on 1 g portlandite. The specific surface area of portlandite was determined prior to adsorption experiments by BET with 14.9 m²/g. The amount of HEC adsorbed per square meter of portlandite surface is:

$$0.0067 \text{ g} / (1 \text{ g} \times 14.9 \text{ m}^2/\text{g}) = 450 \text{ }\mu\text{g}/\text{m}^2$$

Results will be presented in detail in chapter 5.1. Due to technical problems the detector was not calibrated. Therefore the signal-time curve could not be correlated with a certain molecular weight distribution in absolute figures. Nonetheless a comparison between two different distribution curves was possible.

3.9 Powder Diffraction

Standard laboratory and synchrotron X-ray powder diffraction was used to determine the phase composition of mineral mixtures and to monitor the phase development in hydration processes. The monitoring of phase development was supplemented by neutron powder diffraction. Each method needed its own sample treatment. Except for the latest synchrotron experiments which will be described later all formulations were mixed as described in chapter 3.1.

3.9.1 Laboratory X-Ray Powder Diffraction

Due to its long measuring time (approx. 45 min.) the standard X-ray diffractometry was not suitable for in-situ measurements. Therefore the hydration process of the samples stored in controlled climate (23 °C, 50% rel. humidity) had to be stopped before measurements. For this purpose small portions of the sample, prepared as described in chapter 3.1, were taken after certain time intervals and were triturated in acetone. Thereafter the portion was washed

in acetone and vacuum filtered. The acetone removed the water and the hydration processes stopped. The filter residual dried rapidly in the applied vacuum. Triturating, washing and filtering took five minutes per sample. Before the sample was measured it was triturated a second time to produce a fine powder. The X-ray measurements were done with a Panalytical (former Philips) X'pert PW3040 diffractometer at the Institute of Mineralogy of the University of Muenster. This diffractometer uses Cu-K α radiation ($\lambda = 1.54184 \text{ \AA}$) and has a powder diffractometer geometry as described by Azaroff^[Aza1]. The peak-intensities were calculated using the X'pert software. Standard laboratory X-ray diffractometry was performed on OPC with various CE-types only.

3.9.2 Synchrotron X-Ray Powder Diffraction

In-situ XRD-measurements were performed at the Material Science Beamline^[Pat1] of the Swiss Light Source (SLS) at the Paul Scherrer Institute in Villigen/CH for phase-resolved monitoring of the hydration process. The X-radiation of a synchrotron is produced by accelerated high-energy electrons. At the SLS those electrons are produced in the following way: An electron gun emits an electron beam into a linear accelerator (Linac) where the electrons are accelerated up to an energy of 100 MeV. Then they are injected into the booster synchrotron (accelerator ring) where their energy is increased up to a final level of 2.5 GeV. From there the electrons are injected into the storage ring where they circulate at nearly the speed of light.

Although the electrons circulate in high vacuum ($< 10^{-13}$ bar) there is a final probability to collide with atoms of the residual gas. In a conventional synchrotron this electron loss results in a half-life period of the beam of approx. 10 hours. At least once a day the ring has to be refilled. The variation of the electron beam intensity results in changing intensities of the electromagnetic radiation generated at the beamlines. As a consequence the thermal load of the optical components of the beamlines varies, too. To keep a well focused and monochrome beam those optical components has to be readjusted frequently. This problem has been solved for the SLS by the "top-up injection" where all few minutes the electron beam loss is compensated without stopping running experiments. Thus the electron flow is nearly constant and the half-life time has no effects on the experiments.

The electrons are forced into a circular path. Accelerated or retarded (negative acceleration) particles radiate. In case of a circular motion the acceleration is perpendicular to the path. Charged particles that move nearly at light velocity radiate into a narrow cone tangential to the particle's path^[Ger1]. The wavelength (energy) spectrum of the radiation

depends on the velocity of the electrons and the radius of curvature. The radiation intensity depends on the electron current. Electrons can also be forced to move on sinus-shaped tracks by insertion devices (wigglers). They consist of a parallel stacking of small magnets (typically a few mm to cm wide) oriented radially and with alternating magnetization. Depending on the radius of curvature, radiation of any wavelength can be generated.

The Material Science Beamline set-up is described by Gozzo, Schmitt et al. ^[Goz1]. The minigap wiggler of this end station is designed to deliver highly intense hard X-rays with energies from 5 to 40 keV. Behind focusing X-ray optics, a two-crystal monochromator and a set of filters, three different experimental stations are placed in line but only one can be used per session. The diffractometer in second position (fig. A.03, appendix A.1) is equipped with a high-resolution multi-crystal analyser detector and for time-resolved measurements with a multistrip detector (Mythen detector, fig. A.04, appendix A.1). The multistrip detector was designed by B. Schmitt ^[Goz1] and consists of 12 modules, each with 1280 channels (> 15.000 channels in total) covering an angle range of 60°. Between the modules are small blind gaps. The channels are distributed equidistantly on the modules but the gaps may vary in size from module to module. The accurate angle position of each module was measured by moving the modules into the primary X-ray beam with strongly reduced intensity at diffractometer position zero. The zero position was indicated by the intensity maximum of the primary beam. Turning the detector back into its destined position the turning angle was measured at the high precision motor that turned the detector.

The primary X-ray beam was focused as a strip focus into the centre of the diffractometer circle where the sample carrier was mounted. The strip focus had a width of 1.2 mm (slightly broader than the glass capillary diameter $d_S = 1\text{mm}$) and a length parallel to the capillary of $l_F = 10\text{ mm}$. The observed sample volume was $V_S = \pi (d_S / 2)^2 l_F = 7.85\text{ mm}^2$. The correct position of the focus was checked by an X-ray camera in diffractometer angle position zero. The camera produced an image of the primary X-ray beam after passing through the sample. Camera and reduction filters were removed and a primary beam stopper was inserted behind the sample before the experiments started.

The analytical equipment is located in a hut which walls limit a restricted safety area. No person is allowed to stay in the restricted area during experiments. After mounting the sample this restricted area must be checked for persons left in the hut. The safety status must then be stated in an electronic safety system before the shutter of the primary beam can be released. This procedure takes about 30 seconds for experienced personal. This has to be taken into account in time-sensitive experiments.

The samples were freshly mixed at the beamline in the same way as described in chapter 3.1. Directly after stirring the wet paste was sucked into a glass capillary with a diameter of 1 mm and a wall thickness of 0.01 mm. The capillary was sealed at both ends with wax to prevent drying during measurements. The capillary was mounted (glued) into a brass cylinder which itself was mounted and centred on the goniometerhead of the powder diffractometer. With a little experience mixing, filling, mounting and centration took 60 seconds. Another 30 seconds were used to mount the goniometerhead into the diffractometer, to save and lock the restricted beamline area and to start the measurements.

In the latest experiments at the SLS efforts were made to shorten the initial dead time (time between water contact and first data received) from 90 sec. down to zero. Therefore dry cement or pure phase admixtures were filled into the capillary up to the cone-shaped widening near the open end. Efforts had to be taken that the package of the particles in the capillary is dense enough so that no compression by later water pressure occurred. This would have moved the sample partly out of the beam area during the measurements. The upper-most part of the capillary was filled with coarse silica sand. By partly melting the glass, the capillary shrank thermally onto the sand grains and fixed them (fig. A.02, appendix A.1). Care had to be taken that the capillary was not completely sealed by welding. Before the capillary was mounted into a brass sample carrier equipped with a water-inlet, the bottom of the capillary had been broken open.

Next the brass piece with the capillary was mounted and centred on the goniometerhead before water contact. The water-inlet of the brass piece was connected by a flexible rubber hose to a medical syringe filled with fluid. The syringe was mounted onto a remote controlled step drive that pushed the piston of the syringe. After mounting the whole assembly to the diffractometer (fig. A.05, appendix A.1) and locking the restricted area the measurements were started prior to water injection. Water was injected until drops appeared at the open end of the capillary. The air that had filled the voids between particles was pressed through the sand package during water injection while the mineral powder was stopped by the sand. The sample was observed during the full experiments by the means of a standard video camera and monitor system. During the measurements the capillary stayed in contact with the water reservoir in the syringe. The goniometerhead usually spins around an axis through the centre of the glass capillary for better statistics and to counterbalance texture effects. This rotation had to be replaced by oscillation of approx. 120° to prevent the rubber hose to wrap around the glass capillary.

Water injection experiments were done on OPC and a pure phase mixture of 70 mass-% C_3A , 15 mass-% $C\bar{3}H_{0.5}$, and 15 mass-% $C\bar{3}$. In these experiments it was impossible to dry-blend the mineral powder with CE homogenously. Due to the small sample size of approx. 8 mm^3 a homogenous mixture with only a few solid CE particles (0.5 mass-% on mineral phase admixture) could not be prepared. It was tried to dissolve the CE prior to experiments in the water to be injected. But the injection device did not resist the high pressure necessary to pump the viscous CE-solution through the cement-filled capillary. Instead experiments were performed using tap water respectively $Ca(OH)_2$ -saturated solution in order to investigate early hydration processes in dependence of pH-level and Ca^{2+} -ion concentration in the pore water.

All experiments were done with radiation energy of 11.9 keV resulting in a wavelength of 0.104014 nm (1.04014 Å). Rietveld analyses ^[Rie1, You1] were made for the XRD data. For that the Siroquant Quantitative XRD Software by Sietronics ^[Sie1] was used. The software includes a data set of cement phases. All calculations were done on the basis of the data sets of the following phases: cubic C_3A , monoclinic C_3S polymorph M1, β - C_2S , C_4AF , ettringite, gypsum and portlandite. Due to the complexity of the phase compositions observed no efforts have been made to determine the amount of X-ray amorphous phases. An inner standard was not added to the sample because it could not be excluded that either important peaks of the cement phases would be overlain by those of the standard or that the standard interacts with the cement or with the cellulose ether. Fundamentals on Rietveld analysis are given by Taylor ^[Tay2].

3.9.3 Thermal Neutron Powder Diffraction

Samples were mixed and stirred at the beamline in the same way as described in chapter 3.1. But instead of water, di-deuterium monoxide (D_2O , heavy water) was used. After stirring, the paste was filled into an aluminium cylinder with open ends. Two open ends made it easier to fill the cylinder with the viscous paste. The size of the cylinder is 7 cm in length, 1 cm for the inner diameter and 0.1 mm thickness of the Al-wall. One end was equipped with an enforced bottom and an inner thread in which a double-sided screw could be mounted to close this end and to connect the cylinder to the sample carrier of the diffractometer (fig. A.06, appendix A.1). The other end was sealed by a cadmium-lid to prevent drying. During the measurement the bottom of the cylinder together with the mounting screw was wrapped in a cadmium panel to avoid disturbing reflections from the screw. Cadmium is not transparent for thermal neutrons.

The measurements were done at the HRPT beamline of the SINQ neutron source at the Paul Scherrer Institute. The diffractometer has the same geometry as the one of the SLS but with larger diffractometer circle (fig. A.07, appendix A.1). The HRPT-diffractometer is equipped with a multi-channel detector covering 160° with 1200 channels. Between sample and detector radial-oriented Soller slits focus the diffracted signal perpendicular onto the detector to increase the spatial resolution.

The fundamentals of diffraction methods shall not be repeated here since X-ray diffraction is a standard method of mineralogy. Details are given by Azaroff^[Aza1]. But it should be mentioned that neutron diffraction also follows the Bragg's Law^[Bra1]:

$$n \lambda = 2 d \sin \Theta$$

Electromagnetic waves are scattered by the electron shells of atoms and the denser the distribution of heavy atoms in the crystal lattice, the higher the intensity of a diffracted signal. In contrast to electromagnetic radiation, particle waves like neutron radiation are scattered by atom cores. The closer the atom weight to the weight of the radiation particle, the better the impulse transmission. Therefore neutron waves are best scattered by hydrogen since the weight of a single proton is very close to that of a neutron. To reduce background radiation in the diffraction spectra from the pore solution, heavy water was used. It is assumed that the hydration products of cement phases incorporating D₂O are chemically and physically comparable to those hydrated in H₂O. The peak positions in a neutron diffractometer spectrum are the same as in that of X-ray diffraction based on the lattice spacing *d*. But the relative peak intensities differs significantly.

At the SINQ neutron source at the PSI first protons are accelerated in a cyclotron. A part of the protons are shot onto a lead target. The proton bombardment releases neutrons from the Pb-atom cores. The neutrons leave the atomic formation with high speed. The neutron beams are used for high and low speed radiation. For low speed (thermal) the neutrons are retarded by passing a tank with D₂O. These thermal neutrons are used for neutron powder diffractometry. The generated neutron radiation has a wavelength of $\lambda = 1.8857 \text{ \AA}$.

The experimental work at the HRPT beamline was assisted by M. Zwanzig (Hercules Inc.) who at that time was involved in studies at the Heinrich-Hertz-Berufskolleg, a vocational school in Duesseldorf. He and his colleagues from the school took use of the experimental work for an apprenticeship project. A report was written for the Heinrich-Hertz-Berufskolleg [Zwa1].

3.10 Environmental Scanning Electron Microscopy - Field Emission Gun (ESEM-FEG)

At the VDZ Duesseldorf (German Institute of Cement Research) cement pastes with and without CE were investigated in-situ with respect to their hydration behaviour using ESEM in combination with a field emission gun (FEG). The VDZ is equipped with a Philips ESEM XL30 FEG. In contrast to an ordinary scanning electron microscope the ESEM-FEG does not require high vacuum. It was possible to investigate the wet system in-situ since the low-pressure atmosphere is saturated with humidity. During the measurements the samples were exposed to environmental conditions of 5 °C and 4 Torr. Moreover, it was not necessary to sputter the sample for conductivity. So it was possible to observe the surface of the material directly without disturbing coating layer. The cement pastes were prepared as described in chapter 3.1. The images were recorded by K. Lipus, VDZ.

4. Material Characterization

4.1 Defined Portland Cement

The Portland clinker used in this project was ordered from HeidelbergCement AG as a defined clinker produced on a laboratory scale. An X-ray fluorescence analysis (XRF) of this cement is given in table 4.1. The phase composition of the milled and sulphate-blended cement was determined by XRD and Rietveld analysis. One analysis was done at the X-Ray Laboratory Dr. Ermrich, a second analysis was performed by the author based on the synchrotron XRD data (table 4.2). In comparison both analysis showed a fairly good correlation. A significant difference showed up in the silicate contents. Laboratory XRD was done at a wavelength of $\lambda = 1.54184 \text{ \AA}$. The synchrotron radiation had a wavelength of $\lambda = 1.04014 \text{ \AA}$. The higher energy led to a deteriorated spatial resolution of the synchrotron XRD pattern because the diffraction angle decreases with increasing radiation energy as described by Bragg's law. Since most reflections of C_3S and C_2S superimpose each other, the Rietveld analysis software had more difficulties to distinguish between those two phases. The sum of C_3S and C_2S was in both analyses comparable. The software package was for both analyses the same (Sietronics Siroquant 2.5). The difficulty to distinguish the calcium silicates at high radiation energy is also discussed in chapter 5.2.4.

The clinker granules were milled together with 1.5 masspercent of calcium sulphate hemi-hydrate, a stucco from Boergardts, and 1.5 masspercent α -anhydrite III from Sigma-Aldrich (table 4.4). The milling grade should correspond to 4000 cm^2/g Blaine. The particle size distribution (PSD) determined by W. Hildebrandt is given in figure 4.01. The S_V -value calculated on PSD was $1.5 \text{ m}^2/\text{cm}^3$ and the pure density determined by He-pycnometry was $3.21 \text{ g}/\text{cm}^3$ resulting in the geometric surface area of $0.465 \text{ m}^2/\text{g}$ ($= 4650 \text{ cm}^2/\text{g}$) which roughly correlates with the Blaine value. BET delivered a specific surface area of $1.56 \text{ m}^2/\text{g}$. The ratio of geometric and BET-surface of 3.35 was rather small and comes from the aberration of the real grain shape from the ideal sphere. It indicates that the surfaces of the cement particles are rather smooth and that pores in micro- or nano-scale were not to be expected. That means that the difference between the surface area determined by BET (accessible for N_2) and the surface area accessible for water and CE-molecules, is negligibly small. According to its composition and quality the cement was classified as CEM I 42.5 ordinary Portland cement. The Ca-sulphate hemi-hydrate from Boergardts was a plaster of Paris with industrial quality. Its composition was determined by differential thermogravimetry (DTG) by W. Hildebrandt (tab. 4.3).

Oxide component	content [mass-%]	Oxide component	content [mass-%]
SiO ₂	20.70	MgO	1.02
Al ₂ O ₃	5.36	K ₂ O	0.44
TiO ₂	0.25	Na ₂ O	0.05
MnO	0.10	SO ₃	0.16
Fe ₂ O ₃	3.28	loss on ignition	0.09
CaO	68.2	sum	99.92

Table 4.1: Chemical composition of Portland clinker, XRF by HeidelbergCement AG.

Phase	Laboratory XRD [mass-%]	Synchrotron XRD [mass-%]
C ₃ S	69.1	75.3
C ₂ S	11.2	7.9
C ₂ (A,F)	10.5	10.2
C ₃ A	5.4	4.1
M	0.9	0.0
C $\bar{5}$	1.6	1.7
C $\bar{5}$ H _{0.5}	1.3	1.3
sum	100.0	100.6

Table 4.2: Phase composition of Portland cement from HeidelbergCement AG. The laboratory XRD analysis was done by X-Ray Laboratory Dr. Ermrich. The Synchrotron XRD analysis was performed by the author. The sulphate content was known since the addition level was well-defined. The sulphates were not found in synchrotron XRD patterns.

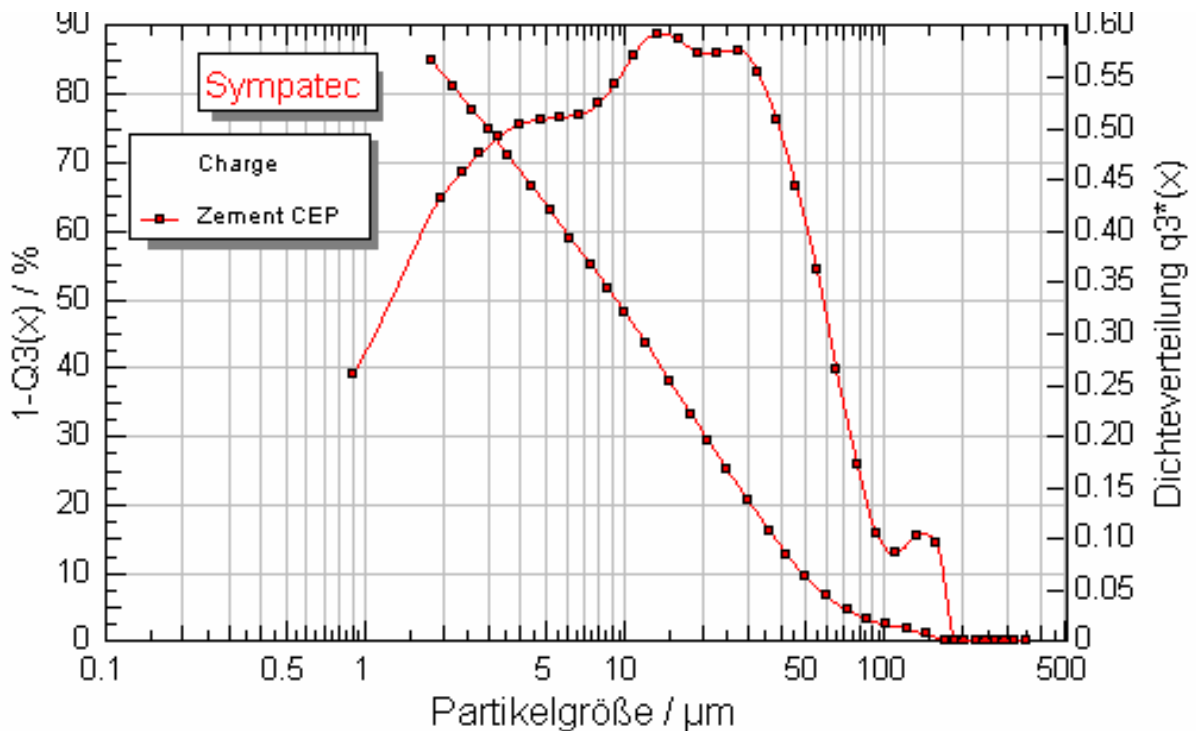


Fig. 4.01: Particle size distribution of Portland cement. The mass distribution (2nd y-axis, right side) is plotted versus the grain size in μm (x-axis). The other curve plots the sieve residual in mass percent (1st y-axis, left side). Laser granulometry by W. Hildebrandt, Hercules Inc.

Phase	Content [mass-%]	Phase	Content [mass-%]
CaSO ₄ ·2H ₂ O	0.8	CaCO ₃	0.8
CaSO ₄ ·½H ₂ O	88.3	SiO ₂	0.0
CaSO ₄	10.1	sum	100.0

Table 4.3: Phase composition of Boergardts stucco. DTG analyses by W. Hildebrandt, Hercules Inc.

Material / Phase	Supplier	Catalogue No.
aluminium sulphate 16-hydrate	Fluka	06421
aluminium hydroxide	BK Giulini Chemie	
tri-calcium aluminat	RWTH Aachen	
calcium hydroxide	Riedel-de Haen	12038
calcium oxide	Sigma-Aldrich	24,856-8
tri-calcium silicate	RWTH Aachen	
calcium sulphate, anhydrite	Sigma-Aldrich	23,731-2
calcium sulphate hemi-hydrate	Riedel-de Haen	12090
alabaster stucco, mainly calcium sulphate hemi-hydrate	Boergardts	

Table 4.4: Sources of mineral phases

4.2 Pure Mineral Phases

Most pure phases used in this investigation were purchased from commercial providers. C₃A and monoclinic C₃S were purchased from the Rheinisch-Westfaelische Technische Hochschule (RWTH) Aachen. They were milled down to a Blaine value of 3000 cm²/g. Calcium sulphate hemi-hydrate and portlandite for adsorption experiments came from Riedel-de Haen. The calcium oxide for the ettringite synthesis and anhydrite to be added to OPC were purchased from Sigma-Aldrich. The aluminium sulphate 16-hydrate for ettringite synthesis came from Fluka (table 4.4). Aluminium hydroxide Al(OH)₃ as additive in Portland cement for laboratory x-ray studies was purchased from BK Giulini Chemie (brand name: Gecedral BZ 111, charge no. 99-65-25). The specific surface area of the gypsum was too low for CE-adsorption experiments (0.2 m²/g) and was therefore triturated until the BET surface was increased up to 1.7 m²/g. The specific surface area and the pure density of some phases were determined and are given in table 4.5. Ettringite was synthesized as described in chapter 3.2. Its purity was confirmed by laboratory XRD at the University of Muenster. This measurement was done by A. Breit. The refraction pattern as shown in figure 4.02 does not show any other peaks than those of ettringite.

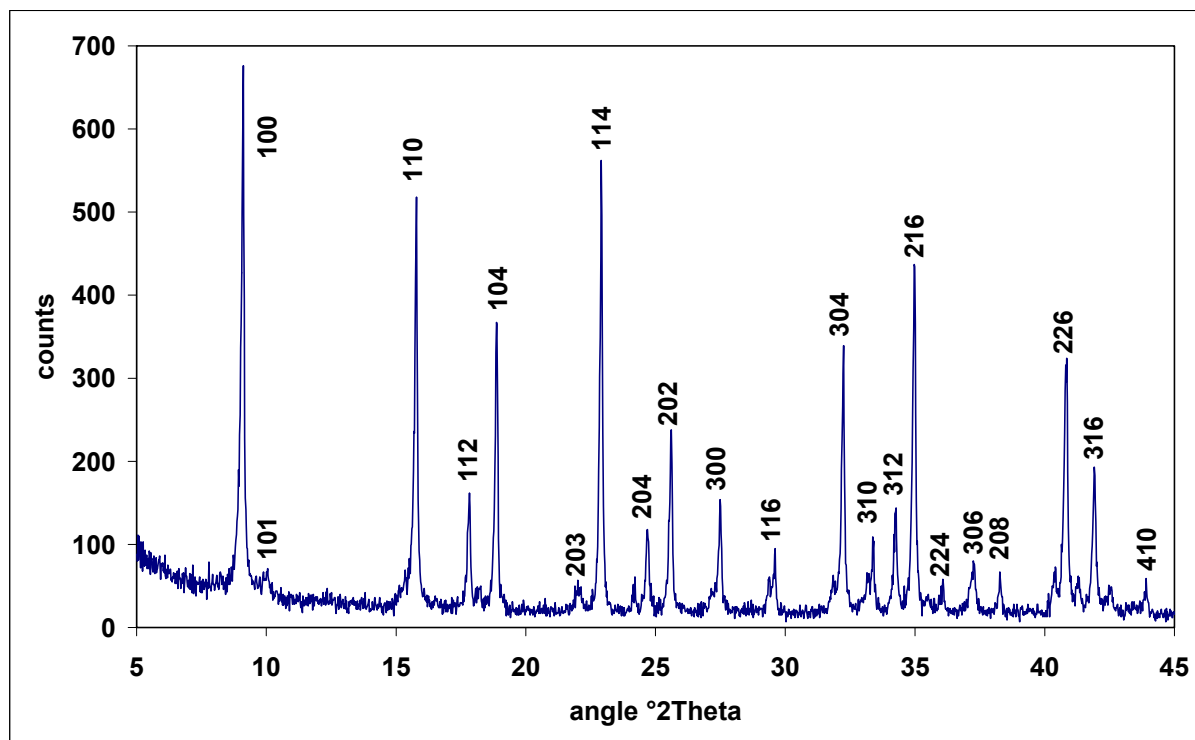


Fig. 4.02: XRD pattern of ettringite using CuK α radiation. All peaks, even those not indicated here, could be ascribed to ettringite. Analysis by A. Breit, University of Muenster.

Material / Phase	OPC	C ₃ A	C ₃ S	CH	AFt	C \bar{s} H ₂	C \bar{s} H ₂ triturated
BET [m²/g]	1.56	0.42	0.54	14.9	6.51	0.21	1.72
Blaine [mm²/g]	4000	3000	3000	n.d.	n.d.	n.d.	n.d.
Pure Density ρ [g/cm³]	3.21	3.02	3.14	n.d.	n.d.	n.d.	n.d.

Table 4.5: Specific surface area and pure densities of OPC and pure phases.

4.3 Cellulose Ethers

All cellulose ethers used in this project are CE-types from Hercules Inc. Two different types of MHPC has been used with DS-values of 1.9 and 1.7, two different types of MHEC with DS-values of 1.7 and 1.5, and two HEC-types with DS-values of 2.0 and 1.1. The milling grades are defined as granulate for the HECs, as powder for the MHPCs and as fine powder for the MHECs. The CE-types have been chosen in a way that the viscosities of 2%-aqueous solutions lie within a range from 15,000 and 25,000 mPas, measured with a Brookfield RV rheometer at 20 °C and 20 rpm. The selection has been made for viscosities as close together as possible. The typical molecule diameters in aqueous solution of those types are between 75 nm (15,000 mPas) and 100 nm (25,000 mPas). The cold water-soluble MHPC and MHEC are common types in construction applications. The hot and cold water-soluble HEC is not a pronounced construction material type but may substitute a part of MHEC or MHPC in some

formulations. Detailed information on those CE-types such as substitution analysis and the accurate trade name must not be disclosed on demand of Hercules Inc. In the following the CE-types are named as follows: MHPC 1.9, MHPC 1.7, MHEC 1.7, MHEC 1.5, HEC 2.0 and HEC 1.1. The numbers return the DS-values of those CE-types.

4.4 Cement and Pure Phase Admixtures

Standard cement wet paste formulation

As far as possible the compositions of wet pastes have been kept constant. In most cases 0.5 mass-% of cellulose ether was dry mixed with ordinary Portland cement or mineral pure phase mixtures before adding water. The reference samples did not contain CE. The water/solid ratio was 0.5. These standard wet paste formulations were used for ultrasonic measurements, heat calorimetry (partly), XRD (lab and synchrotron) and neutron diffraction (D_2O instead of H_2O). If not described otherwise untreated tap water was used. The wet pastes were prepared as described in chapter 3.1.

Heat flux calorimetry

Beside the standard cement wet paste, pure C_3S and a mixture of 70 mass-% C_3A , 15 mass-% bassanite and 15 mass-% anhydrite were used. The CE addition level on dry powder was 0.5 mass-%. The water/solid ratio for the C_3S could be kept comparable to OPC ($w/s = 0.5$). The aluminate/sulphate mixture had a higher water demand of $w/s = 0.8$.

Adsorption experiments

The formulations for that method had the broadest variety. This was necessary because the liquid/CE/mineral phase ratios had to be adjusted to the specific surface area of the investigated mineral phase. A list of those formulations is given in table 5.1. The reference samples for these tests were CE-solutions that had no contact to mineral phases.

Form. No.	Mineral sample	Exp. condition	Solution	w/s	CE	CE in solution [mass-%]	CE on solid [mass-%]
F21	none	reference	tap water		HEC 1.1	0.133	
F22	OPC	dynamic	tap water	0.5	HEC 1.1	0.133	0.067
F23	C ₃ S	dynamic	tap water	0.5	HEC 1.1	0.133	0.067
F24	C ₃ A	dynamic	tap water	0.5	HEC 1.1	0.133	0.067
F25	C ₃ A+C \bar{S} +C \bar{S} H _{0.5}	dynamic	tap water	0.5	HEC 1.1	0.133	0.067
F26	CH	dynamic	tap water	0.5	HEC 1.1	0.133	0.067
F27	none	reference	CH-sat.		HEC 1.1	0.5	
F28	CH	stable	CH-sat.	2	HEC 1.1	0.5	1
F29	CH	stable	CH-sat.	3	HEC 1.1	0.5	1.5
F30	CH	stable	CH-sat.	4	HEC 1.1	0.5	2
F31	none	reference	CH-sat.		MHPC 1.9	0.5	
F32	CH	stable	CH-sat.	2	MHPC 1.9	0.5	1
F33	CH	stable	CH-sat.	3	MHPC 1.9	0.5	1.5
F34	CH	stable	CH-sat.	4	MHPC 1.9	0.5	2
F35	none	reference	CH-sat.		MHPC 1.7	0.5	
F36	CH	stable	CH-sat.	2	MHPC 1.7	0.5	1
F37	CH	stable	CH-sat.	3	MHPC 1.7	0.5	1.5
F38	CH	stable	CH-sat.	4	MHPC 1.7	0.5	2
F39	none	reference	CH-sat.		MHEC 1.7		
F40	none	reference	CH-sat.		MHEC 1.5		
F41	CH	stable	CH-sat.	2	MHEC 1.7	0.5	1
F42	CH	stable	CH-sat.	2	MHEC 1.5	0.5	1
F43	none	reference	CH+C \bar{S} H ₂ -sat.		MHPC 1.9	0.2	
F44	none	reference	CH+C \bar{S} H ₂ -sat.		MHPC 1.7	0.2	
F45	none	reference	CH+C \bar{S} H ₂ -sat.		MHEC 1.7	0.2	
F46	none	reference	CH+C \bar{S} H ₂ -sat.		MHEC 1.5	0.2	
F47	none	reference	CH+C \bar{S} H ₂ -sat.		HEC 1.1	0.2	
F48	C \bar{S} H ₂	stable	CH+C \bar{S} H ₂ -sat.	1	MHPC 1.9	0.2	0.2
F49	C \bar{S} H ₂	stable	CH+C \bar{S} H ₂ -sat.	1	MHPC 1.7	0.2	0.2
F50	C \bar{S} H ₂	stable	CH+C \bar{S} H ₂ -sat.	1	MHEC 1.7	0.2	0.2
F51	C \bar{S} H ₂	stable	CH+C \bar{S} H ₂ -sat.	1	MHEC 1.5	0.2	0.2
F52	C \bar{S} H ₂	stable	CH+C \bar{S} H ₂ -sat.	1	HEC 1.1	0.2	0.2
F53	none	reference	CH+AFt-sat.		MHPC 1.9	0.2	
F54	none	reference	CH+AFt-sat.		MHPC 1.7	0.2	
F55	none	reference	CH+AFt-sat.		HEC 1.1	0.2	
F56	AFt	stable	CH+AFt-sat.	3	MHPC 1.9	0.2	0.6
F57	AFt	stable	CH+AFt-sat.	3	MHPC 1.7	0.2	0.6
F58	AFt	stable	CH+AFt-sat.	2	HEC 1.1	0.2	0.4
F59	C ₃ S	dynamic	CH-sat.	1	MHPC 1.9	0.2	0.2
F60	C ₃ S	dynamic	CH-sat.	1	MHPC 1.7	0.2	0.2
F61	C ₃ S	dynamic	CH-sat.	1	MHEC 1.7	0.2	0.2
F62	C ₃ S	dynamic	CH-sat.	1	MHEC 1.5	0.2	0.2
F63	C ₃ S	dynamic	CH-sat.	1	HEC 1.1	0.2	0.2

Table 5.1: Formulations for CE-adsorption experiments and SEC analyses.

5. Results

5.1 The Adsorption of Cellulose Ethers on Cement Phases

The adsorption of cellulose ether on crystal faces was measured in two different kinds of experiments:

1. Under stable conditions the hydrated pure phases were in stable equilibrium with the fluid phase. All solutions were $\text{Ca}(\text{OH})_2$ -saturated to increase the pH-value as high as in Portland cement pastes. To avoid dissolution of the solids all solutions were ion-saturated in respect of the investigated phases. Cellulose ethers were predissolved in those ion-saturated solutions. Under the assumption that changes in specific surface areas during the experiments were negligibly small, the amount of adsorbed CE per area was calculated on the basis of BET surface analyses of the pure phases. Since all investigated phases had specific surface areas below $15 \text{ m}^2/\text{g}$ it can be assumed that the grain surfaces were rather smooth and no micropores occurred. Thus the difference between measured surface areas accessible for nitrogen and the surface accessible for CE molecules in aqueous solution is negligibly small.

2. In dynamic experiments active phases reacted with water to form several hydration products. Since the actual specific surface area of the products could not be determined during the experiments, only qualitative and comparative statements were made. The cellulose ethers were predissolved in the water prior to experiments. The formulations used for the adsorption tests are listed in table 5.1.

Formulation F27 (highly alkaline) was analysed after 24 hours and was compared to F21 (neutral) by SEC to check if low-DS cellulose ether (HEC 1.1) is stable in high alkaline environment for this time. No differences between F21 and F27 were found. The higher the DS the higher the resistance of CE against alkaline degradation. Since the low-DS type was stable, the other types were stable, too. This result correlates with those of Pourchez ^[Pou2].

Dynamic experiments did not produce absolute values but they allowed a time-resolved monitoring of CE-adsorption during hydration (fig. 5.01). Exposure times of solids to CE-solution were 1, 4, 8 and 24 hours plus 30 minutes of centrifugation each. The dynamic experiments were done with HEC 1.1 only. The reference formulation for all dynamic experiments was F21. The adsorption of the HEC 1.1 on cement phases during the hydration of OPC (formulation F22) increased with increasing hydration time. The OPC hydration took place as described in chapter 2.5.3. The adsorption performance correlated with results of pure C_3S -hydration (F23), where the pure clinker phase reacted with water to CSH and CH. Since the phase content changed in these experiments no statement can be given on which

phases CE adsorbed. Since OPC and pure C_3S showed similar results and since C_3S was with more than 70 mass-% the main component of OPC, it is assumed that in Portland cement CE adsorbed mainly on C_3S and its hydration products portlandite and CSH. The amount of HEC 1.1 adsorbed in experiments with pure C_3A (F24) in absence of sulphates increased also with the hydration time with exception of the 1-hour value. During these experiments C_3A hydrated to mainly C_4AH_{19} . The adsorption performance of HEC 1.1 changed significantly in formulations where calcium sulphates were added to the C_3A (F25). C_3A reacted with calcium sulphate and water forming ettringite and probably some supernatant sulphate reacted with water to gypsum. The amount of HEC adsorbed in these hydration processes was small in comparison to the processes where no sulphate was involved. For comparison pure portlandite was used in dynamic experiments (F26), too. But it turned out that a CE-amount of 0.067 % on portlandite was too small. Before the portlandite surface was CE-saturated HEC 1.1 was used up.

Pure phase experiments with stable phases (in saturated solutions) allowed to quantify the CE-adsorption based on specific surface area. The exposure time of the solids to the solution was one hour plus 30 minutes of centrifugation. Since in the dynamic experiment series the HEC-amount on portlandite (0.067 mass-%) was too small, a series with varying CE/portlandite ratio from 0.01 to 0.02 (1-2 mass-% on CH) was done to find the ideal composition. It was found that all tested ratios would do. The CE/CH ratio was varied by varying the water ratio (solution/solid) keeping the initial CE-concentration in the primary solution constant. The results showed that the maximum amount of HEC 1.1 that can be adsorbed on portlandite is independent of the amount of supernatant CE in solution. The threshold of CE-adsorption with this specific HEC on portlandite is $440 \pm 30 \mu\text{g}/\text{m}^2$. The results also showed good reproducibility. The experiments using HEC 1.1 and portlandite are listed in table 5.2. Comparable test sequences were performed with MHPC 1.9 (tab. 5.3) and MHPC 1.7 (tab. 5.4). Both MHPCs showed a tendency to increase CE-adsorption slightly with increasing MHPC/CH ratio.

A comparison between the molecular weight distributions in the residual pore water after adsorption showed that the distribution depends on the HEC1.1/CH-ratio (fig. 5.02). The lower the ratio the more is the average molecular weight of HEC 1.1 shifted to higher molecular weights. That means that adsorption started with smaller polymer molecules when the HEC/CH is high. With decreasing HEC/CH ratio the amount of smaller molecules was not sufficient to saturate the portlandite surface with adsorbed CE and larger molecules followed. Smaller molecules might be preferred for adsorption because of their higher mobility in

aqueous solution. The same trends were observed for MHPC 1.9 (fig. 5.03) and MHPC 1.7 (fig 5.04).

The next sequence of experiments was performed to compare the adsorption behaviour of different CE-types on various cement phases. The adsorption of CE on portlandite is independent of the DS within the range of error (fig. 5.05; F27, F28, F31, F32, F35, F36, F39-F42). On gypsum CE adsorbed DS-dependently (F42-F52). The lower the DS the higher the adsorption with exception of MHEC 1.7 (F51) which might be caused by experimental error. Beside this CE-type the trend is significant. Nearly no CE adsorbed on ettringite (F53-F58). Little adsorption was found for MHPC 1.9 (adsorption = $30 \mu\text{g}/\text{m}^2$, F56). The adsorption values for MHPC 1.7 (F57) and HEC 1.1 (F58) were negative. All values were in a range of error of $\pm 30 \mu\text{g}/\text{m}^2$. The conclusion is that no CE adsorbed on ettringite.

A last series of experiments was done with C_3S in $\text{Ca}(\text{OH})_2$ -saturated solution (F43-F47, F59-F63). Since C_3S is not stable in an aqueous environment, the exposure time was reduced down to 15 minutes plus further 30 minutes of centrifugation. On the other hand the presence of cellulose ethers retarded the hydration processes significantly as will be shown later. If the exposure time is kept short no significant amounts of hydration products will be formed and changes in BET-surface will be negligibly small. ESEM-FEG images as given in chapter 5.2.7 indeed gave evidence that not much CH or CSH was formed within 45 minutes. CE adsorption actually took place on the surface of C_3S . In comparison to each other the results showed clearly that the lower the DS the higher the CE-adsorption (fig. 5.05). C_3S probably started to dissolve during the experiments. Thus the specific surface area of C_3S , determined by BET prior to experiments, was rather slightly different from the actual surface accessible for CE during the experiments. Nonetheless it is assumed that differences were small. If the surface area decreased due to dissolution, the quantified amount of CE adsorbed per surface area determined in those tests was slightly smaller than the adsorption capacity of C_3S really was.

Conclusions

- Cellulose ethers, even those with low DS, are stable in high alkaline environment over 24 hours.
- In dynamic hydration processes the amount of CE adsorbed on the surfaces of the solids increases with progressing hydration time.
- Significant amounts of CE are adsorbed during C₃A hydration in absence of sulphates.
- CE-adsorption during C₃A hydration is strongly inhibited in the presence of sulphates.
- CE-adsorption on C₃S is DS-specific: the lower the degree of substitution the stronger the adsorption. C₃S showed the highest CE-adsorption capacity of all investigated phases.
- Significant amounts of CE adsorbs on portlandite DS-independently.
- CE-adsorption on gypsum is also DS-specific: the lower the DS the stronger the adsorption. Significantly less CE adsorbs on gypsum than on C₃S.
- No CE adsorbs on ettringite.
- Within the given molecular weight distribution of the CE in aqueous solution, the molecular weight of the CE adsorbed on portlandite depends on the CE/CH ratio: The smaller the CE/CH ratio the higher the molecular weight of the adsorbed CE molecules.

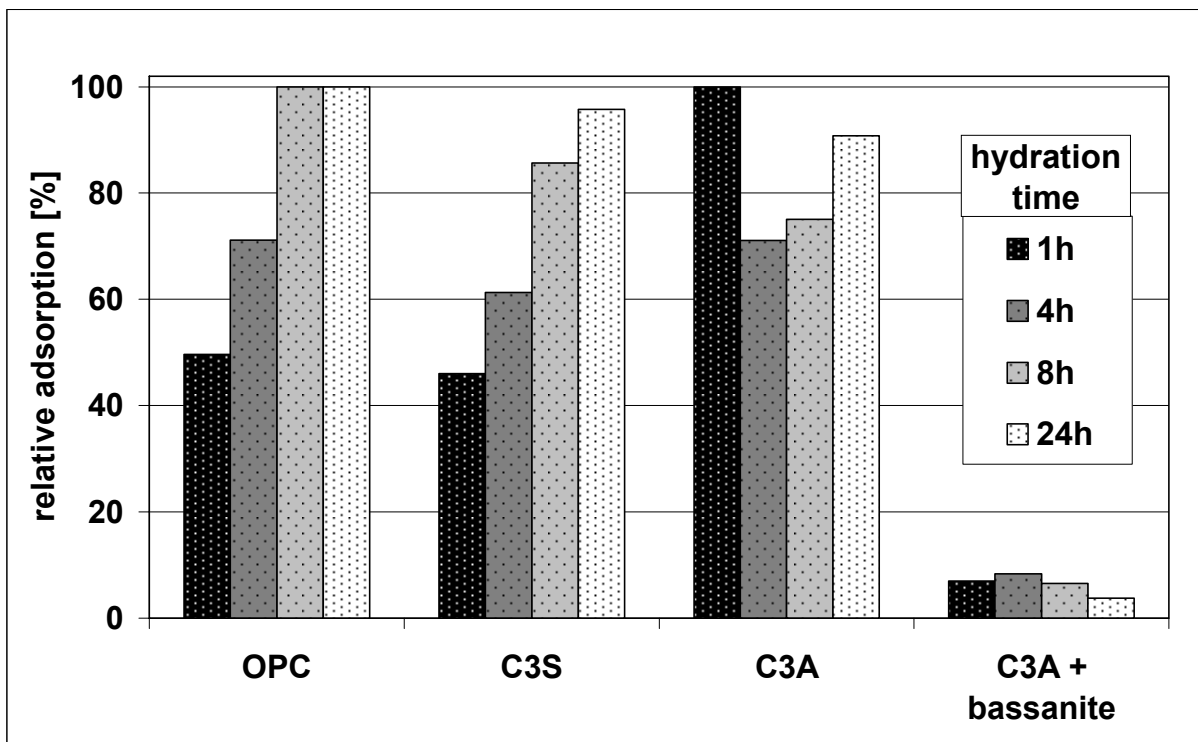


Fig. 5.01: Relative adsorption rates of HEC 1.1 on different cement phases determined in dynamic experiments.

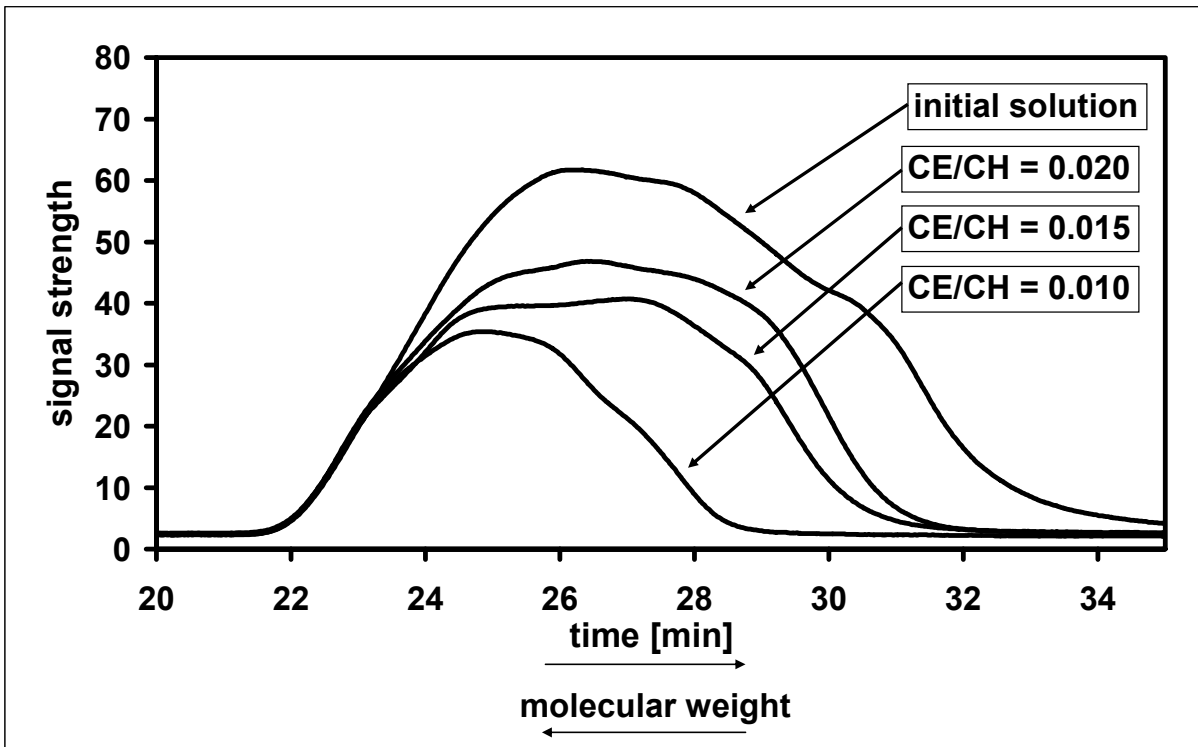


Fig. 5.02: Molecular weight distribution of HEC 1.1 in residual pore water depending on HEC/CH ratio

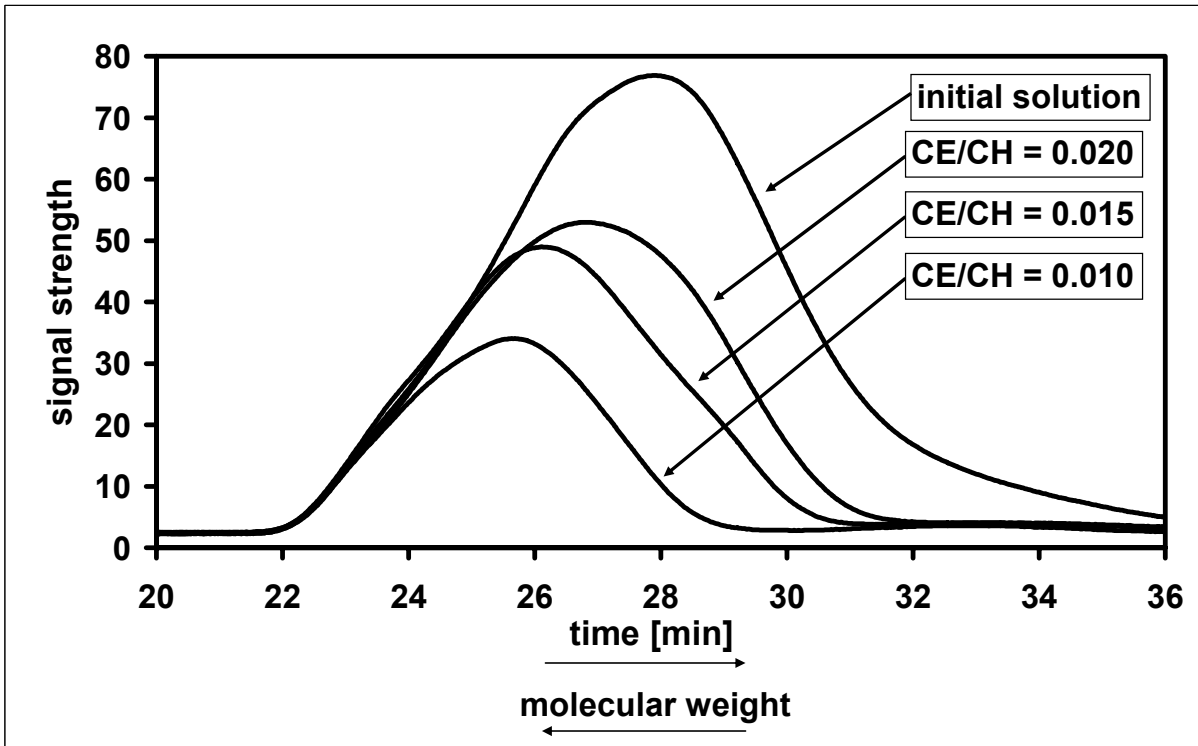


Fig. 5.03: Molecular weight distribution of MHPC 1.9 in residual pore water depending on MHPC/CH ratio.

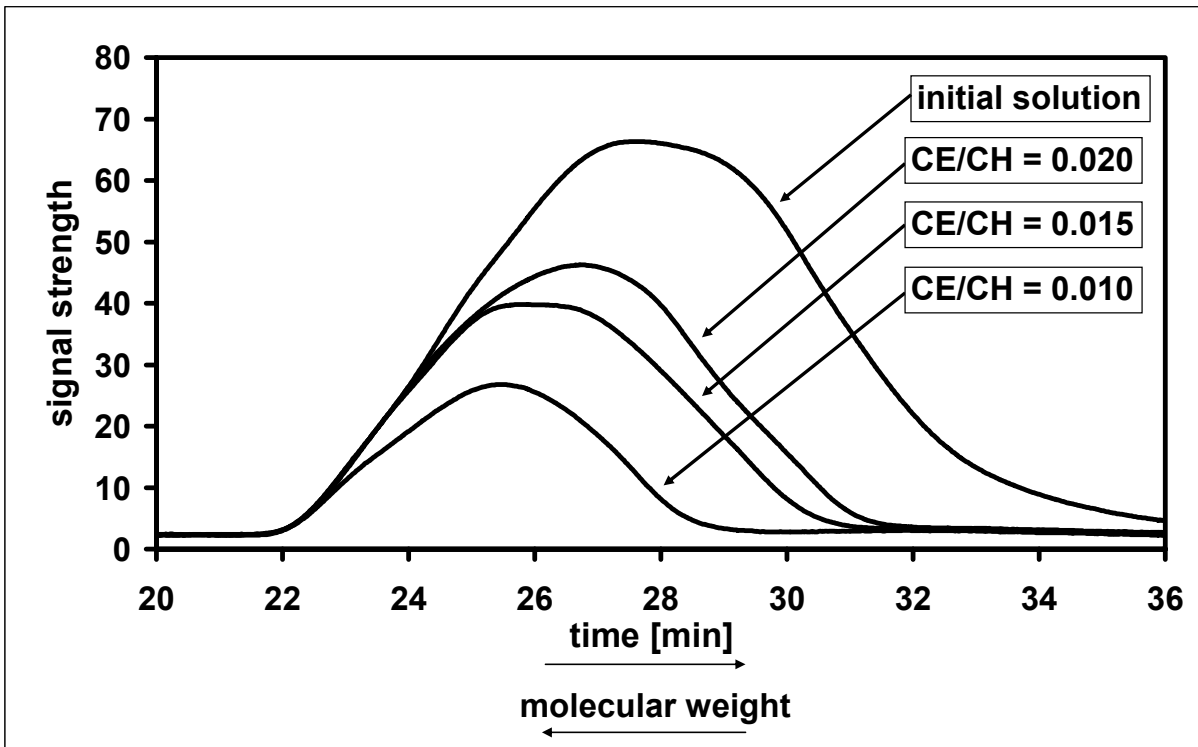


Fig. 5.04: Molecular weight distribution of MHPC 1.7 in residual pore water depending on MHPC/CH ratio.

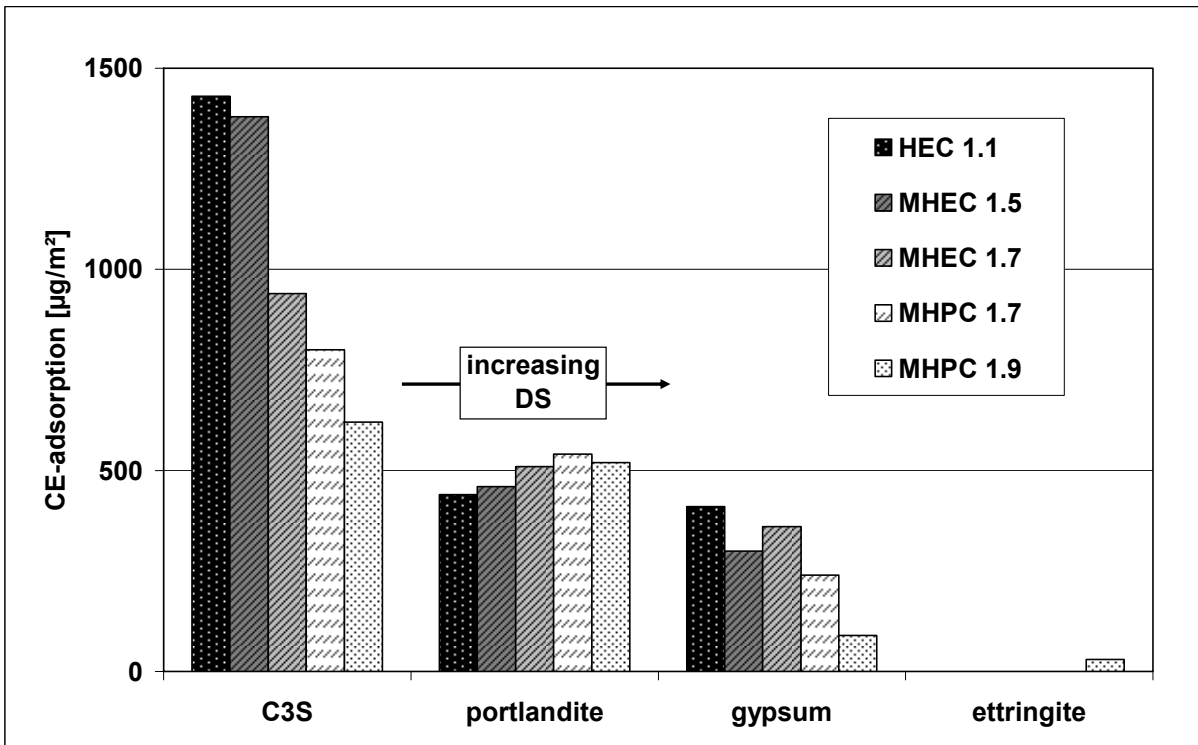


Fig. 5.05: Quantitative determination of CE-adsorption depending on CE-type and substrate.

Formulation No.	water/solid ratio	% HEC 1.1 on portlandite	relative adsorption ¹⁾ [mass-%]	absolute adsorption [$\mu\text{g}/\text{m}^2$]
F-28	2	1	67	450
F-29	3	1,5	45	450
F-30	4	2	33	440
F-28	2	1	70	470
F-29	3	1,5	44	440
F-30	4	2	32	430
F-28	2	1	63	420
F-27	reference		average	440 \pm 30

Table 5.2: Adsorption of HEC 1.1 on portlandite.

Formulation No.	water/solid ratio	% MHPC 1.9 on portlandite	relative adsorption ¹⁾ [mass-%]	absolute adsorption [$\mu\text{g}/\text{m}^2$]
F-32	2	1	72	490
F-33	3	1,5	52	530
F-34	4	2	41	550
F-31	reference		average	520 \pm 30

Table 5.3: Adsorption of MHPC 1.9 on portlandite.

Formulation No.	water/solid ratio	% MHPC 1.7 on portlandite	relative adsorption ¹⁾ [mass-%]	absolute adsorption [$\mu\text{g}/\text{m}^2$]
F-33	2	1	78	520
F-34	3	1,5	56	570
F-35	4	2	47	630
F-32	reference		average	575 \pm 55

Table 5.4: Adsorption of MHPC 1.7 on portlandite.

¹⁾ based on initial CE-concentration

5.2 The Retarding Effect of Cellulose Ethers on Early Portland Cement Hydration

5.2.1 Ultrasonic Measurements

The retarding effect of cellulose ether on the Portland cement hydration is well known in construction material industries since the strength development of the cement is DS-specifically retarded. This can be easily detected by Vicat needle penetration tests but also with ultrasonic measurements. The latter showed clearly that cement setting is DS-specifically retarded by CE. The lower the DS the larger the retarding effect (fig. 5.06). The reference sample without CE (F01) showed the fastest strength development. The acoustic coupling between sender and receiver was disturbed after approx. four hours. After dismantling the experimental set-up, it was found that the hardened sample had fine cracks. Those cracks were caused by cement shrinkage during hydration. The shrinking cement probably built up tension forces to the mould walls which leads to crack formation in the inner sample volume. Furthermore the shrinkage might have caused contact loss to the transmitters. Reproduction tests showed that this problem only occurred in experiments without CE (fig 5.07). The reproducibility was good until crack formation. The loss of acoustic contact was indicated by a sudden decline in the time curves. From this point on the measurement did not deliver reliable results. Cellulose ethers improved the adhesion of cement pastes to the transmitters and also improved cohesion within the cement paste. No cracks occurred within 24 hours and the acoustic coupling between sender and receiver was good over all the time. Experiences in product development shows that cellulose ether increases cement shrinkage. Nevertheless crack formation is reduced due to improved cohesion within the cement. The reproducibility of the tests with CE-blended samples was very good.

Conclusions

- The strength development of Portland cement is DS-specifically retarded by CE: the lower the degree of substitution the stronger the retardation.
- Crack formation within the hardening cement is effectively reduced by the presence of cellulose ethers.

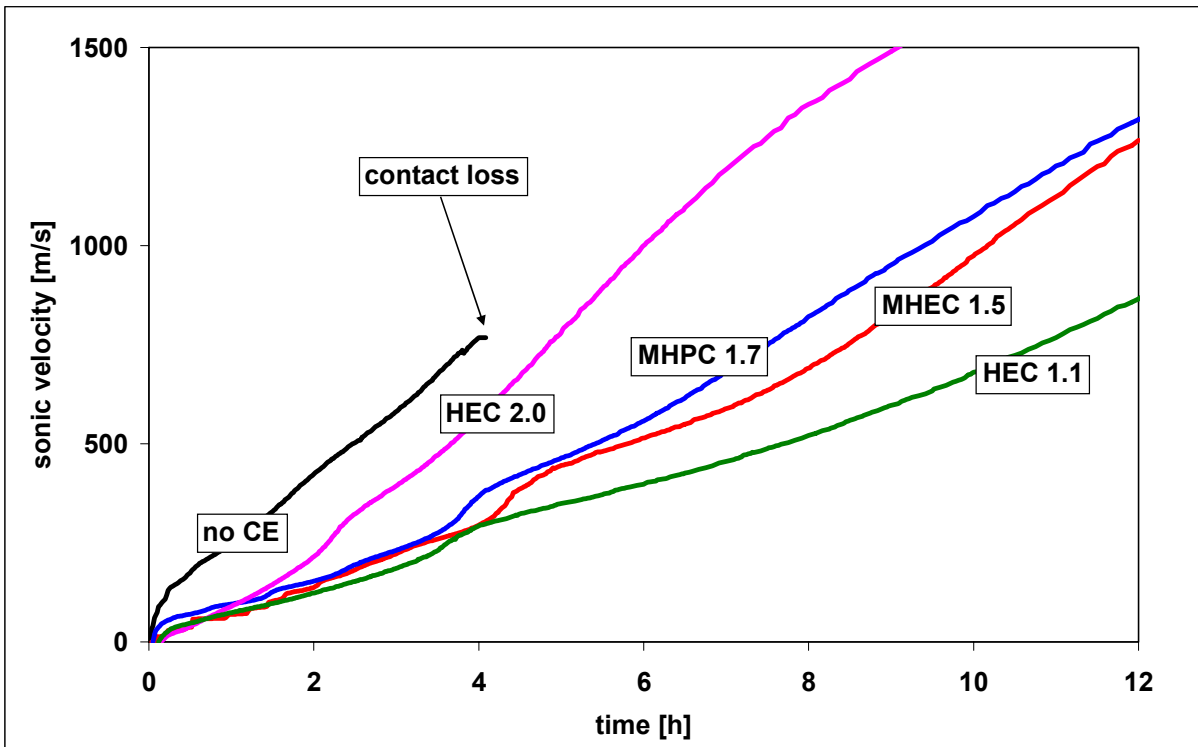


Fig. 5.06: DS-specific, CE-caused retardation of strength development in OPC monitored by ultra sonic measurements.

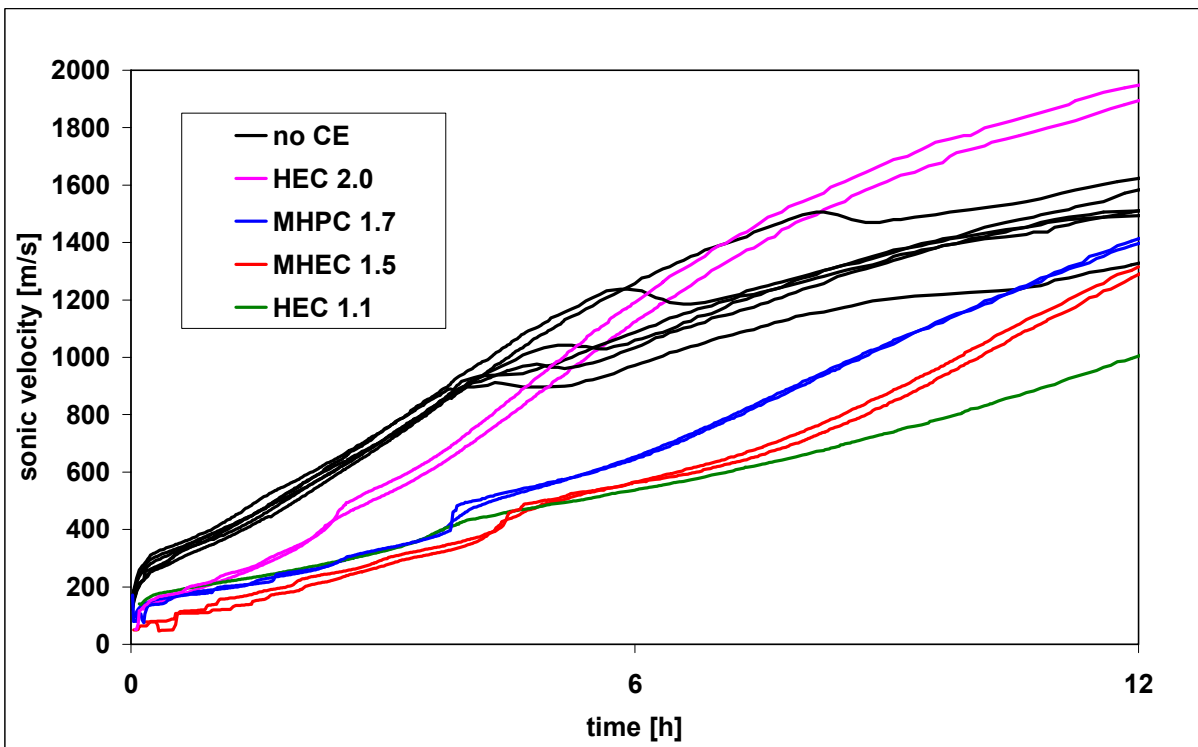


Fig. 5.07: The reproducibility of ultrasonic tests is very good until crack formation in the reference samples without CE leads to disturbed acoustic coupling between sender and receiver.

5.2.2 Heat Flux Calorimetry

The results were confirmed by heat flux calorimetric measurements of setting Portland cement (fig. 5.08, table 5.5). The lower the DS the longer the retardation times. The heat evaluation curve usually started with a strong, sharp peak. Its origin lay mostly in the dissolution heat plus first crystallization heat. Since the water was added prior to measurements this peak could not be observed except for the rest of the sharp drop down in the very left of the diagram. The main hydration took place in a time frame of 3-20 hours with its maximum between 6 and 13 hours depending on the DS of the added CE. According to Taylor ^[Tay1] this heat development correlates with strong CSH-formation in the hydration process of C₃S. The downward trend of the heat evaluation curve hereafter showed a weak shoulder. Taylor associates this shoulder with increased ettringite and monosulphate formation. This process was, like the main hydration, DS-specifically retarded.

Heat flux calorimetry can also produce information on phase-dependent retardation if single phases are used. Instead of cement pure C₃S was mixed with water prior to measurements. The heat evaluation curves here showed a significant retardation of the mean hydration caused by CE (fig. 5.09, tab. 5.6), much clearer than in experiments with cement. The lower the DS of the added CE the stronger the retardation. Since C₃S was the only clinker phase in these experiments the heat evaluation curves did not show shoulders of C₃A-hydration. Due to the lower milling grade (3000 cm²/g Blaine) the hydration times were significantly longer than those of the Portland cement (4000 cm²/g Blaine).

Further experiments were carried out with mixtures of 70 % C₃A, 15 % anhydrite and 15 % calcium sulphate hemi-hydrate. The heat development curves showed that the main hydration of C₃A took place approx. 30 minutes after water contact when no CE was added (fig. 5.10). All CE-types showed a slight retarding effect of approx. 25 minutes, independent of DS. It is assumed that the retardation was an unspecific effect of increased viscosity of the pore solution which inhibited the ion mobility in crystallization processes.

Since a single time point for the climax of hydration processes can be determined (i.e. the point of maximum heat development), it was possible to plot the retardation times versus the degree of substitution. Figure 5.11 shows the DS-dependent retardation times for the three different hydration processes described above. The hydration process of the pure C₃S is much slower than that of Portland cement due to coarser particle sizes.

Conclusions

- The main hydration processes of Portland cement and C_3S pure phase are strongly and DS-specifically retarded by CE: the lower the degree of substitution the stronger the retardation.
- The hydration of C_3A in presence of Ca-sulphates is slightly and DS-independently retarded by CE.

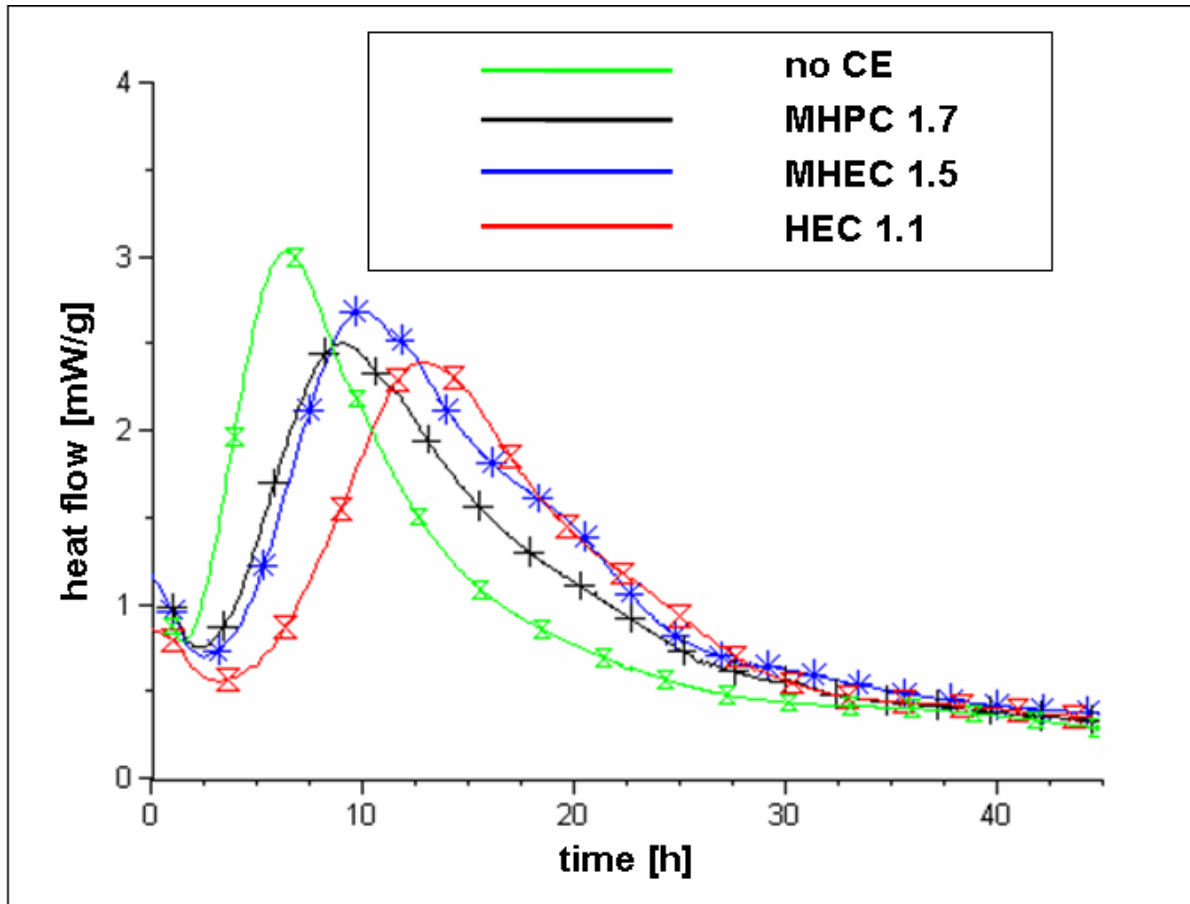


Fig. 5.08: DS-specific retardation of cement hydration monitored by heat flux calorimetry. Analyses by S. Hucko and M. Zwanzig, Hercules Inc

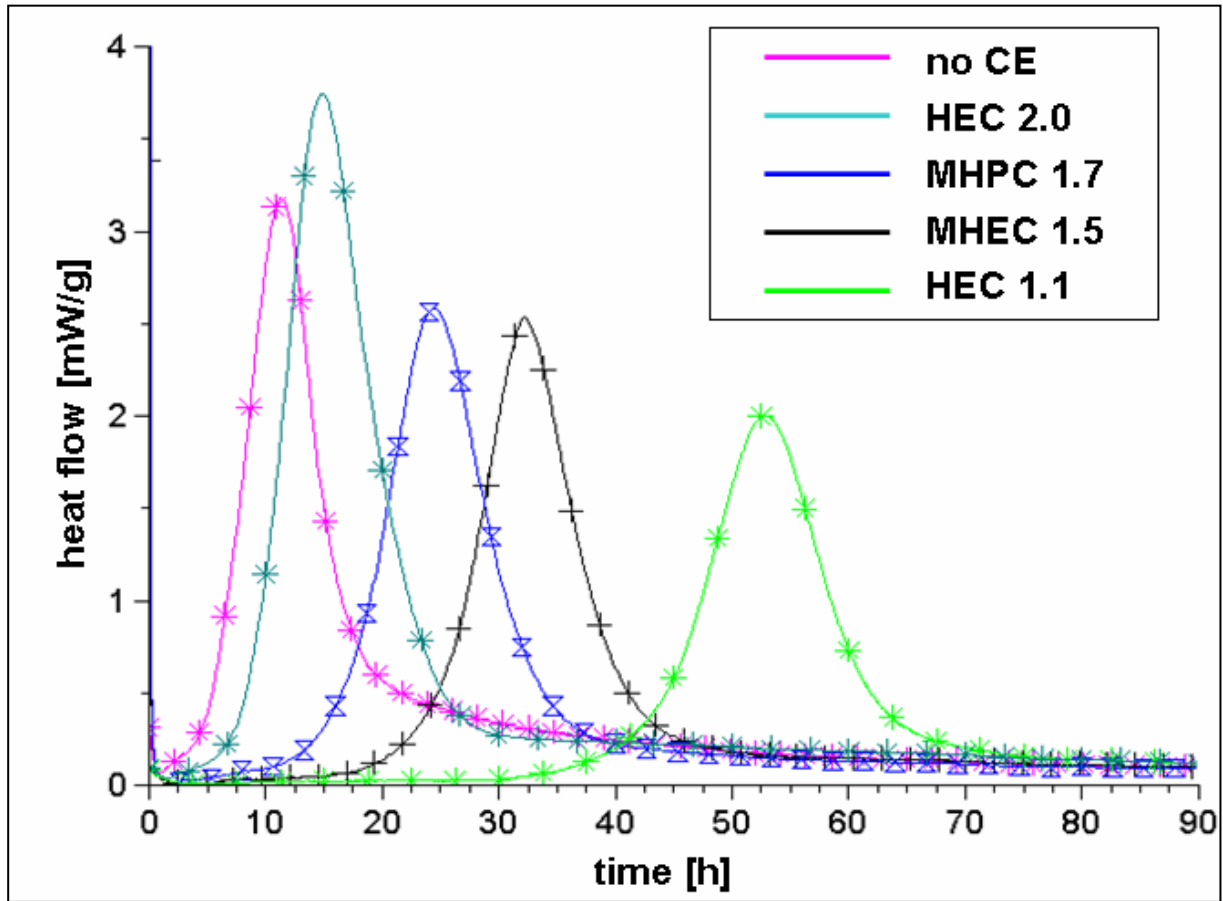


Fig. 5.09: DS-specific retardation of C_3S -hydration monitored by heat flux calorimetry. Analyses by S. Hucko and M. Zwanzig, Hercules Inc

CE-type	no CE	MHPC 1.7	MHEC 1.5	HEC 1.1
main hydration time [h]	6:15	8:45	10:00	13:00
retardation time [h]		2:30	3:45	6:45

Table 5.5: CE-caused retardation of Portland cement hydration determined by heat flux calorimetry.

CE-type	no CE	HEC 2.0	MHPC 1.7	MHEC 1.5	HEC 1.1
main hydration time [h]	11:00	15:00	24:30	32:00	53:00
retardation time [h]		4:00	12:30	21:00	42:00

Table 5.6: CE-caused retardation of C_3S hydration determined by heat flux calorimetry.

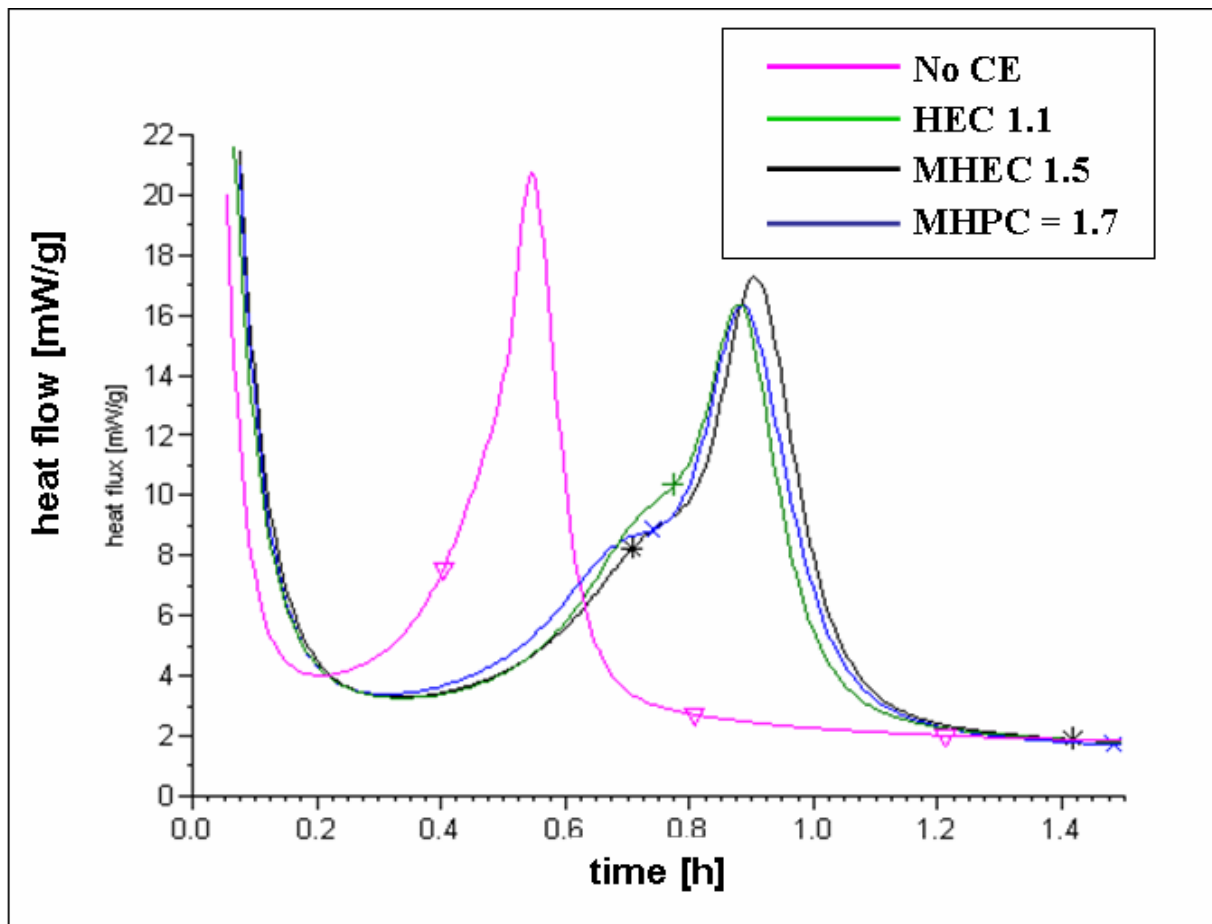


Fig. 5.10: DS-independent retardation of C_3A -hydration in presence of sulphates monitored by heat flux calorimetry. Analyses by S. Hucko and M. Zwanzig, Hercules Inc.

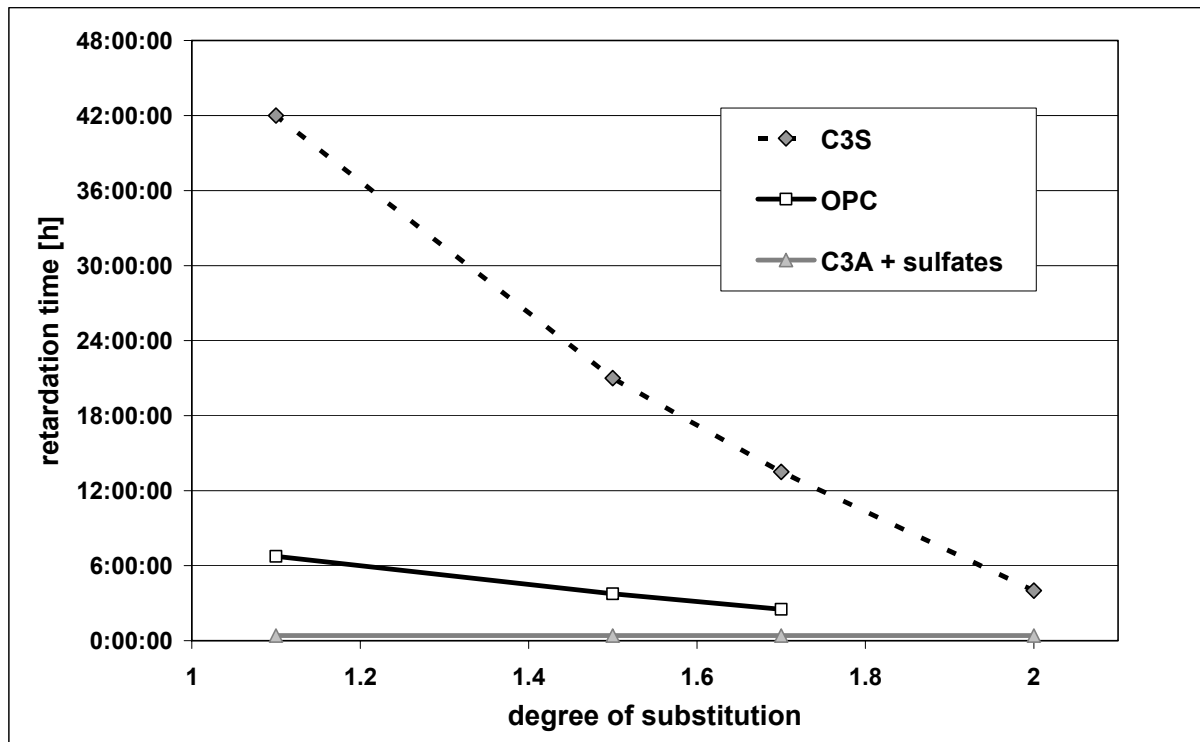


Fig. 5.11: DS- and phase-specific expansion of hydration times.

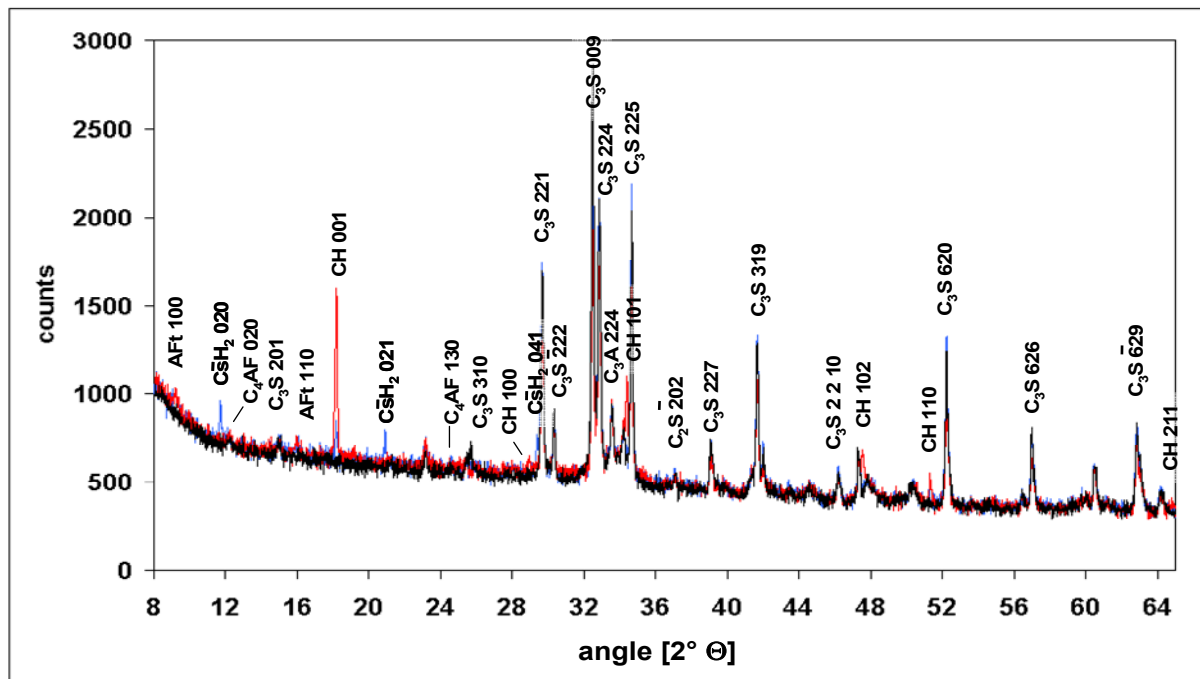


Fig. 5.12: XRD pattern of Portland cement: black: fresh OPC, not hydrated; blue: 4 hours of hydration; red: 21 hours of hydration. $\lambda = 1.54184 \text{ \AA}$ (CuK α).

5.2.3 Laboratory XRD

Ultrasonic measurements cannot monitor the influence of CE on cement hydration phase-resolved. Heatflux calorimetry can do that in pure-phase experiments only. Therefore the phase development of Portland cement was monitored by X-ray powder diffractometry. A series of samples was tested with standard laboratory XRD at the Institute of Mineralogy of the University of Muenster using Cu-K α -radiation with a wavelength of 0.154184 nm (1.54184 \AA). Since the scanning time of 45 minutes was too long for in-situ measurements for each time interval the hydration process was stopped in sample portions individually as described in chapter 3.91.

First, all peaks of the diffraction pattern must be identified. Therefore the diffraction patterns of three cement samples with different hydration times were plotted (fig. 5.12). The cement was fresh (black pattern), hydrated for 4 hours (blue) and 21 hours (red). The peak positions were compared to those of pure phases recorded in the ICDD-database^[1cd1]. Since cement phases, especially the silicates, are solid solutions with varying chemical composition, the ICDD data did not coincide with experimental data completely. Variations in cell parameters and d-values were expected. The peak intensities were integrated with the help of the X'Pert software by Phillips. Difficulties resulted from multiple superimposition of peaks from different phases. C₂S for example showed no peak with sufficient intensity standing alone. Its reflections overlapped mainly with those of C₃S. The only single peak of C₃S was at

angle position $51.7^\circ 2\Theta$ (620). The strongest reflection of C_4AF (141) became overlapped by a strong portlandite peak (101) with proceeding hydration. Some minor peaks of this phase are (020), (130) and (040). Other peaks did not overlay them, but they had low intensity. C_3A had only one peak (224) without superimposition at $33.2^\circ 2\Theta$. In contrast to clinker phases the hydration products ettringite, portlandite and gypsum had their main reflections standing alone in the low angle range. Ettringite has its main reflections at $9.1^\circ 2\Theta$ (100) and $15.8^\circ 2\Theta$ (110). Due to the small amount of ettringite none of the smaller peaks were found. Gypsum showed three distinct peaks at $11.6^\circ 2\Theta$ (020), $20.7^\circ 2\Theta$ (021) and $29.2^\circ 2\Theta$ (041). Portlandite has three strong peaks: (001), (101) and (110). (101) was partly superimposed by C_4AF (141) and C_3S (225). Calcium sulphate hemi-hydrate and anhydrite also have distinct main reflections but their content in cement (approx. 1.5 mass-% each) was too low. No peaks of those two phases could be detected.

To monitor the phase development in the hydration process and to compare the hydration kinetics of different cement-CE-blends it was not necessary to determine the phase content quantitatively as can be done by Rietveld analysis. In this first test series the development of peak intensities of one specific phase was compared in different formulations. For better statistics the intensities of several selected reflections of one phase were summed up. A list of all used reflections is given in table 5.7. The peak intensities were integrated and calculated by using X'Pert peak identification and fitting software. The plot of the sum of intensities versus time shows the phase development during hydration.

Figure 5.13 shows the phase development of ettringite over time. About two third of all observed ettringite was formed within the first ten minutes of hydration. This result correlates basically with the estimation of Cerulli (80 mass-%, chapter 2.6). The rest crystallized slowly over 24 hours. Cellulose ethers did not show any effect on ettringite crystallization.

Aft	C\bar{S}H₂	C₄AF	C₃S	CH	C₃A	C₂S
1 0 0	0 2 0	0 2 0	2 0 1	0 0 1	2 2 4	$\bar{2}$ 0 2
1 1 0	0 2 1	1 3 0	3 1 0	1 0 0		
	0 4 1	0 4 0	$\bar{2}$ 2 2	1 0 1		
		1 4 1	2 2 7	1 1 0		
			2 2 10	2 1 1		
			6 2 0			
			6 2 6			
			$\bar{6}$ 2 9			
			6 2 9			
			8 0 4			

Table 5.7: Selected peaks suitable to determine the phase development in OPC.

After the first rapid ettringite crystallization the supernatant primary sulphate carriers hydrated to gypsum (fig 5.14). Gypsum crystallization was slightly retarded by CE depending on the degree of substitution. The lower the DS the stronger the retardation. The delay of gypsum crystallization was smaller than that of gypsum consumption. The consumption of gypsum in the ongoing ettringite formation was strongly retarded by CE but the DS-dependent trend was disturbed by the two types MHEC 1.5 and MHPC 1.7. HEC 1.1 showed the strongest effect. MHPC 1.7 showed a stronger retarding effect than MHEC 1.5. HEC 2.0 showed the weakest retarding effect.

The portlandite formation was significantly and DS-specifically retarded in the presence of CE (fig. 5.15). The lower the DS the stronger retardation, with exception of HEC 2.0, which seemed to have a stronger effect than MHEC 1.5 and MHPC 1.7. The consumption of C_3S in the hydration process is shown in figure 5.16. This process was also DS-specifically affected. The lower the DS the stronger the retardation.

The influence of aluminium hydroxide on early ettringite formation was studied by adding 0.5 mass-% of $Al(OH)_3$ on cement without CE. Figure 5.17 shows that the amount of ettringite formed within the first minutes of cement hydration was significantly increased when $Al(OH)_3$ was added. Since more sulphate was consumed in the enforced ettringite formation less gypsum crystallized (fig. 5.18)

The time-curves of phase development were not smooth which made the interpretation difficult. The reason for this was the individual sample treatment for each measurement. Rietveld analyses of the data could not improve the results significantly. The observation of C_3A , $C_2(A,F)$ and C_2S development did not deliver satisfying results. All these phases had too few suitable peaks and too weak peak intensities. The reproducibility was poor due to insufficient statistic.

Conclusions

- Cellulose ether does not effect the rapid ettringite crystallization.
- Gypsum crystallization is slightly, gypsum dissolution strongly and DS-specifically retarded by CE: the lower the DS the stronger the retardation.
- Portlandite precipitation and the corresponding C_3S consumption is strongly and DS-specifically retarded: the lower the DS the stronger the retardation.
- The addition of aluminium hydroxide increases the amount of ettringite that crystallizes during early hydration of OPC while gypsum formation is reduced.

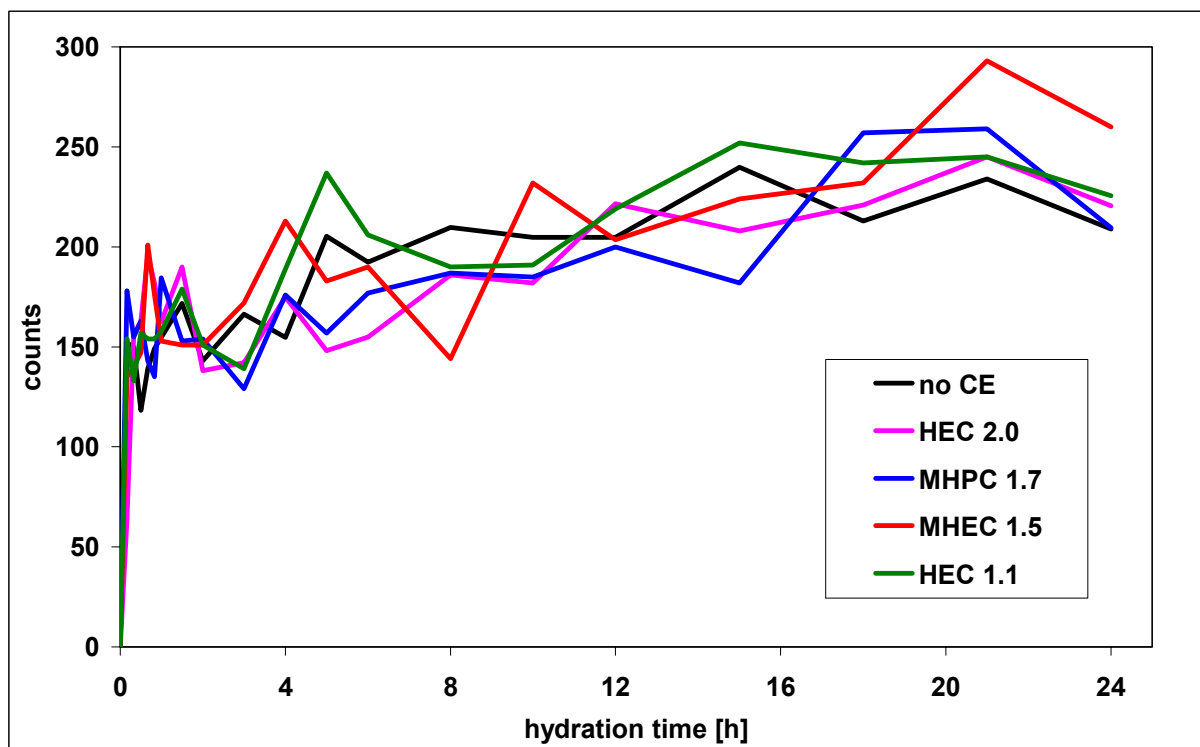


Fig. 5.13: Phase development of ettringite in OPC. The dry cement powder did not contain any ettringite before water contact. Laboratory XRD, samples quenched with acetone.

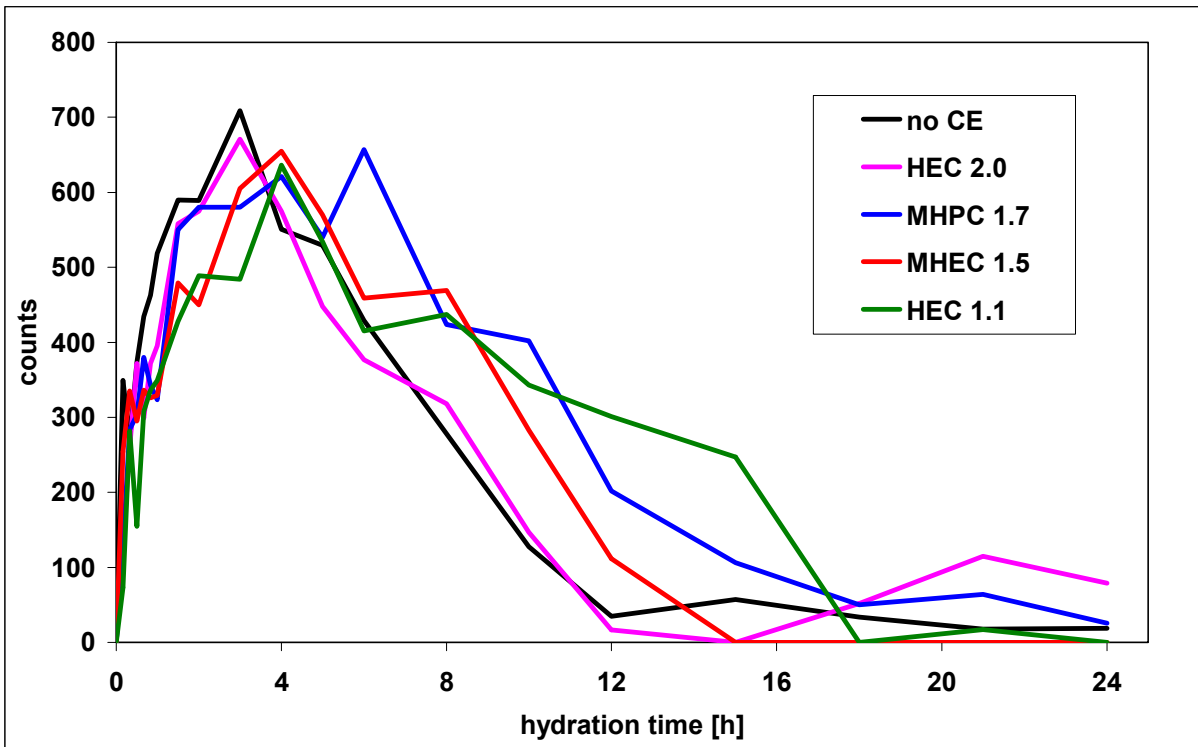


Fig. 5.14: Phase development of gypsum in OPC. Laboratory XRD, samples quenched with acetone.

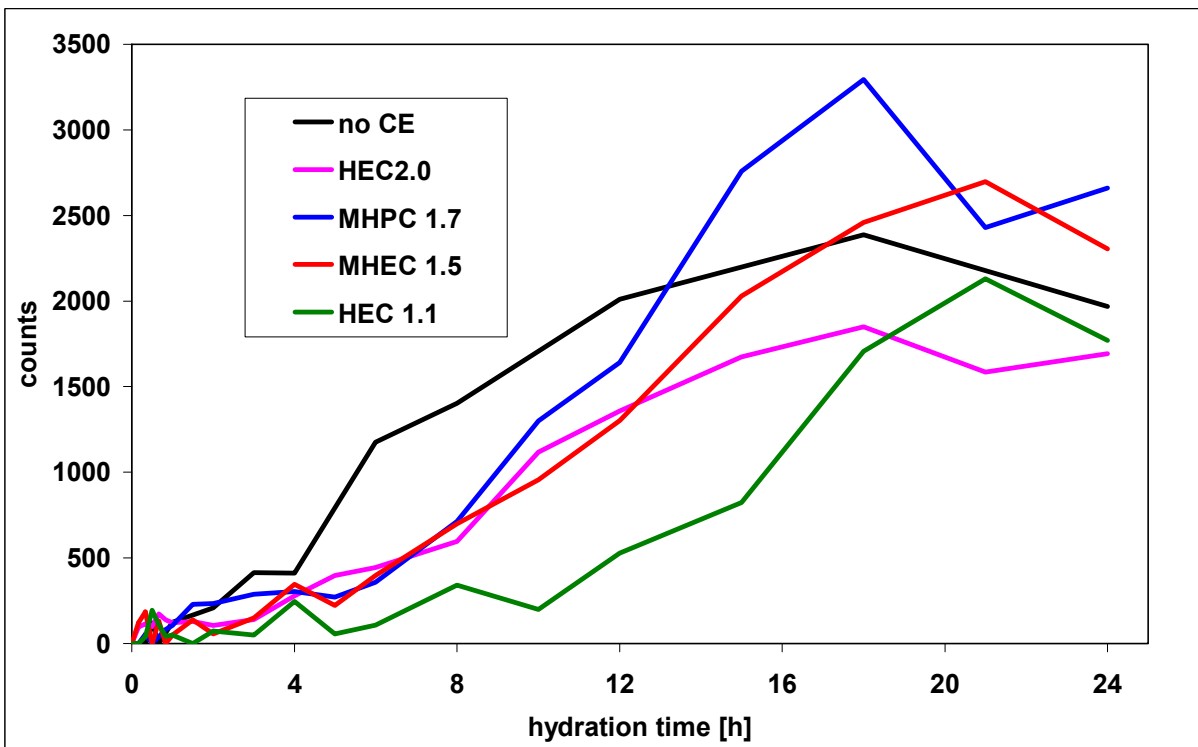


Fig. 5.15: Portlandite precipitation in OPC. Laboratory XRD, samples quenched with acetone.

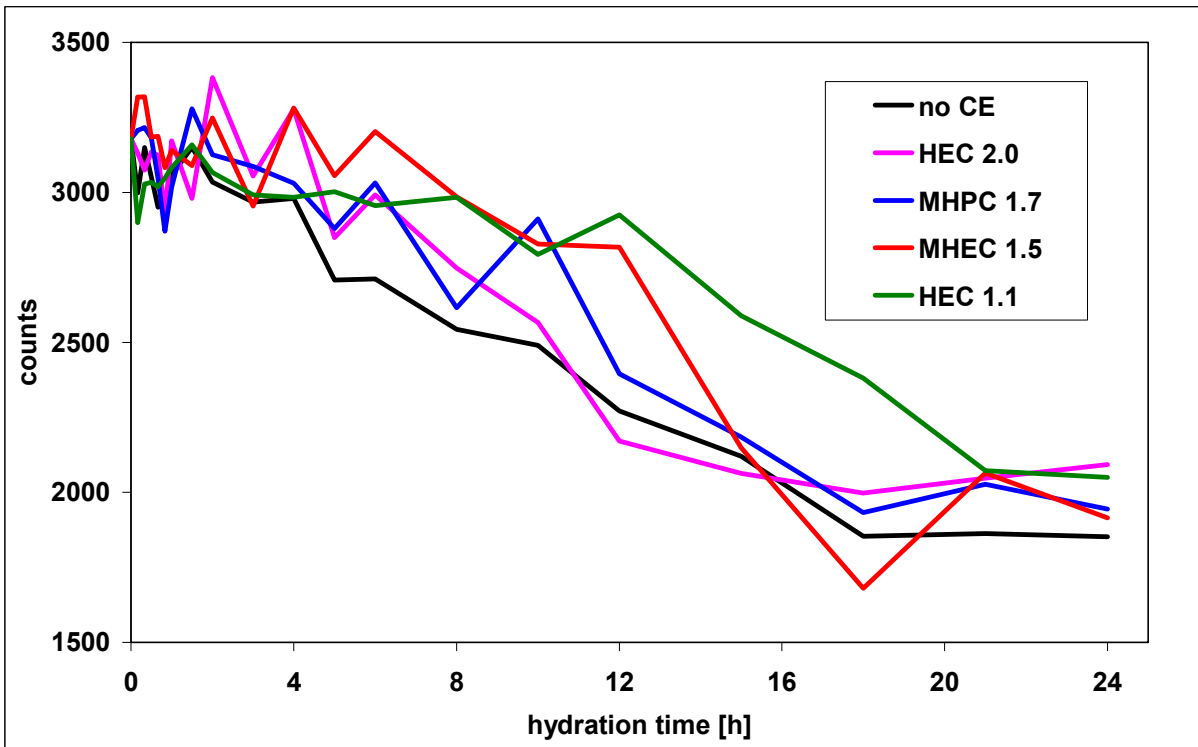


Fig. 5.16: C₃S consumption during OPC hydration. Laboratory XRD, samples quenched with acetone.

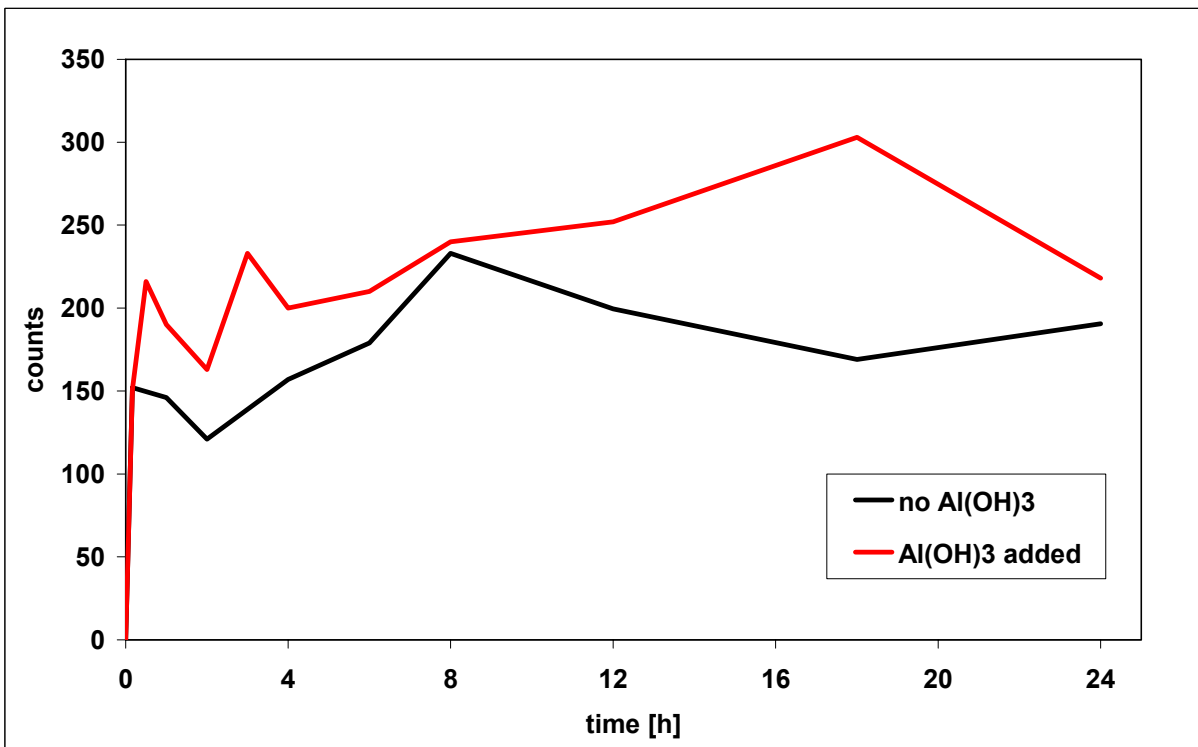


Fig. 5.17: Increased ettringite formation in OPC with addition of 0.5 mass-% Al(OH)₃. Laboratory XRD, samples quenched with acetone.

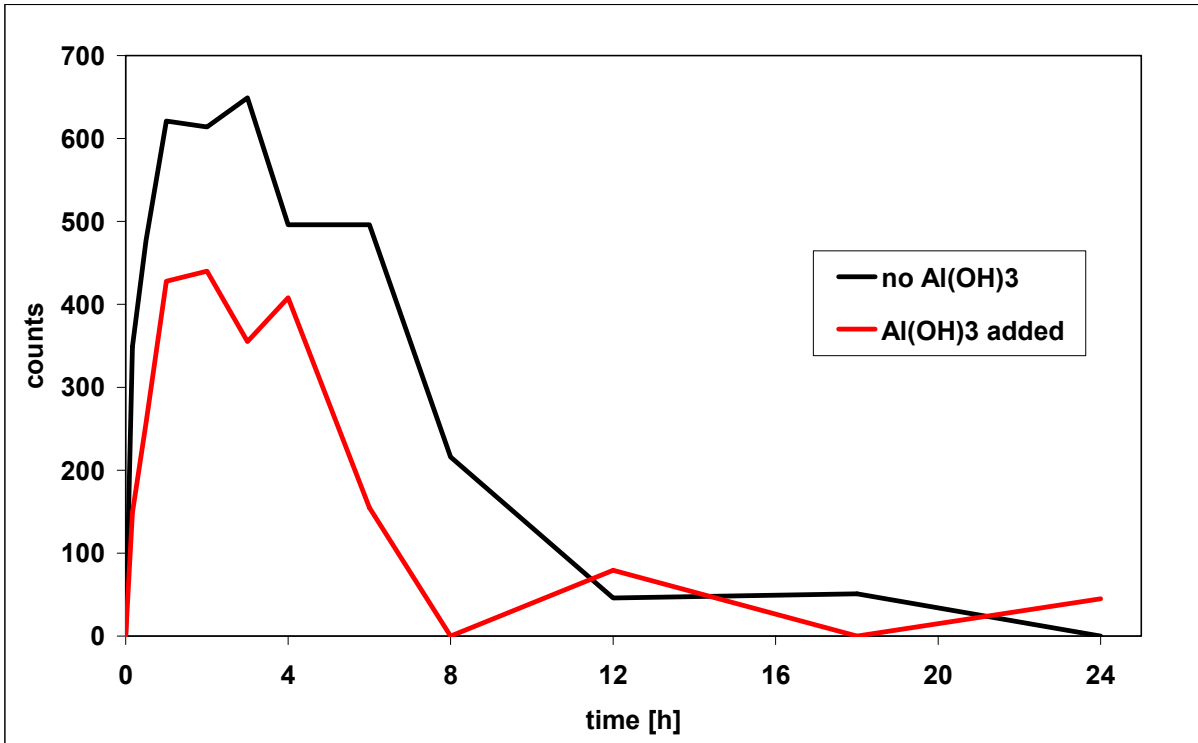


Fig. 5.18: Reduced gypsum formation in OPC with addition of 0.5 mass-% Al(OH)₃. Laboratory XRD, samples quenched with acetone.

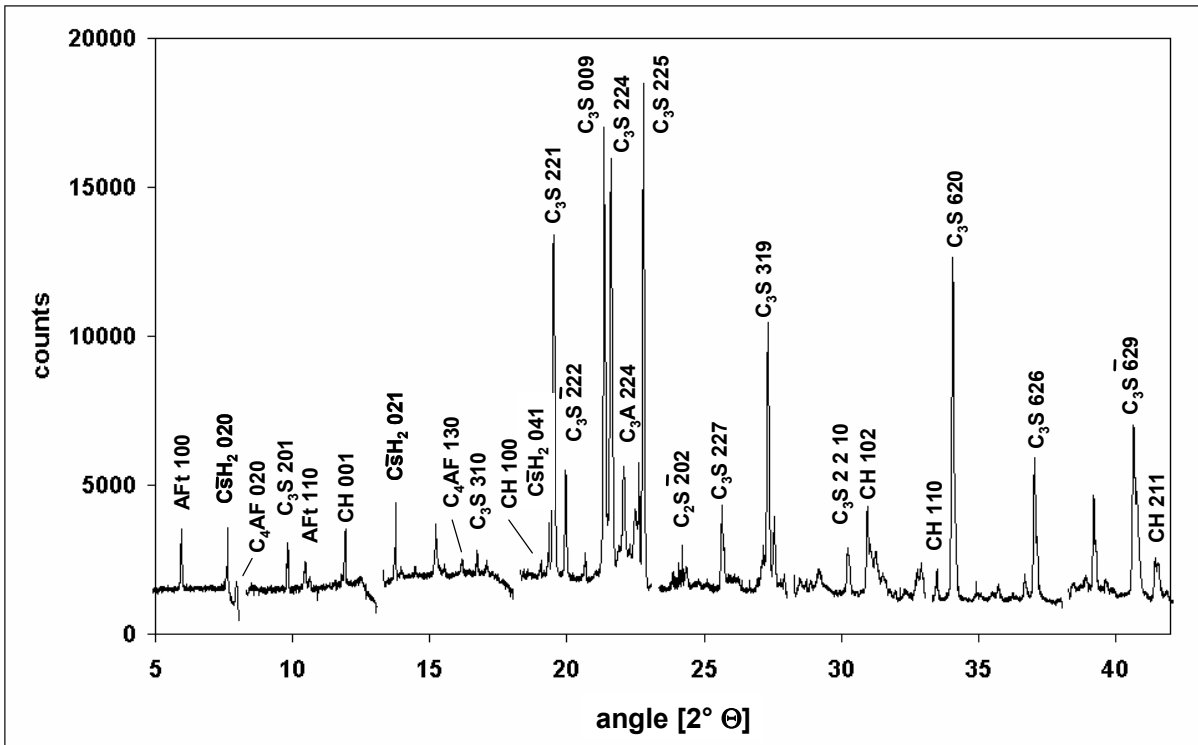


Fig. 5.19: Synchrotron XRD pattern of Portland cement after 5 hours of hydration. $\lambda = 1.04014 \text{ \AA}$.

5.2.4 Synchrotron XRD

The incontinuity of measurements as described in the chapter before, can only be avoided if the same sample is monitored in-situ over time. Synchrotron radiation with high brilliance (up to 10^{13} ph/s) in combination with simultaneous detection of diffracted beams over the whole angle range allows in-situ measurements with a temporal resolution of 10 seconds. During a measuring time of 24 hours a huge amount of data was produced (approx. 8600 data files per day). Only a small part of all data could be used for data analysis in a reasonable time. The time-resolution was high at the beginning of hydration to monitor the rapid ettringite crystallization and was more and more reduced with progressing hydration time. Rietveld analyses were done without consideration of the so-called amorphous phases. Calcium silicate hydrates and the X-ray amorphous ettringite as observed by Eckart and Stark ^[Eck1] had not been taken into account. Therefore the calculated phase content given in masspercent is based on the sum of all observed phases:

$$[X] = 100 m_X / \Sigma m_n$$

with $[X]$ = content of phase X in masspercent, m_X = mass of X and Σm_n = sum of masses of all *observed* phases including X. The following phases could be observed: C₃A, C₄AF, C₃S, C₂S, ettringite, portlandite and gypsum (fig. 5.19). Since the ignored content of amorphous phases increased with proceeding hydration time, the calculated content of all observed phases was higher than their content in cement actually was. The difference between calculated and actual content increased with progressing hydration time. Furthermore free water was not considered. A part of the pore water was incorporated into crystalline hydration products and contributes to the mass of observed phases. However, this did not disturb the comparing approach of hydration kinetics.

The first ettringite was formed within the first five minutes of hydration (fig. 5.20). CE had no effect on the first ettringite crystallization. This correlates well with results from laboratory XRD. Whereas conventional XRD showed a rather continuous ettringite formation hereafter, the synchrotron XRD gave three other results: 1. After a few minutes the first ettringite formation stopped and the phase content of ettringite was constant for some hours. After some hours a renewed growth of ettringite started. 2. The apparent amount of ettringite formed during first crystallization was less in in-situ experiments than in quenched samples. This correlates with the observations made by T. Cerulli ^[Cer1] (s. chapter 2.6). 3. The second ettringite formation is strongly DS-specifically retarded by CE. MHPC 1.9 showed nearly no retardation closely followed by MHEC 1.7. The next was MHEC 1.5 followed by MHPC 1.7. The strongest retardation was shown by HEC 1.1. After 24 hours the second ettringite

formation had just started in the HEC 1.1 formulation. The second ettringite formation proceeded simultaneously with gypsum dissolution, a phase that was consumed in this process.

Gypsum crystallization was significantly retarded by CE depending on DS (fig. 5.21). The lower the DS the stronger the retardation. An exception is MHEC 1.5, which showed a slightly stronger retardation than HEC 1.1. The disappearance of gypsum proceeds simultaneously with the second ettringite formation indicating that gypsum is consumed in this crystallization process. The retarding effects of various CE-types was here in line with their DS-value. The lower the DS the stronger the retardation.

After complete consumption of gypsum, ettringite should react with C_3A and water forming calcium aluminate monosulphate hydrate. The monosulphate has only one strong peak very close to ettringite (100). Due to the partly superposition of both peaks and the high radiation energy with decreased spatial resolution, monosulphate could not be distinguished from ettringite. However, it was assumed that only negligibly small amounts of monosulphate were formed during the first 24 hours of hydration. Theoretically no monosulphate should appear in this time since the pore solution is more supersaturated in respect of ettringite than of monosulphate (Rothstein^[Rot1]). Thus ettringite is a stable phase at this stage of hydration. This correlates with results presented by Stark^[Sta1, Sta2], who did not observe monosulphate formation in the first 24 hours of cement hydration.

A comparison of the calculated development of C_3S and C_2S showed that the Siroquant software had difficulties to distinguish between those two phases (see also chapter 4.1). Sudden drop downs of the calculated C_3S -content were always associated with a sharp increase of C_2S (fig. 5.22). This indicates that in some analyses Siroquant identified C_3S peaks as those of C_2S . Therefore both phases were summarized as calcium silicates which led to a steady course of the time curves. This made it easier to compare the kinetics of the phase development in different samples. The comparison between C_3S and C_2S shows that it is rather the C_3S that was consumed in the silicate hydration in which portlandite and X-ray amorphous CSH is formed. C_2S seemed to be stable over 24 hours. This result was in line with those of Taylor and Scrivener^[Tay1, Scr1]. Thereafter C_2S is less active and reacts in cement over years. The consumption of calcium silicates was retarded DS-specifically (fig. 5.23). The lower the DS the stronger the retardation. The phase development of calcium silicates correlated perfectly with the simultaneous portlandite crystallization (fig. 5.24). The HEC 1.1 showed the strongest retardation: after 24 hours the amount of calcium silicates hardly decreased and only little CH was formed.

The content of $C_2(A,F)$ seemed to increase after eight hours (fig. 5.25). This apparent DS-dependent increase was an artefact since the increase of a clinker phase during hydration makes no sense. Assuming that the mass of $C_2(A,F)$ was constant over observation time, which is reasonable since $C_2(A,F)$ is the most stable clinker phase, its calculated content increased because Σm_n decreased due to its contribution to CSH-formation whose mass was not included in the sum.

The same argumentation explains the apparent DS-specific C_3A -growth after eight hours (fig. 5.26). C_3A contributes to ettringite formation. The stoichiometric equation



transformed into a balance of molecular masses:

$$270 + 516 + 468 = 1254$$

indicates that the mass contribution of C_3A is approx. one fifth of the mass of ettringite. A slight decrease of C_3A content in cement is to be expected, as the figure shows for the initial stage of hydration. Due to the impossibility to describe the phase development of the last two phases, no statement can be made on the influence of cellulose ethers on those developments.

All in all it could be said that the cellulose ether had a DS-dependent effect on the hydration process of the calcium silicates and on the second ettringite formation together with gypsum consumption. The lower the DS the stronger the retarding effect. A comparison between MHECs and MHPCs shows that MHPCs had stronger retarding effects on the hydration kinetics than MHECs. Samples containing MHPC 1.7 were always delayed for longer times than samples with MHEC 1.7. In respect of second ettringite formation the MHPC 1.7 was close to MHEC 1.5. This indicated that the chemistry of the substituent had also an influence on hydration kinetics. Within one group of cellulose ethers the CE-caused retardation was DS-specific. HEC 1.1 with its extremely low DS showed always the longest retardation times.

Additionally to the quantitative phase analyses based on synchrotron XRD data, a Rietveld analysis of the reference sample that had been hydrated for 24 hours without CE was made at the X-Ray Laboratory Dr. Ermrich to confirm the results. The results are given in table 5.8. The comparison is satisfying. The differences between the ettringite contents showed that the laboratory XRD result fits better since a cement sample without CE should have a higher content of ettringite after 24 hours of hydration (see also fig. 5.20).

Conclusions

- Ettringite crystallization takes place in two stages: the rapid first ettringite formation is not effected by CE. The second ettringite formation after several hours of rest is strongly and DS-specifically retarded by CE: the lower the DS the stronger the retarding effect.
- Gypsum crystallization is significantly, gypsum dissolution strongly and DS-specifically retarded by CE: the lower the DS the stronger the retardation.
- Portlandite precipitation and the corresponding C₃S consumption is strongly and DS-specifically retarded: the lower the DS the stronger the retardation.
- The retarding effect of MHPC is stronger than that of MHEC with the same DS (1.7). Within one group of CE the retarding effect increases with decreasing DS.

Phase	Laboratory XRD [mass-%]	Synchrotron XRD [mass-%]
C ₃ S	47.5	50.9
C ₂ S	10.2	6.7
C ₂ (A,F)	9.4	12.9
C ₃ A	5.4	4.5
M	0.4	0.0
C \bar{s}	0.0	0.0
C \bar{s} H _{0.5}	0.0	0.0
C \bar{s} H ₂	0.0	0.0
CH	16.2	16.9
AFt	10.9	7.9
amorphous	0.00	0.0
sum	100.0	99.6

Table 5.8: Phase composition of hydrated Portland cement without CE after 24 hours. The laboratory XRD analysis was done by X-Ray Laboratory Dr. Ermrich. The Synchrotron XRD analysis was performed by the author. The correlation is satisfying. A significant difference occurs with ettringite.

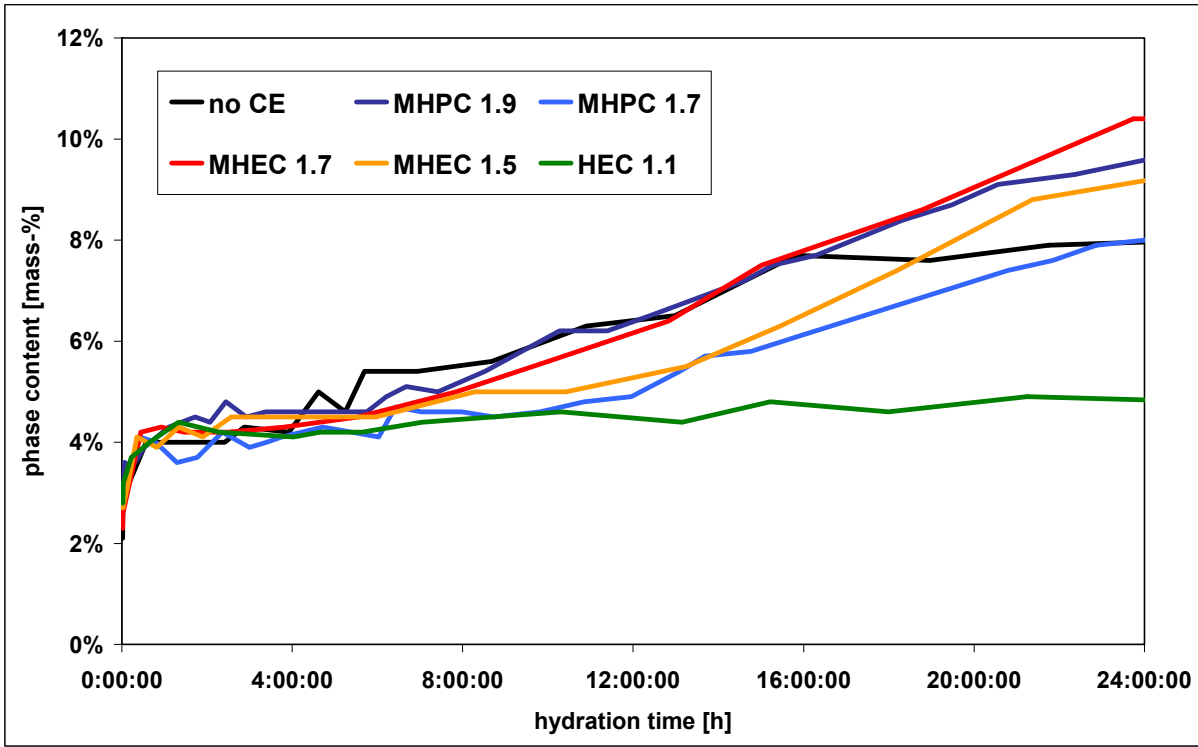


Fig. 5.20: Phase development of ettringite in OPC. The dry cement powder did not contain any ettringite before water contact. Rietveld analyses based on synchrotron XRD data.

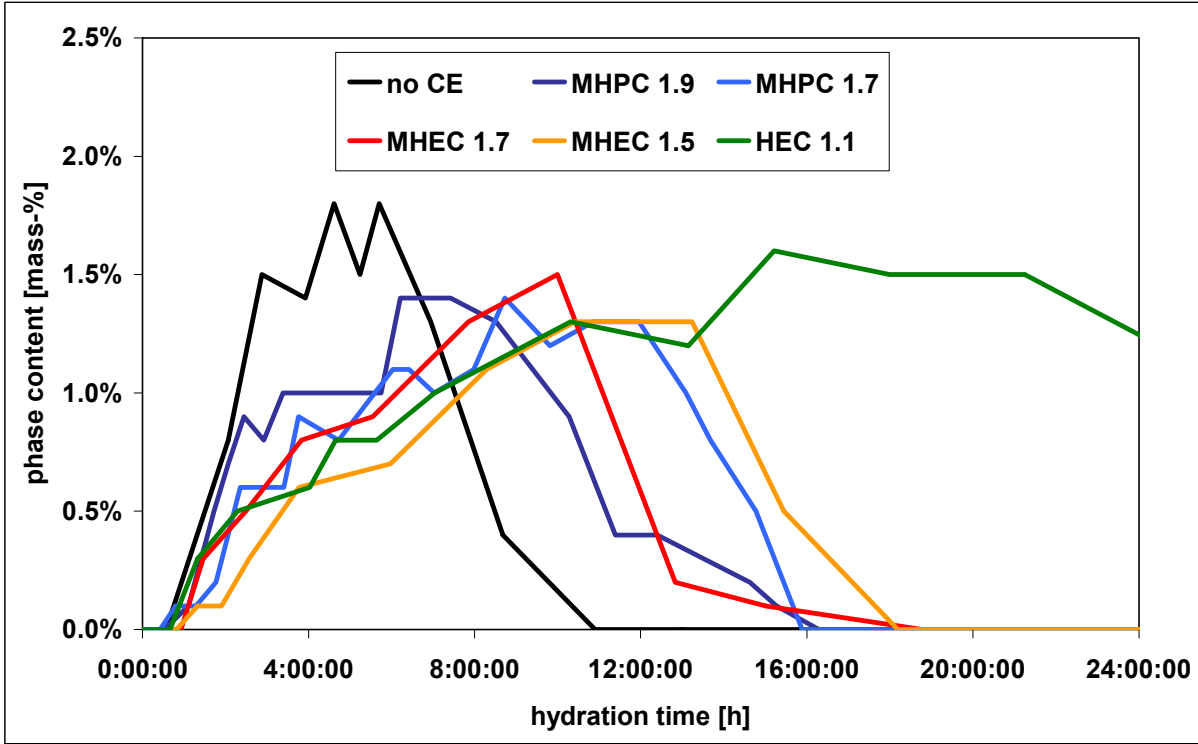


Fig. 5.21: Phase development of gypsum in OPC. Rietveld analyses based on synchrotron XRD data.

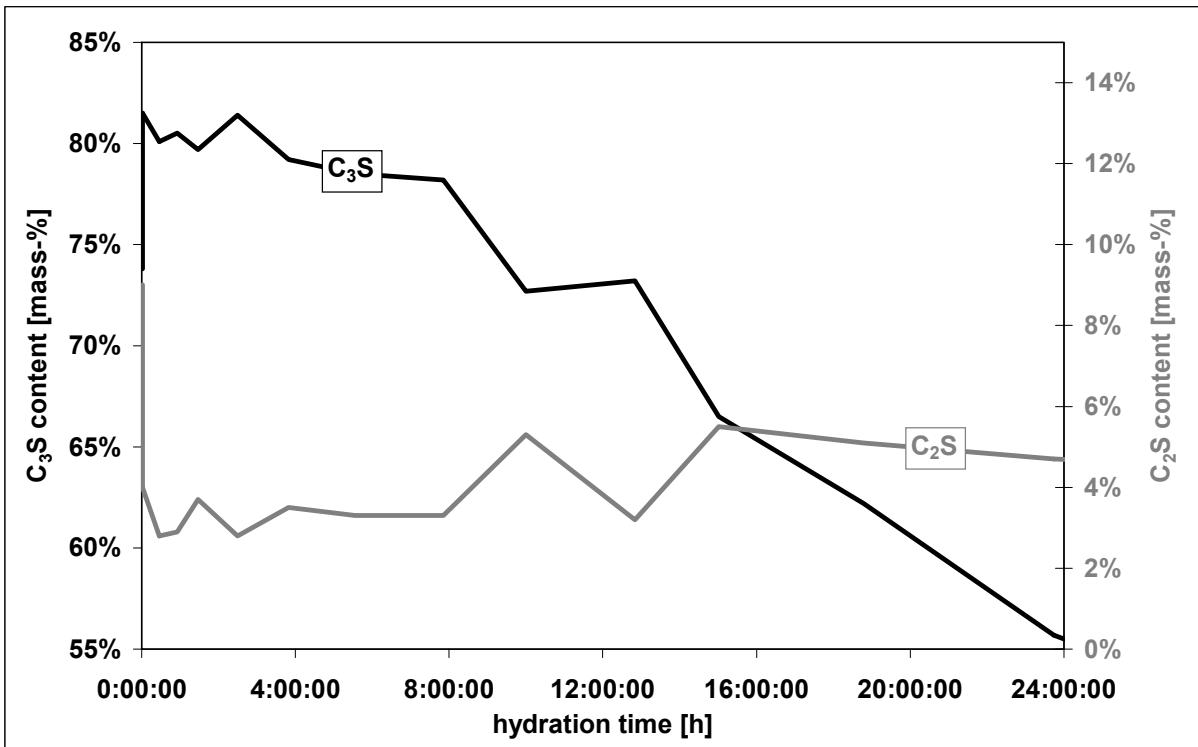


Fig. 5.22: Calculated phase content of C_3S and C_2S over hydration time. Any incline of the apparent C_3S amount correlates with a decline of the C_2S content. Obviously the Rietveld analysis software had difficulties to distinguish between C_3S and C_2S reflexes.

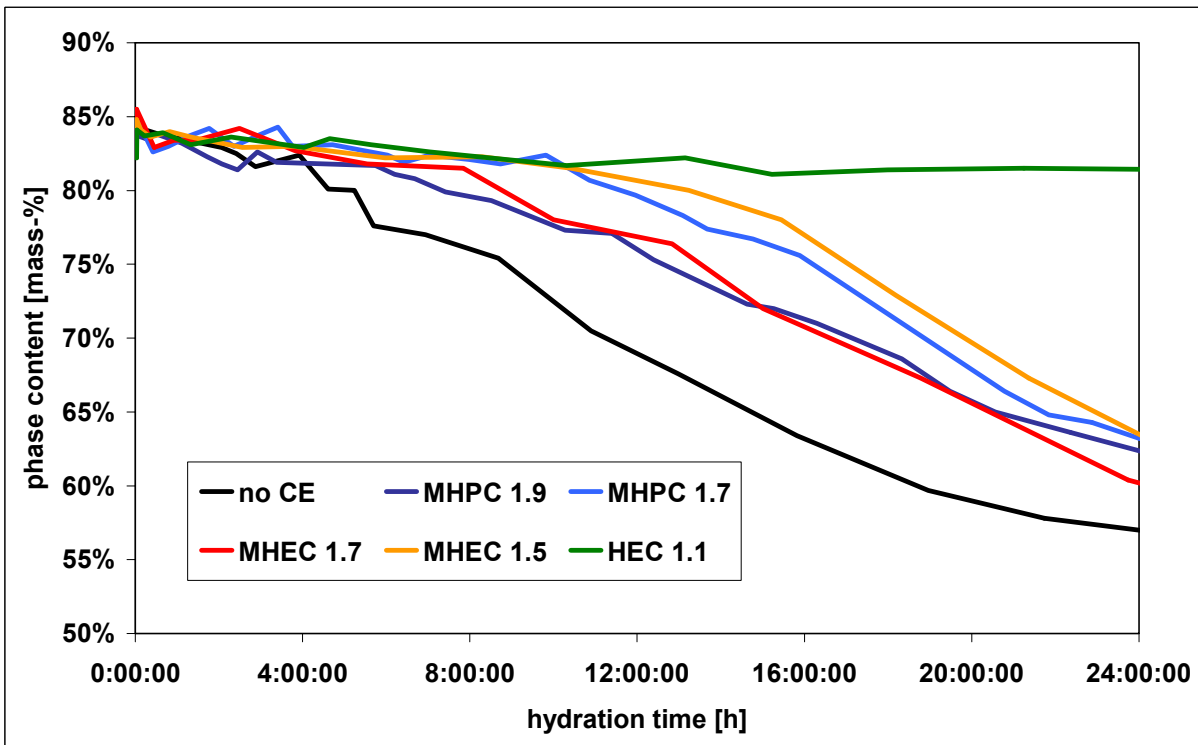


Fig. 5.23: Consumption of Ca-silicates ($C_3S + C_2S$) in the hydration process of OPC. Rietveld analyses based on synchrotron XRD data.

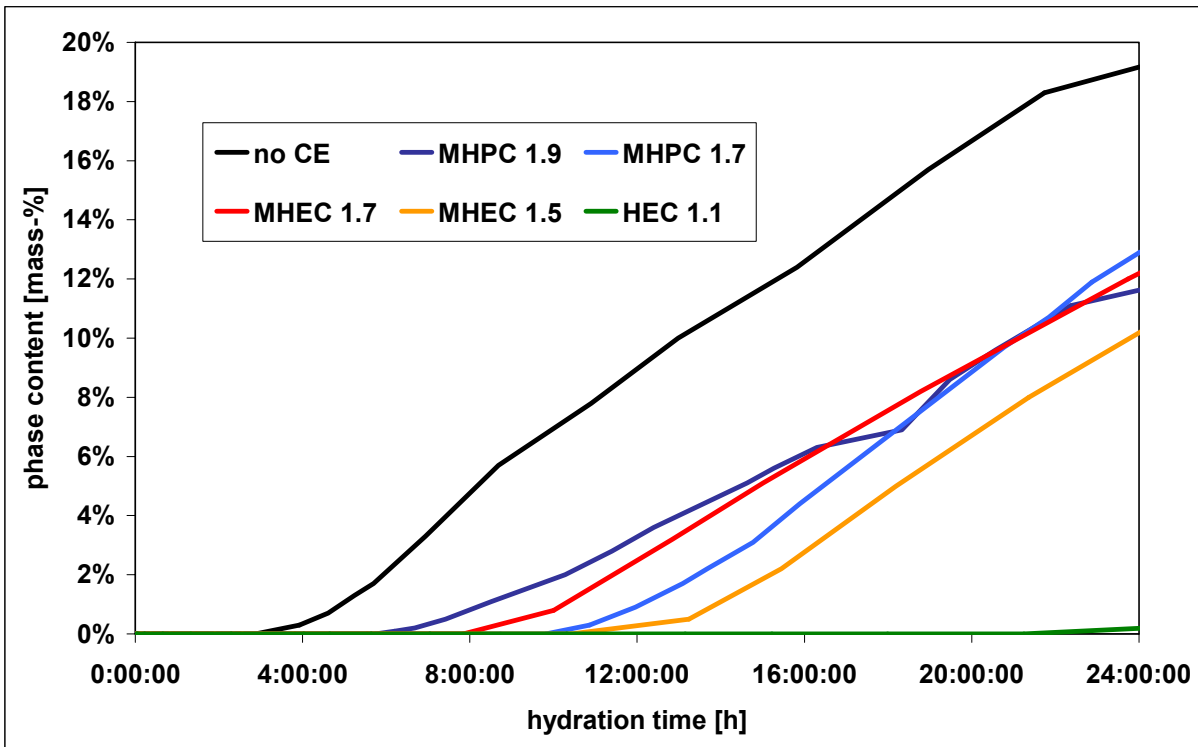


Fig. 5.24: Portlandite precipitation in Portland cement. Rietveld analyses based on synchrotron XRD data.

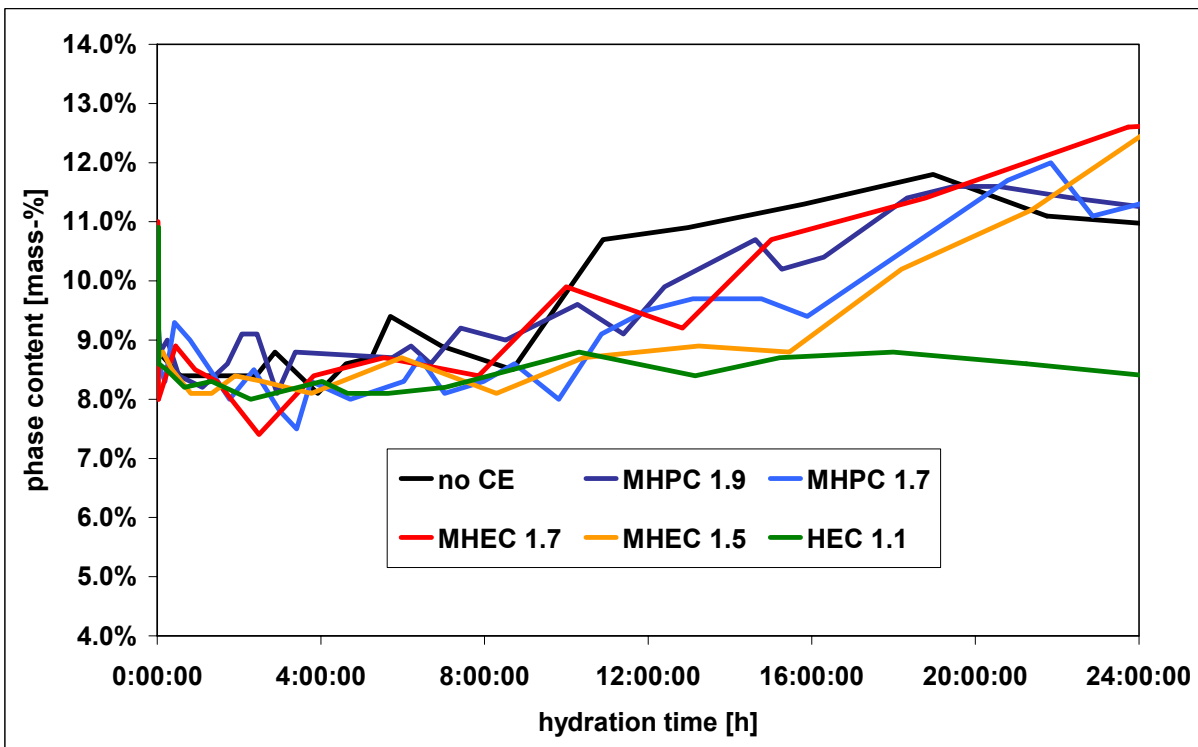


Fig. 5.25: The content of $C_2(A,F)$ in Portland cement as calculated by Rietveld analysis of synchrotron X-ray data. The apparent increase of the amount of $C_2(A,F)$ is an artefact since the increasing contribution of X-ray amorphous phases to the total mass was not considered.

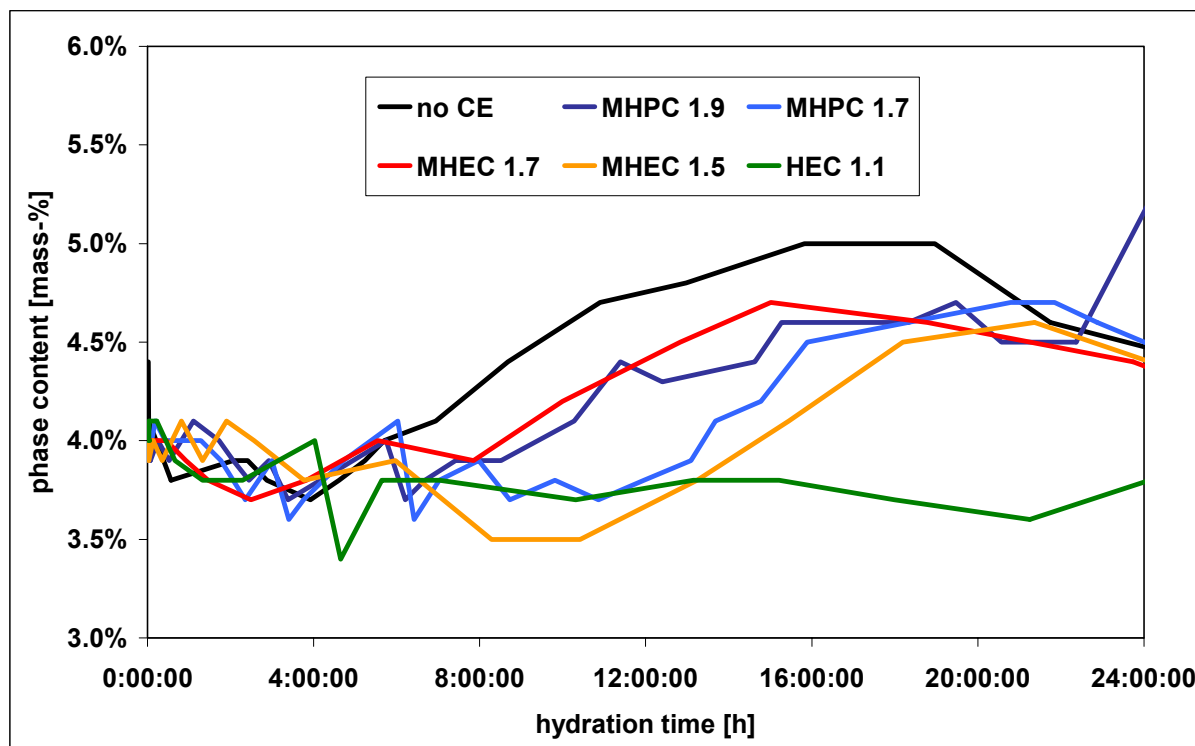


Fig. 5.26: The apparent increase of the amount of C_3A during OPC hydration determined by Rietveld analysis - an artefact since the increasing contribution of X-ray amorphous phases to the total mass was not taken into account.

5.2.5 Synchrotron XRD with Liquid Injection

The attempt to minimize the initial dead time by injecting the water after the measurement had been started, worked well with low viscous aqueous solutions (s. chapter 3.9.2). Problems appeared when CE-solutions with high viscosities were tried to be injected. The sealing did not resist the pressure needed to pump the thickened fluid through the cement powder. To use the given beam time at the synchrotron efficiently the experiments with CE were stopped. Another problem occurred with the progressive ettringite formation in the C_3A + sulphates + water formulation (F10). The expansive crystal growth of ettringite frequently broke the glass capillary during the experiments. If the break happened out of the range of X-ray illumination it did not matter. Otherwise the experiment had to be repeated.

Instead of experiments with various CE-types, cement samples and samples consisting of 70 % C_3A , 15 % anhydrite and 15 % calcium sulphate hemi-hydrate were exposed to water and to $Ca(OH)_2$ -saturated aqueous solution at a pH of 12.6. The focus of examination was on ettringite development. The background was that the author could not explain the different effects of CE on first and second ettringite formation at this point. CE had no effect on the kinetics of the first generation at all, whereas a CE-specific retardation of the second ettringite crystallization could be observed. The precipitation process is the same in both cases

independent of the educts (different sulphates) if the nuclei are formed out of aqueous solution as Taylor and Scrivener suggested ^[Tay¹, Scr¹] (s. chapter 2.5.3). This means that adsorption of CE on ettringite and surface intoxication cannot explain the effect on renewed ettringite growth. But the crystallization kinetics can be affected by the dissolution rate of the educts and/or the ion-concentration in the pore water. Scrivener saw a relation between second ettringite formation and C₃S hydration. This relation could be confirmed by the results of synchrotron XRD. A comparison between second ettringite crystallization and portlandite precipitation showed clearly, that indeed renewed ettringite growth always started synchronically with portlandite crystallization (fig. 5.27). The common component of both processes is calcium and it was assumed that the calcium concentration in pore water is the key. If the ion-balance in solution plays a role, even the first ettringite formation must be affected by variations of calcium concentration in water.

Graphical comparison of the development of the ettringite reflections (100) and (110) within the first 45 minutes of hydration showed that the crystallization started immediately after water contact. In the pure phase mixture of C3A + sulphates with water the ettringite formation was a continuous and steady process (fig. 5.28). Comparison of the two sulphate phases showed that the hemi-hydrate was consumed while the anhydrite was more stable (fig. 5.29). After 4 hours gypsum appeared while ettringite was still slowly growing. The bassanite was long gone and the anhydrite began to dissolve. In a time range of a few hours it was clear that the dissolution of anhydrite was a slow but continuous process (figures 5.30 and 5.31).

If Ca(OH)₂-saturated solution was used, only little ettringite seemed to crystallize directly after contact with the fluid. The further precipitation of (well-crystalline) ettringite was efficiently inhibited by Ca²⁺ respectively (OH)⁻ ions in aqueous solution (fig. 5.32). Simultaneously only little bassanite and no anhydrite were consumed (fig. 5.33). The initial amount of ettringite was comparable to the first ettringite formation in OPC. After one hour ettringite was slowly growing, much slower than in the experiment with tap water. Instead much more gypsum was formed by the hydration of bassanite. Anhydrite was much more stable in Ca(OH)₂ saturated solution (figures 5.34 and 5.35).

In experiments with Portland cement the additional Ca(OH)₂ dissolved in water prior to cement contact had no significant influence on the results. In OPC Ca(OH)₂-saturation is quickly achieved after water contact anyway, even if no additional Ca(OH)₂ was given into solution before the experiment started (figures 5.36 and 5.37).

Conclusions

- Ettringite crystallization starts immediately after water contact.
- In Portland cement the second ettringite crystallization always takes place contemporaneously with portlandite precipitation.
- In pure phase admixtures of C_3A and Ca-sulphates (in absence of silicates) the ettringite formation is a continuous process.
- High $Ca(OH)_2$ -concentration in the pore water inhibits the ettringite formation significantly.
- Calcium sulphate hemi-hydrate is more reactive than the water-soluble anhydrite used in this investigation.

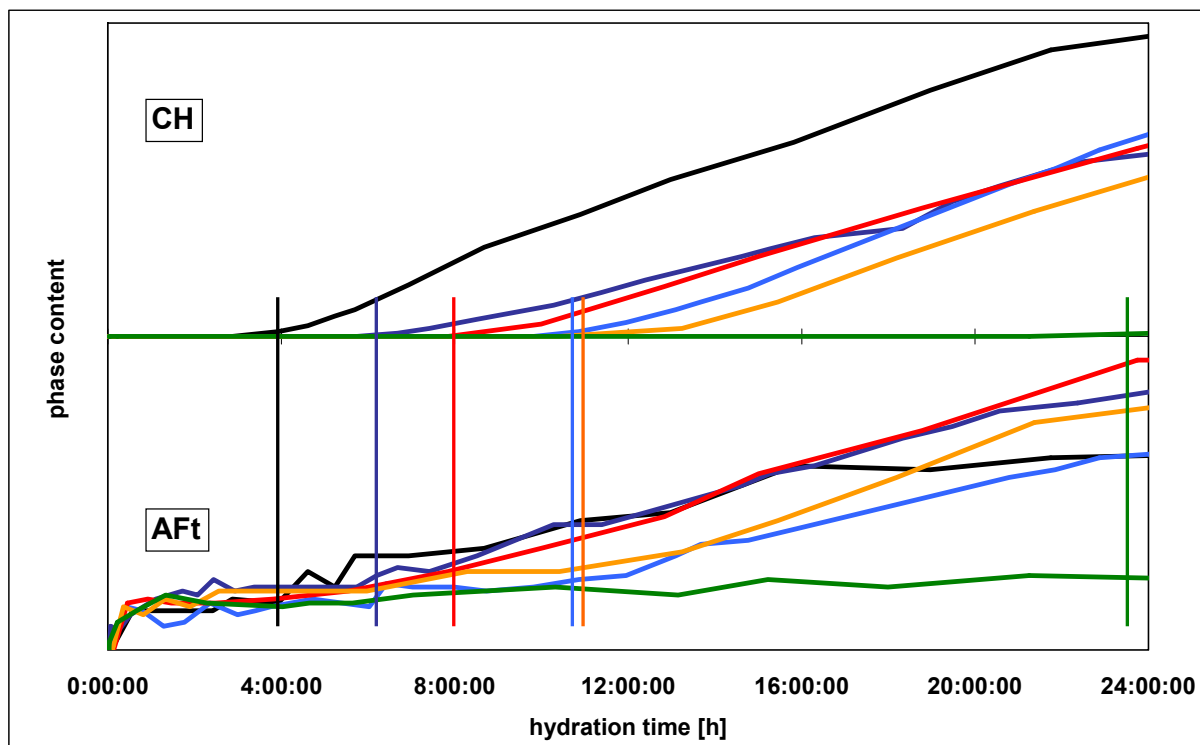


Fig. 5.27: Portlandite (CH) and second ettringite (AFt) crystallization in comparison. Depending on the cellulose ether both processes starts at the same time. Black: no CE; dark blue: MHPC 1.9; red: MHEC 1.7; light blue: MHPC 1.7; orange: MHEC 1.5; green: HEC 1.1.

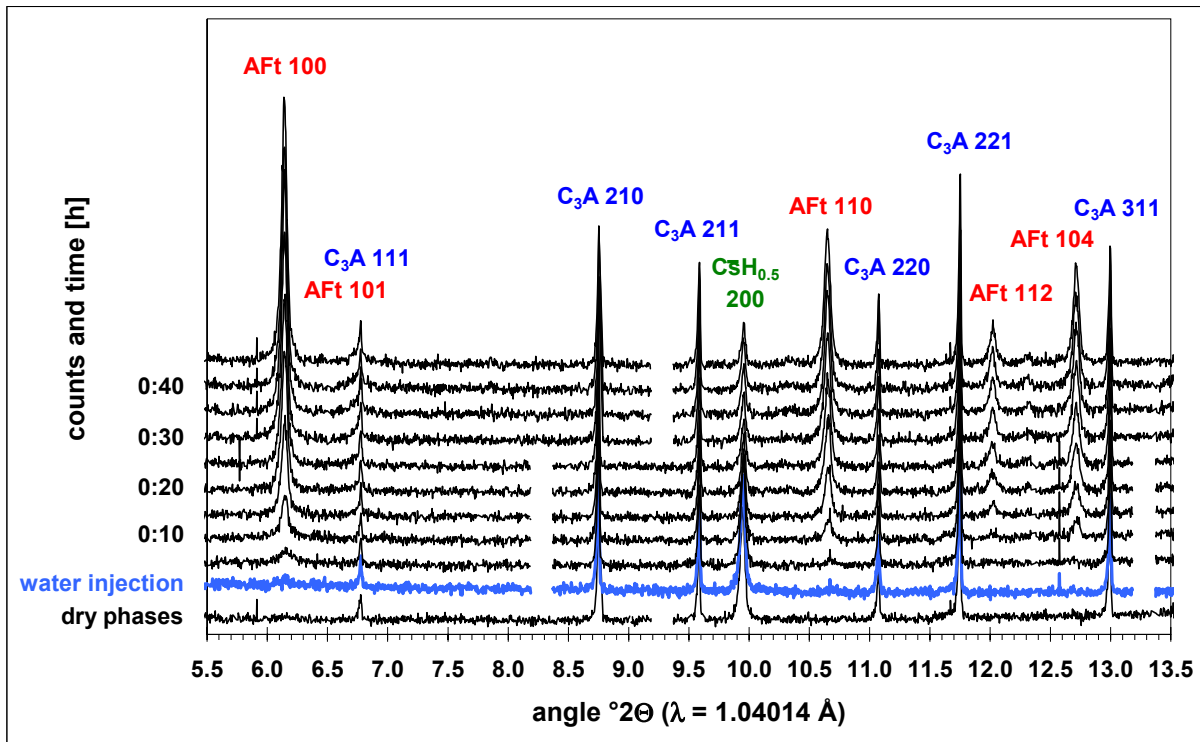


Fig. 5.28: Early ettringite formation in a pure phase mixture of 70 mass-% C_3A , 15 mass-% anhydrite and 15 mass-% bassanite plus water. The anhydrite does not show reflexes in this angle range.

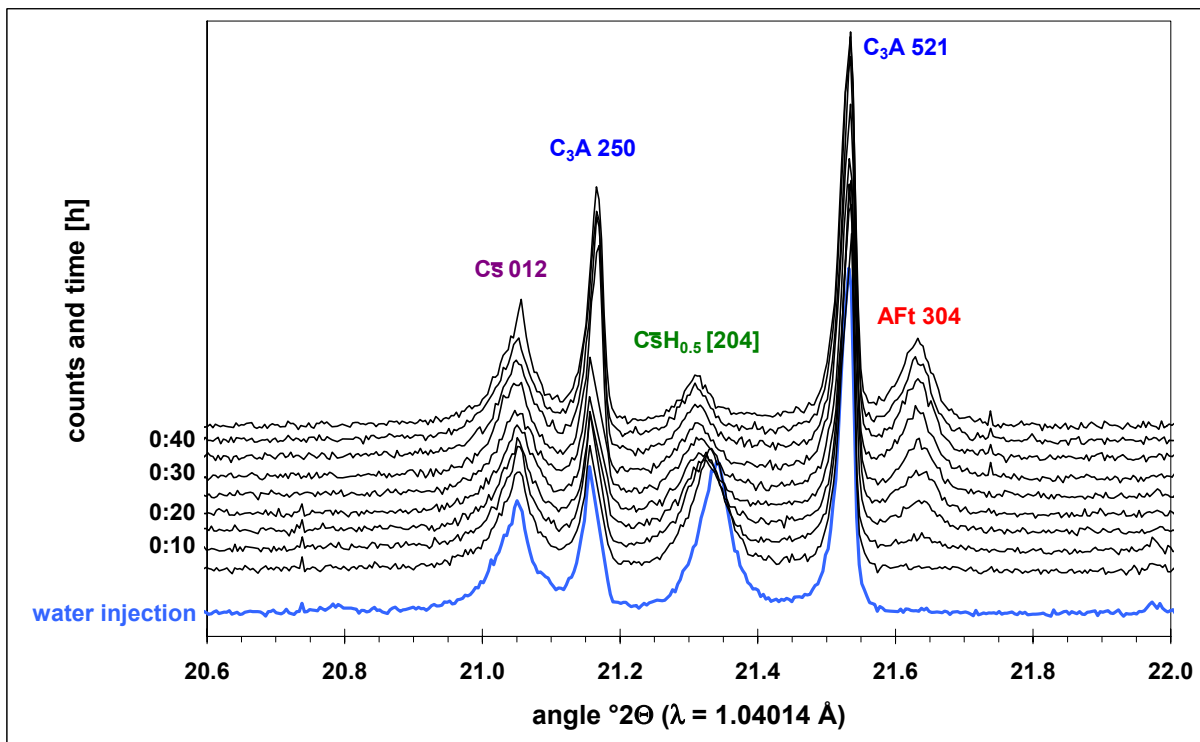


Fig. 5.29: Ca-sulphate consumption during early ettringite formation in a pure phase mixture of 70 mass-% C_3A , 15 mass-% anhydrite and 15 mass-% bassanite plus water. The anhydrite is less active than the bassanite.

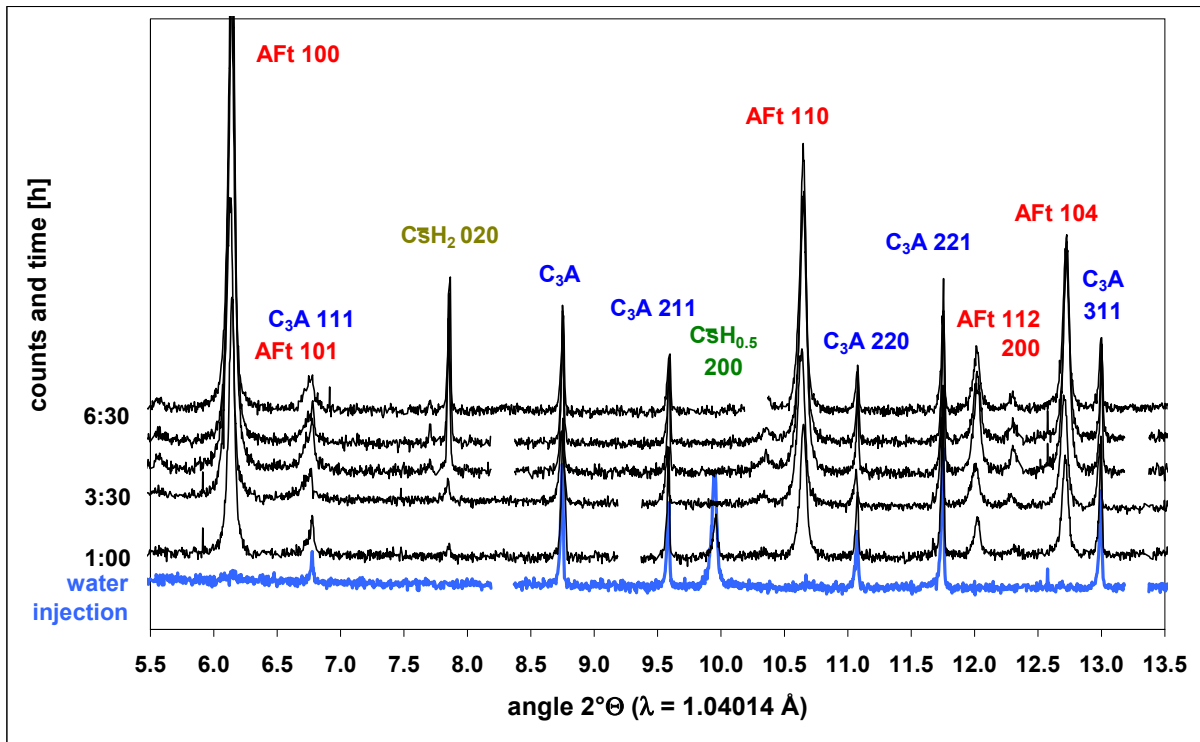


Fig. 5.30: Ettringite formation in a pure phase mixture of 70 mass-% C_3A , 15 mass-% anhydrite and 15 mass-% bassanite plus water. The anhydrite does not show reflexes in this angle range.

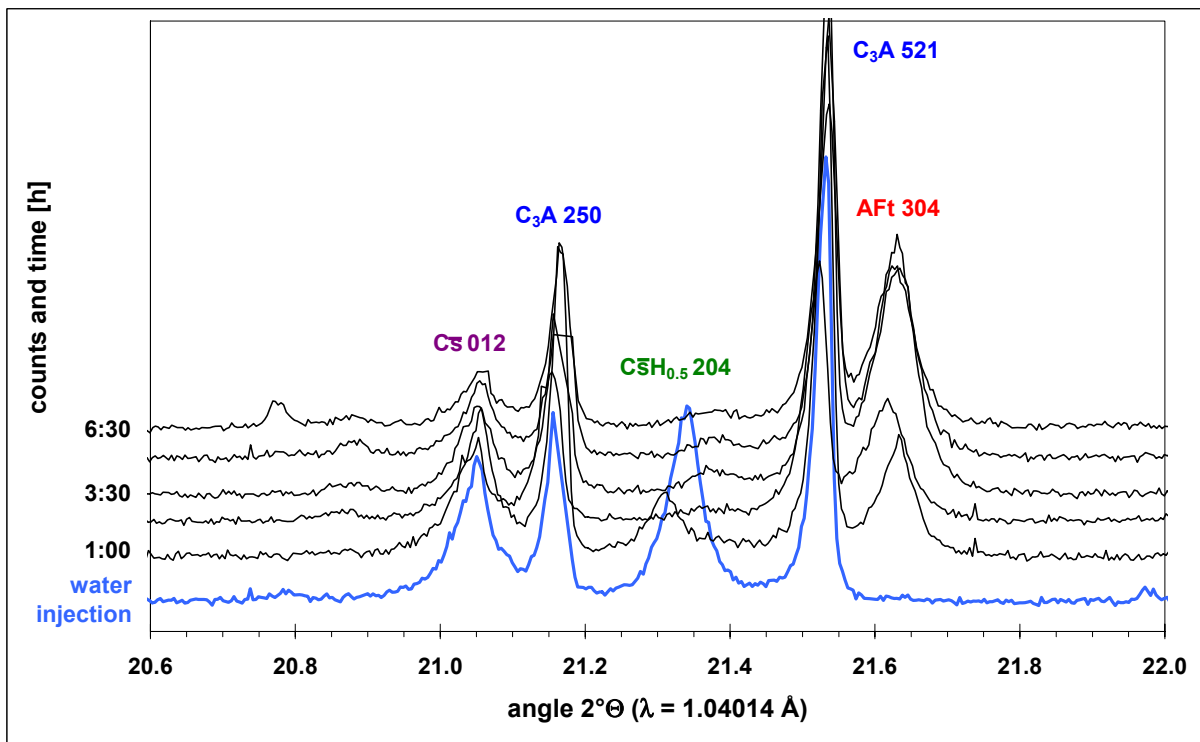


Fig. 5.31: Ca-sulphate consumption during ettringite formation in a pure phase mixture of 70 mass-% C_3A , 15 mass-% anhydrite and 15 mass-% bassanite plus water. The anhydrite is less active than the bassanite.

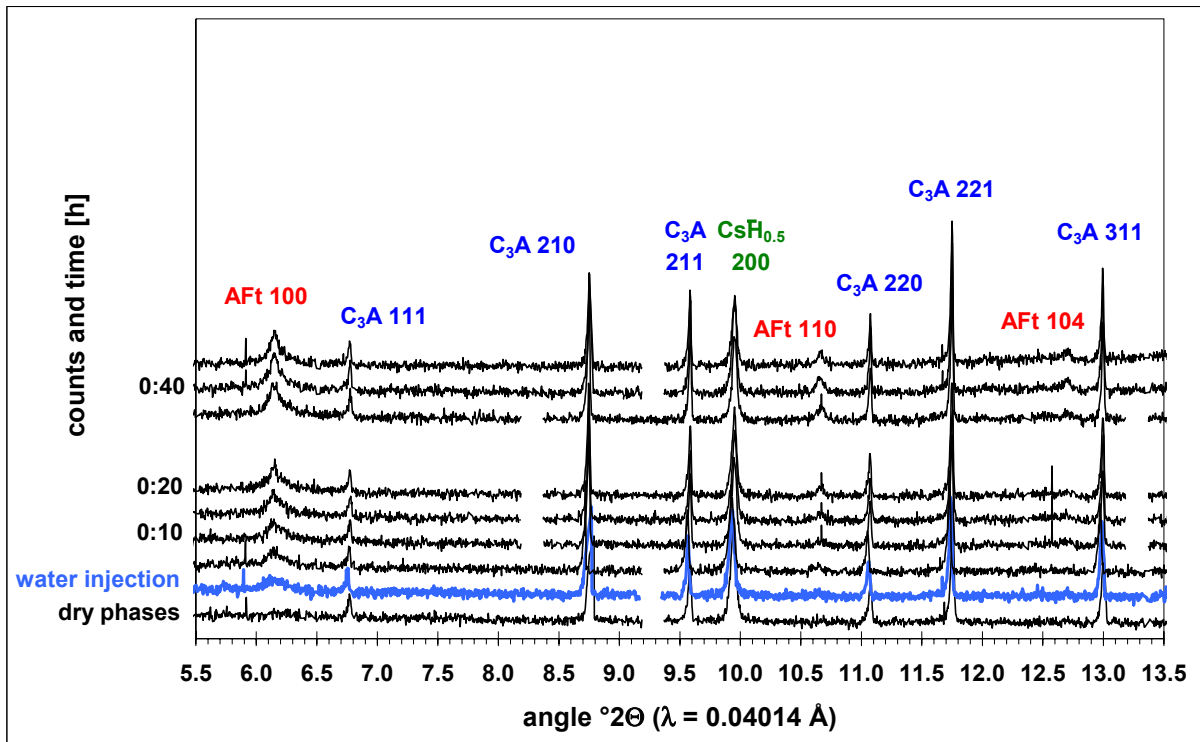


Fig. 5.32: Disturbed early ettringite crystallization in $\text{Ca}(\text{OH})_2$ -saturated aqueous solution. This experiment was performed with a pure phase mixture of 70 mass-% C_3A , 15 mass-% anhydrite and 15 mass-% bassanite.

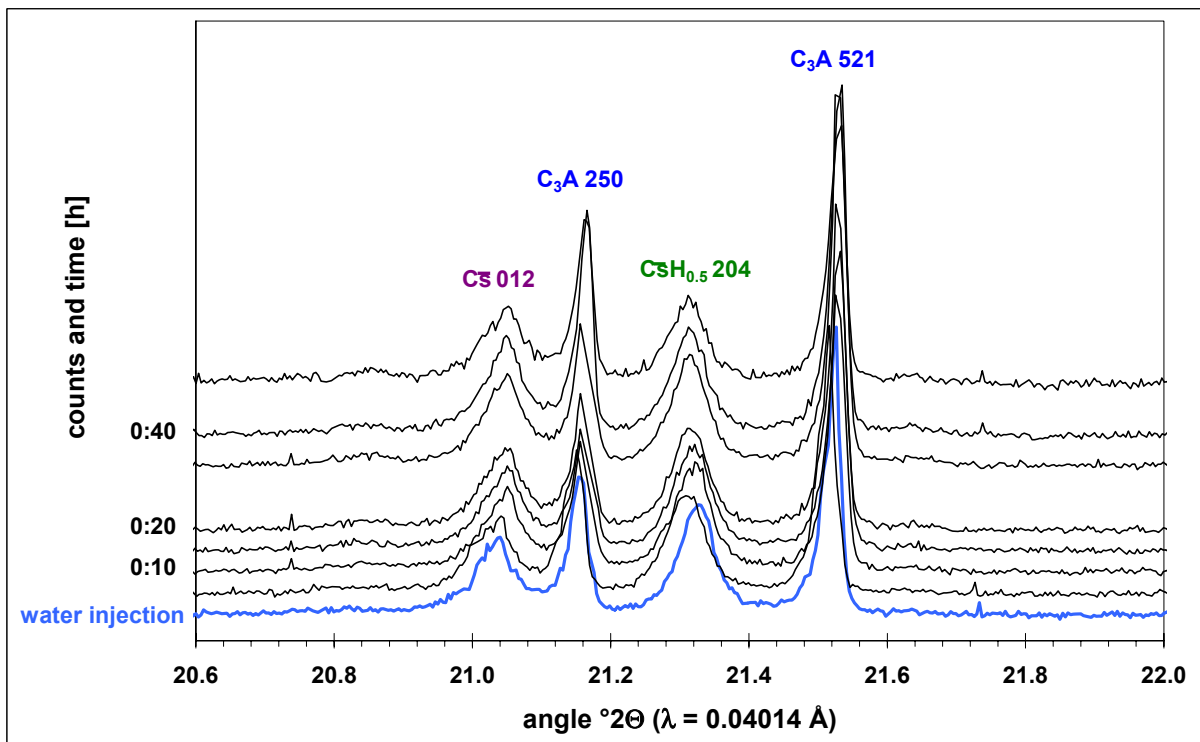


Fig. 5.33: Disturbed early ettringite crystallization in $\text{Ca}(\text{OH})_2$ -saturated aqueous solution. Only little Ca-sulphate was consumed.

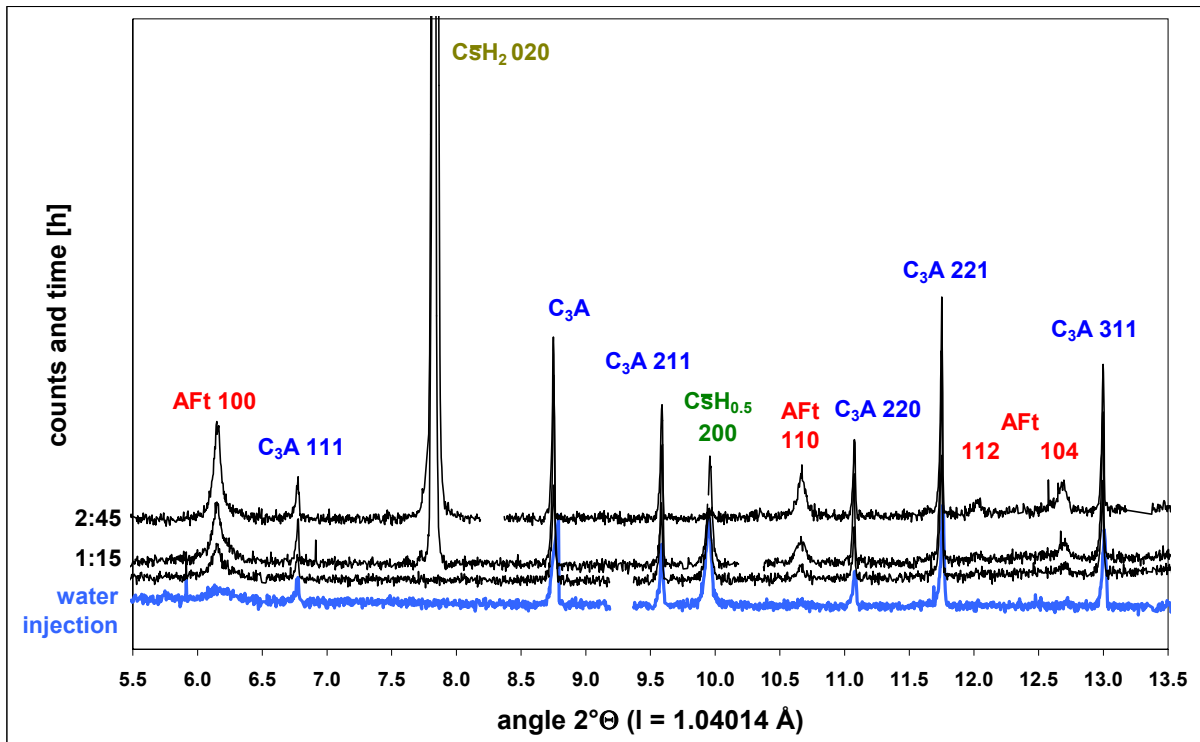


Fig. 5.34: Disturbed ettringite crystallization in $\text{Ca}(\text{OH})_2$ -saturated aqueous solution. This experiment was performed with a pure phase mixture of 70 mass-% C_3A , 15 mass-% anhydrite and 15 mass-% bassanite. Instead of ettringite much more gypsum hydrated from bassanite than in low-pH solutions.

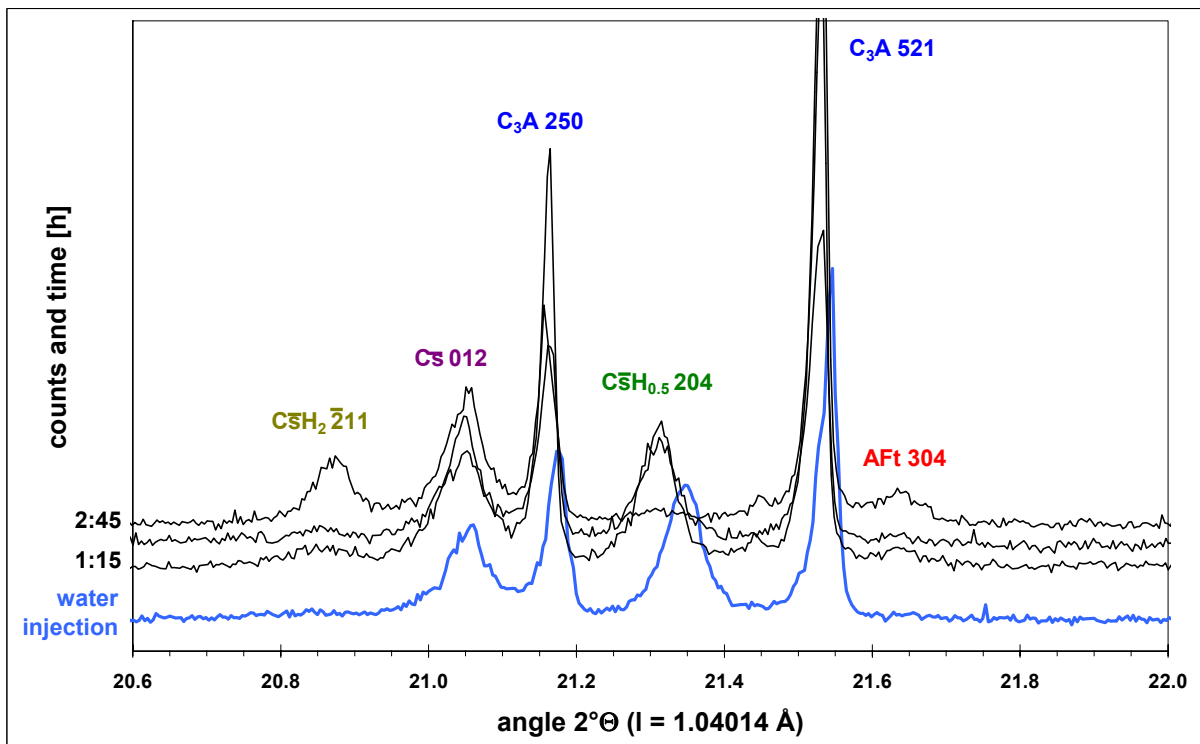


Fig. 5.35: Disturbed ettringite crystallization in $\text{Ca}(\text{OH})_2$ -saturated aqueous solution. Bassanite is consumed in gypsum formation.

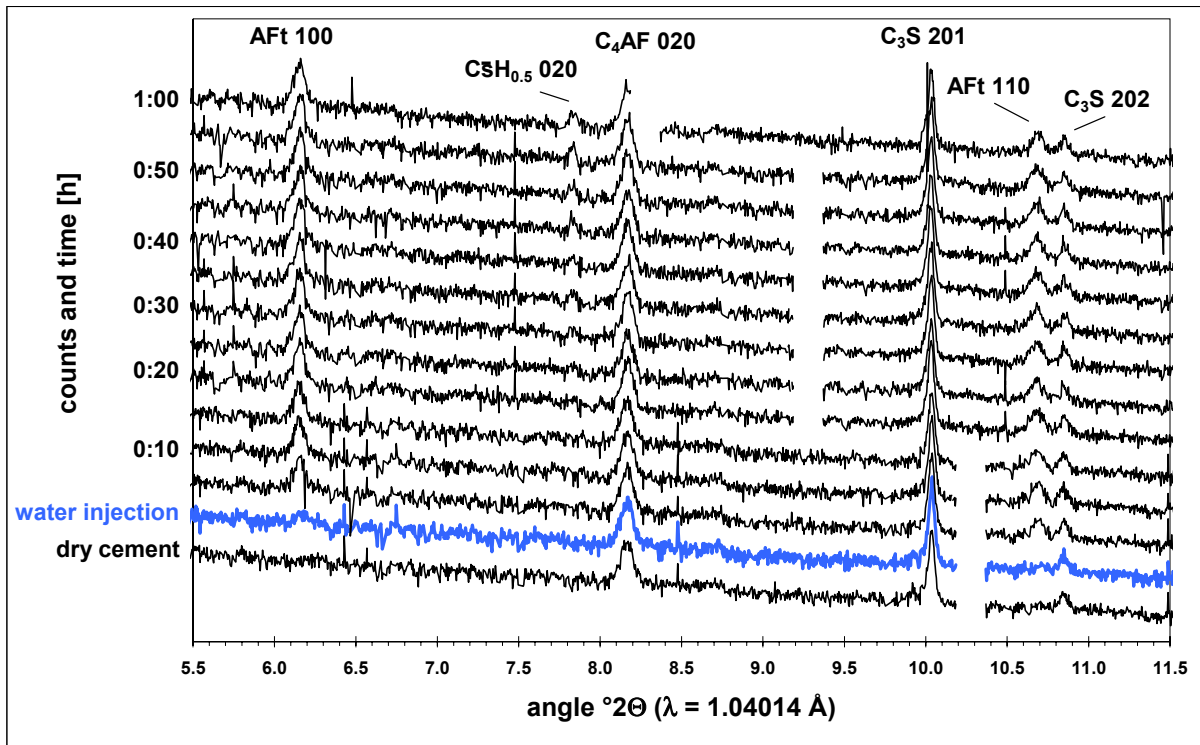


Fig. 5.36: Early hydration of Portland cement. During running measurements of synchrotron XRD tap water was injected into the sample.

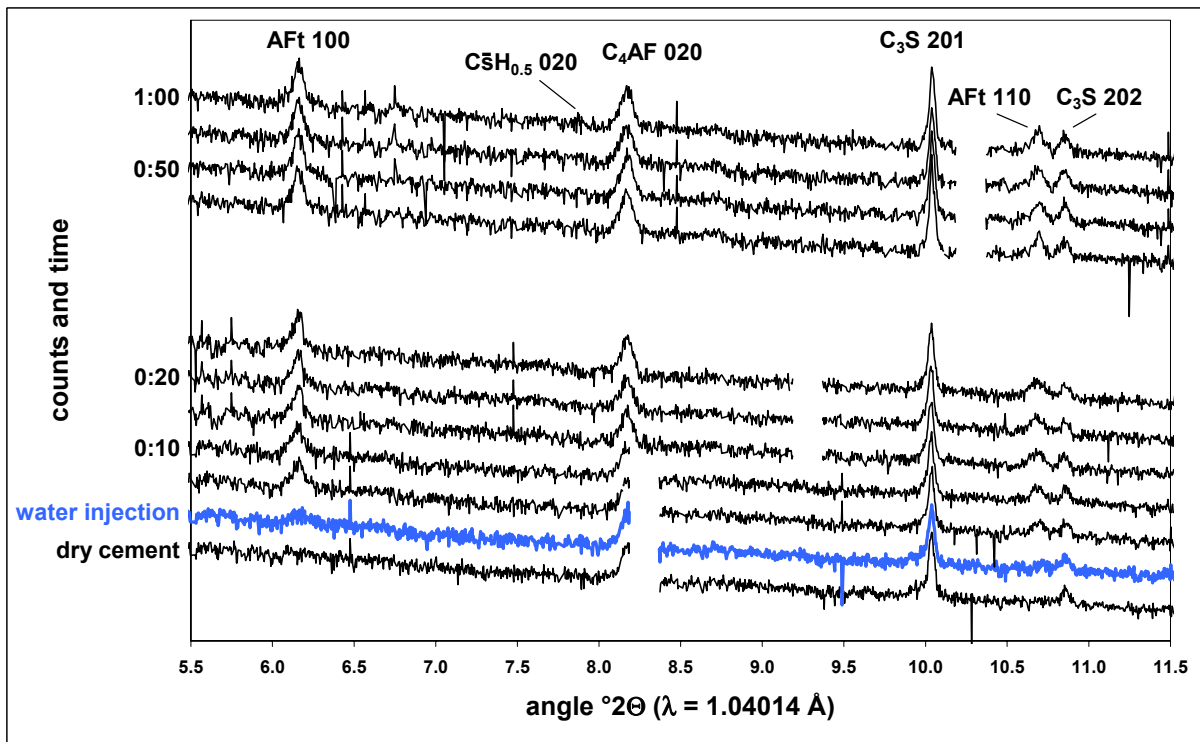


Fig. 5.37: Early hydration of Portland cement. During running measurements of synchrotron XRD $Ca(OH)_2$ -saturated aqueous solution was injected into the sample.

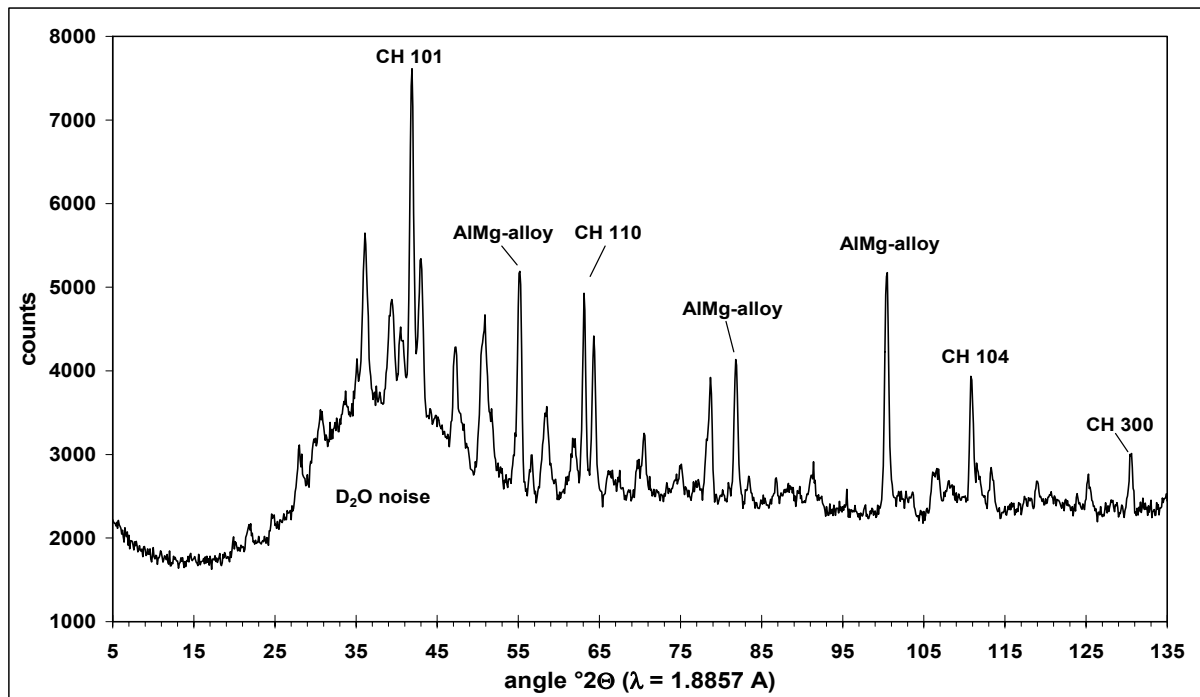


Fig. 5.38: Neutron diffraction pattern of a cement without CE after 24 hours hydration time in a slurry with heavy water (D_2O). Indicated are the strongest peaks of portlandite and the AIMg-alloy, the material of the sample carrier.

5.2.6 Thermal Neutron Powder Diffraction

During the work at the SLS there was also the opportunity to monitor cement hydration by thermal neutron diffractometry at a wavelength of 0.18857 nm (1.8857 Å). Neutron diffraction follows Bragg's law like X-ray diffraction. That means that the peak positions plotted over d_{hkl} are principally the same in both methods. While X-rays are diffracted by the electron shells, neutrons are scattered by collision with the atom cores. This results in different intensities at the same d-position. The differences can be enormous since very low intensities down to zero might occur with one method while the other gives a distinct peak at same d-value.

A disadvantage of neutron diffractometry is the long integration time of 30 minutes and the lower spatial resolution (1200 channels/160° 2θ), both caused by less intense radiation. Nevertheless a pilot test using an aged sample from earlier synchrotron measurements was promising despite of the long integration time. The ettringite and portlandite peaks were much stronger than measured with X-rays. Neutron diffractometry put emphasis on phases with light elements especially with water because the impulse transmission from nucleus to neutron is the better the closer the atomic mass is to that of the neutron. Hydrogen works best. To avoid high background from pore water, heavy water (D_2O) with lower refractive capacity was used. The hydration of cement took place in heavy water over 24 hours. It was assumed

that "deuterated" cement develops comparable phases to hydrated cement. The results of wet paste experiments were disappointing. Ettringite and gypsum peaks were hard to see. Rietveld analysis was not reasonable because two important phases were missing. Instead the portlandite peaks still were very strong (fig. 5.38). The kinetics of portlandite crystallization in absence and presence of different CE-types was evaluated qualitatively by single peak intensity analysis. Since the peaks were strong and sharp, the measurement of their height above background was efficient enough to study the influence of various cellulose ethers on the crystallization kinetics of this phase in comparison. The sum of all measured peak heights of CH per scan was set in relation to that of the AlMg-alloy of which the sample carriers were made. Figure 5.39 shows the DS-specific retarding effect of the MHPC types. MHEC 1.5 is close to MHPC 1.7, a result that confirms that beside the DS the type of substituent also determines the influence on hydration kinetics (see also chapter 5.2.4). Small amounts of portlandite already crystallized at the start of cement hydration. This result is in line with Stark's result who also reported an early CH precipitation^[Sta1, Sta2]. Neutron Diffraction reconfirmed the results achieved with other methods, but in comparison to synchrotron XRD it did not provide any new insights with respect of CE-caused retardation.

Conclusion

- Small amounts of Portlandite are already formed in the early stage of hydration.

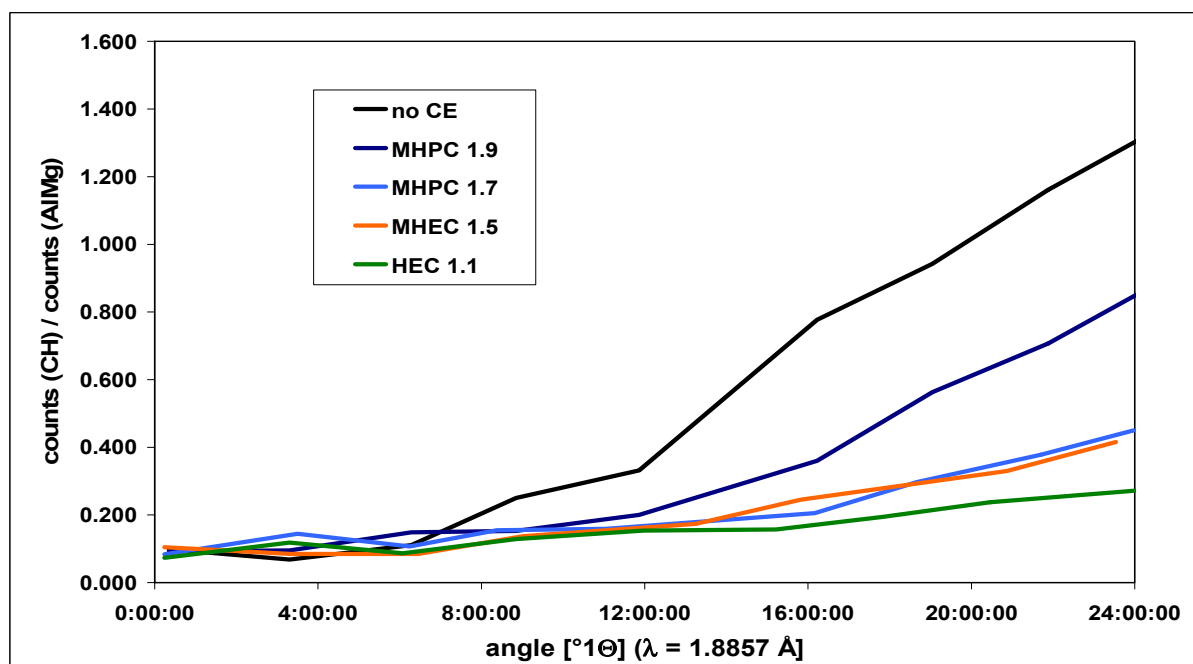


Fig. 5.39: Phase development of portlandite and the DS-specific retarding effect on CE, monitored by neutron diffraction in-situ.

5.2.7 ESEM-FEG

ESEM-FEG images were taken from MHPC 1.7 and HEC 1.1 blended samples as well as from a reference without CE. In the reference sample small and very few ettringite crystals without distinct crystal morphology could already be seen after 15 min (fig. 5.40). First needle-shaped CSH-crystals of sizes of about 500 nm appeared after 4 hours (fig. 5.41). At this time ettringite appeared as short prismatic hexagonal crystals. After 7 hours of hydration (fig. 5.42) the cement particles were densely covered with CSH-needles and large CH crystals appeared in former voids. The MHPC 1.7 sample showed a similar picture as the reference after 15 minutes. After 4 hours of hydration the very first tiny CSH needles could be observed. They were smaller and fewer than those of the reference after the same time of hydration. Three hours later the CSH crystals had grown and their number increased. But the cover of the primary clinker particles is not as dense as it was in the reference sample at the same hydration time. HEC 1.1 showed the strongest retardation effect. Even at a hydration time of 4 hours, CSH could not be observed. At 7 h the state of hydration is similar to the state of the MHPC 1.7 sample at 4 h (fig. 5.43 - 5.47).

Samples containing cellulose ethers showed a homogeneous, massy texture 15 minutes after stirring. In contrast, the texture of the reference sample without CE was inhomogeneous. Particles agglomerated in clusters with larger voids in between (fig. 5.48, 5.49). This confirms that the cohesion within the paste is improved in presence of CE as could be seen during ultrasonic measurements (chapter 5.2.1). This correlates with the results of SEM studies made by Ridi et al. [Rid1] who described the texture of cementitious extrusion pastes as more dense in presence of MHEC than without CE.

Conclusions

- The primary clinker particles are less densely covered by hydrated phases in presence of CE than in samples without CE at any time of hydration. The amount of hydration products depends on the DS of the added CE. The lower the DS the less hydration products precipitate at the same hydration time.
- CE-blended cement samples have a homogenous texture. Samples without CE show particles agglomerated in clusters with large gaps between. This confirms the improved cohesion of the particles within the cement in presence of CE.

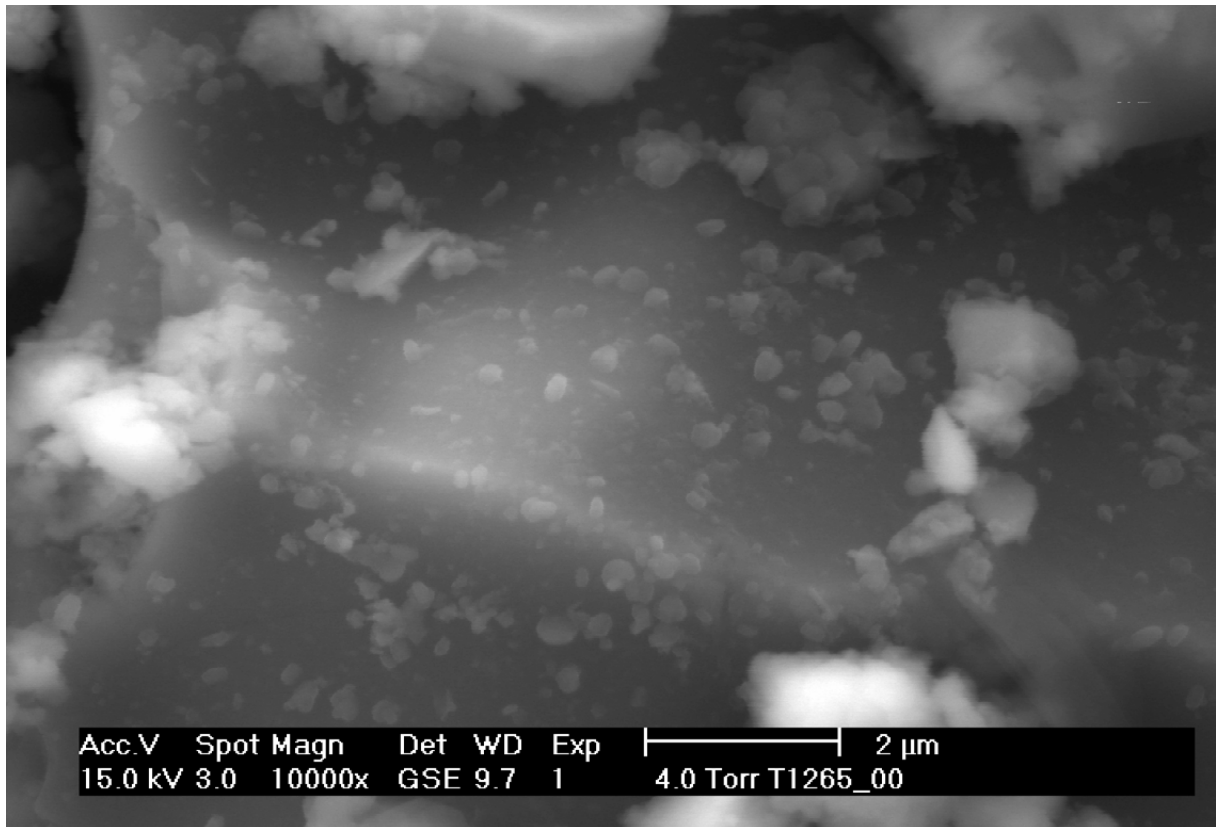


Fig. 5.40: ESEM-FEG image of a Portland cement without CE after 15 minutes of hydration. Tiny ettringite crystals are formed on the surface of a primary clinker particle.

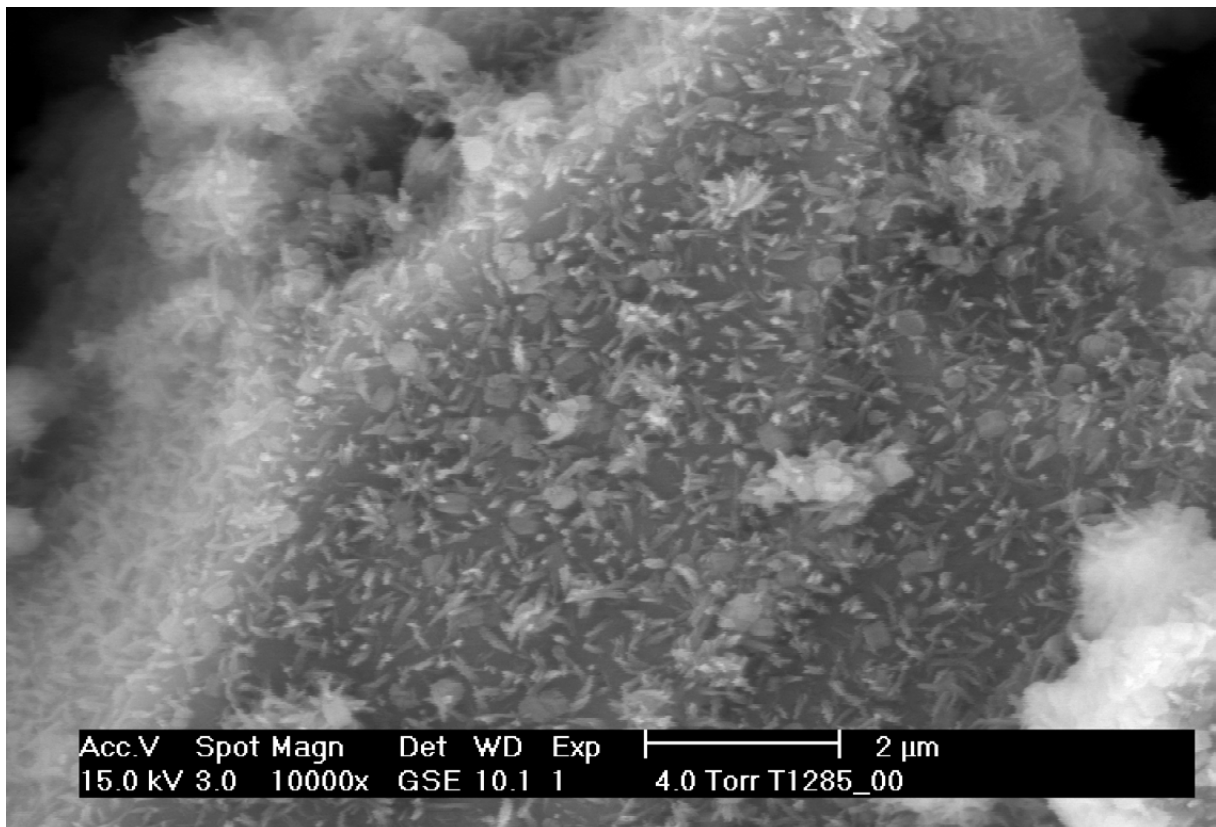


Fig. 5.41: ESEM-FEG image of a Portland cement without CE after 4 hours hydration time. Needle shaped CSH crystals occur beside short prismatic ettringite.

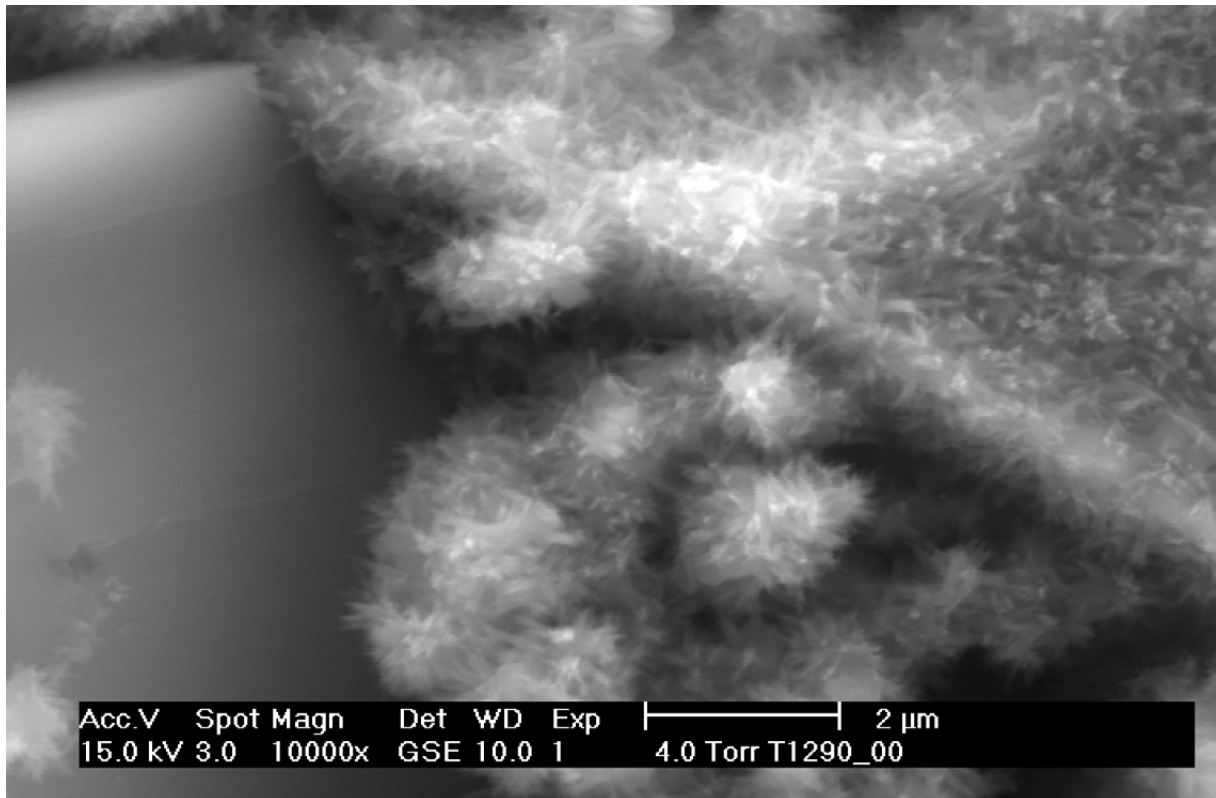


Fig. 5.42: ESEM-FEG image of a Portland cement without CE after 7 hours hydration time. The primary cement particles are densely covered by needle-shaped CSH crystals. A big CH crystal can be seen on the left side.

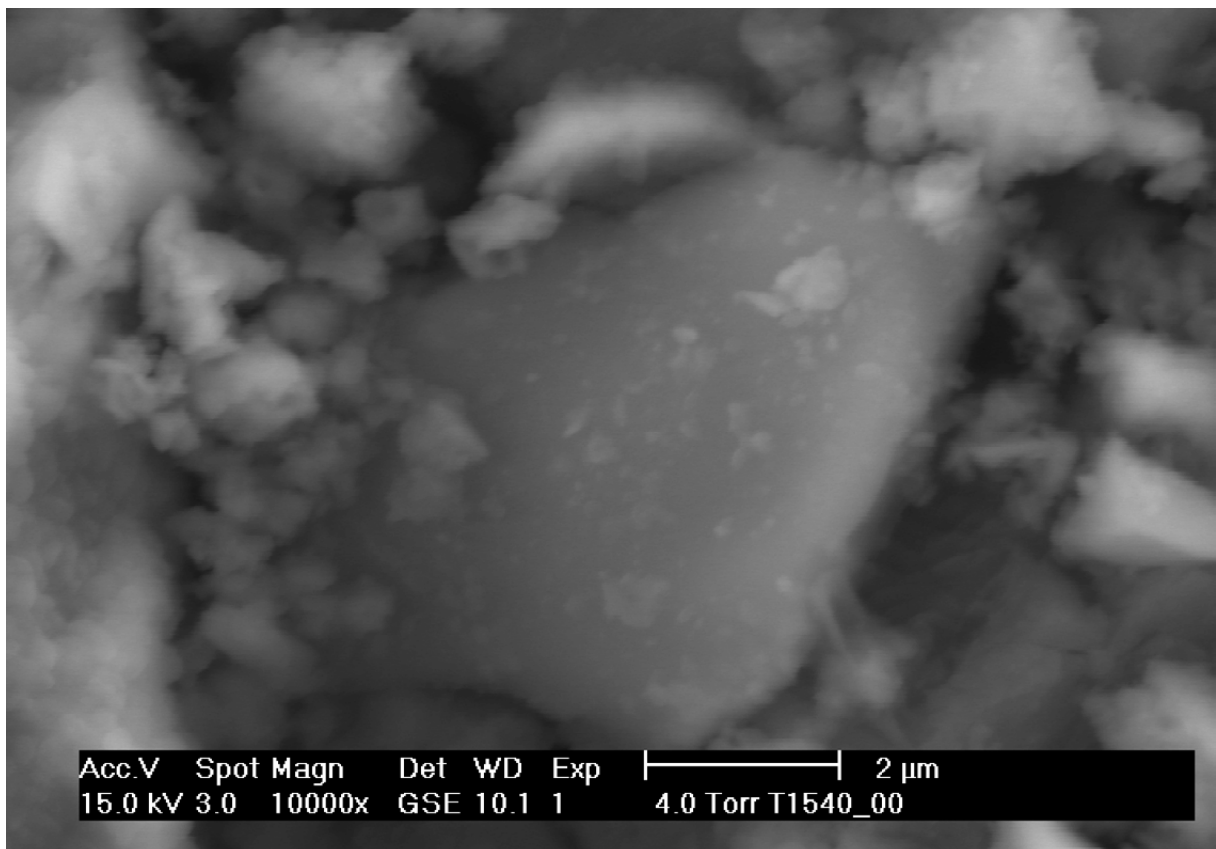


Fig. 5.43: Portland cement with MHPC 1.7 after 15 minutes hydration time.

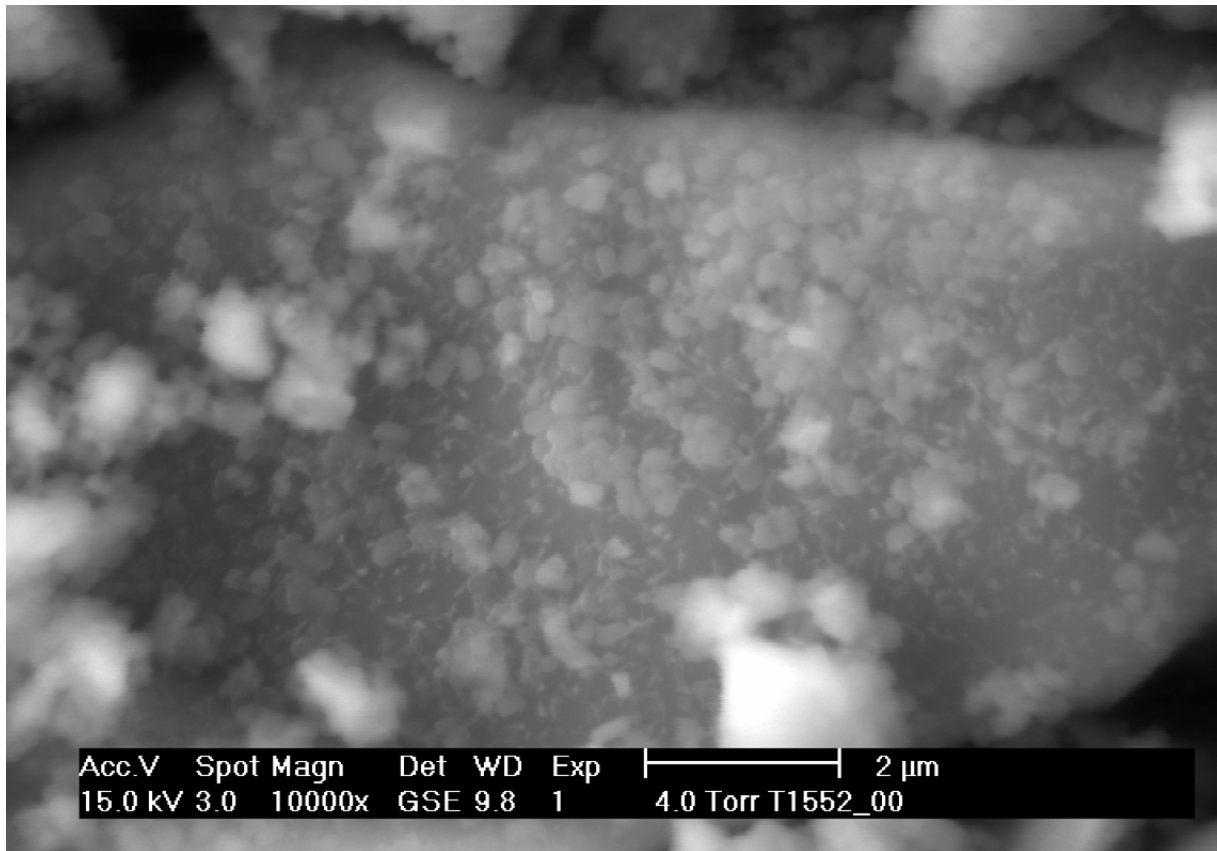


Fig. 5.44: Portland cement with MHPC 1.7 after 4 hours hydration time.

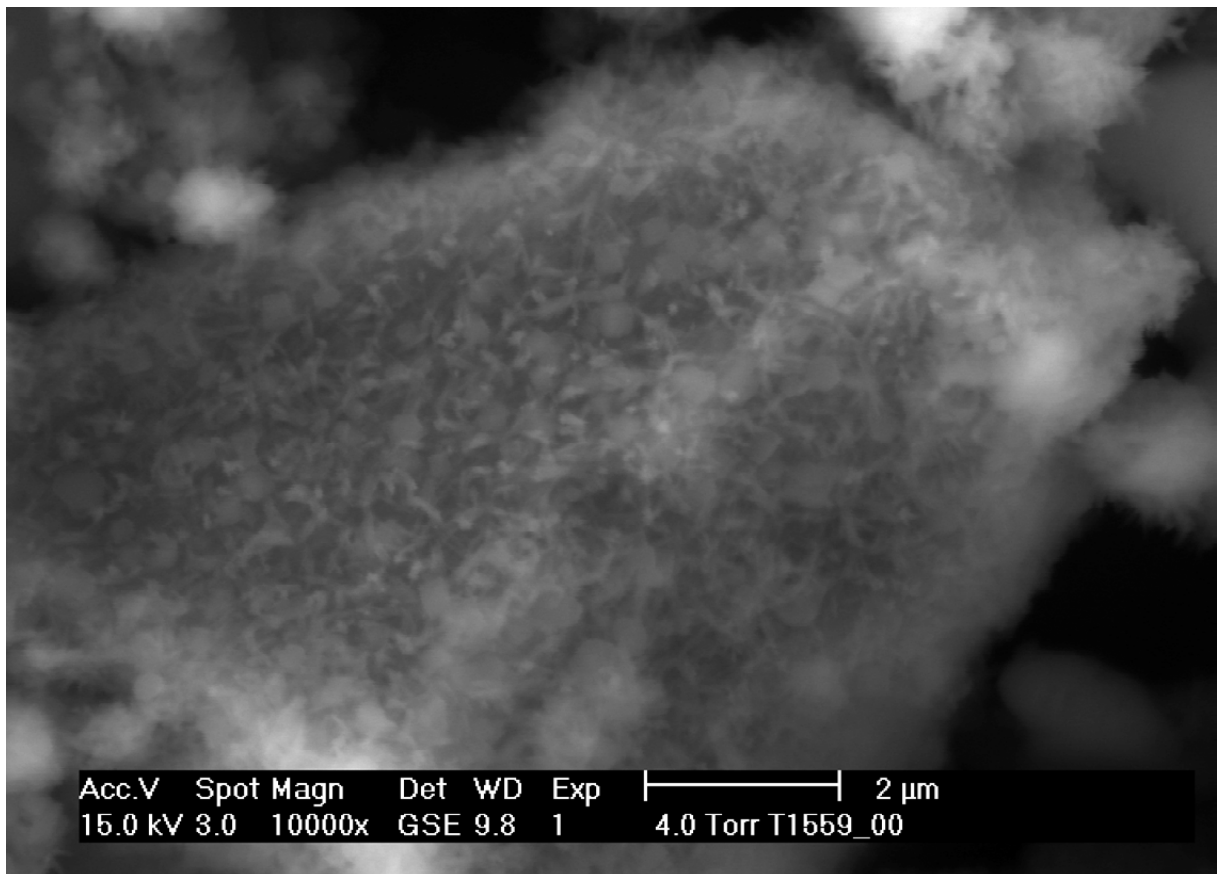


Fig. 5.45: Portland cement with MHPC 1.7 after 7 hours hydration time.

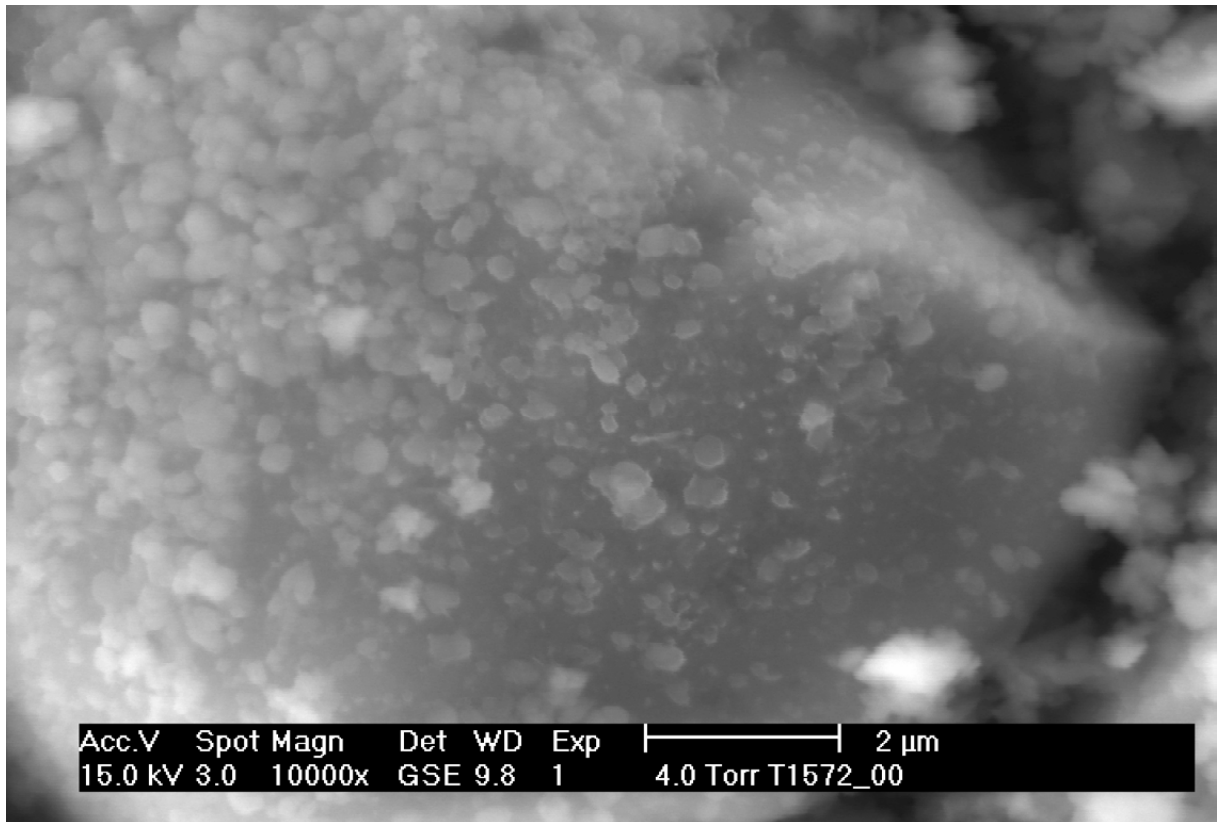


Fig. 5.46: Portland cement with HEC 1.1 after 4 hours hydration time.

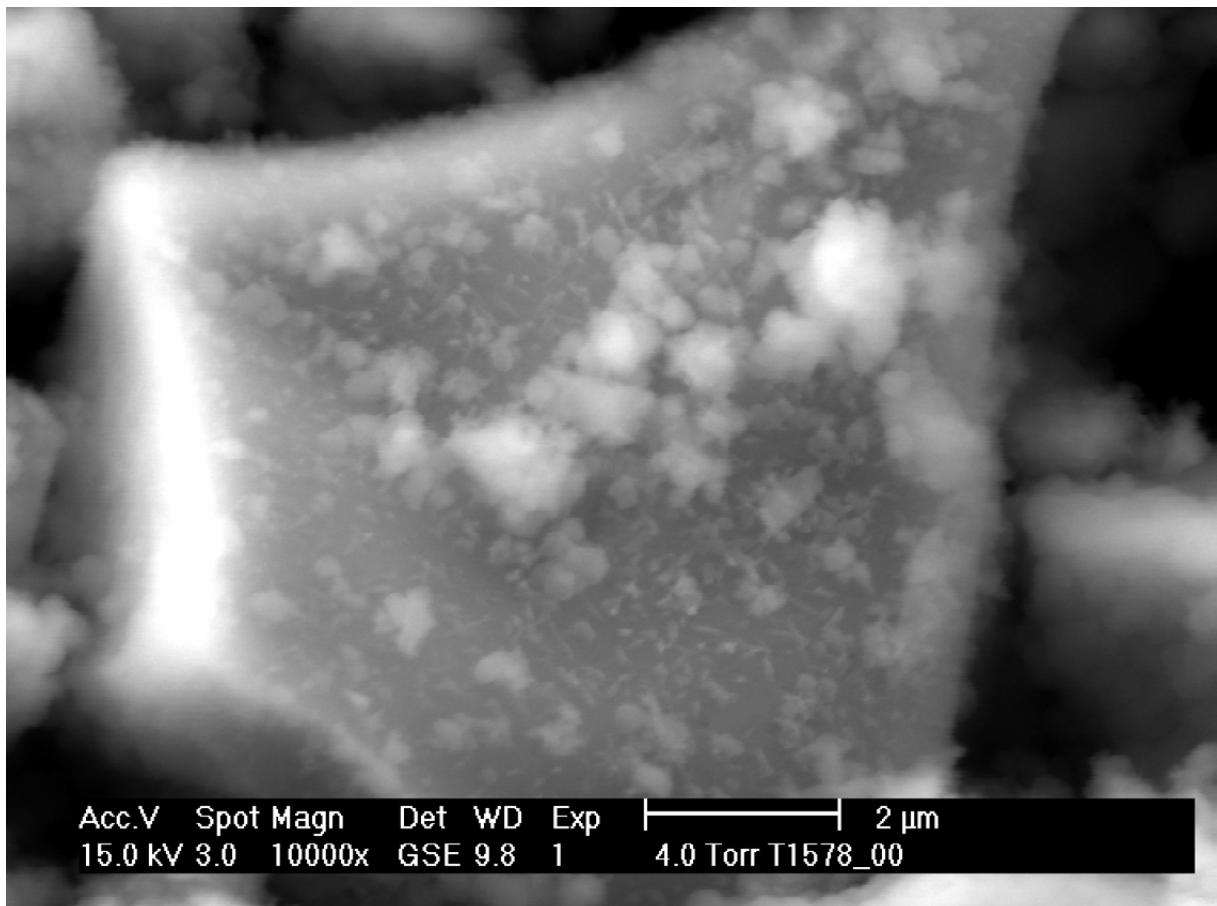


Fig. 5.47: Portland cement with HEC 1.1 after 7 hours hydration time.

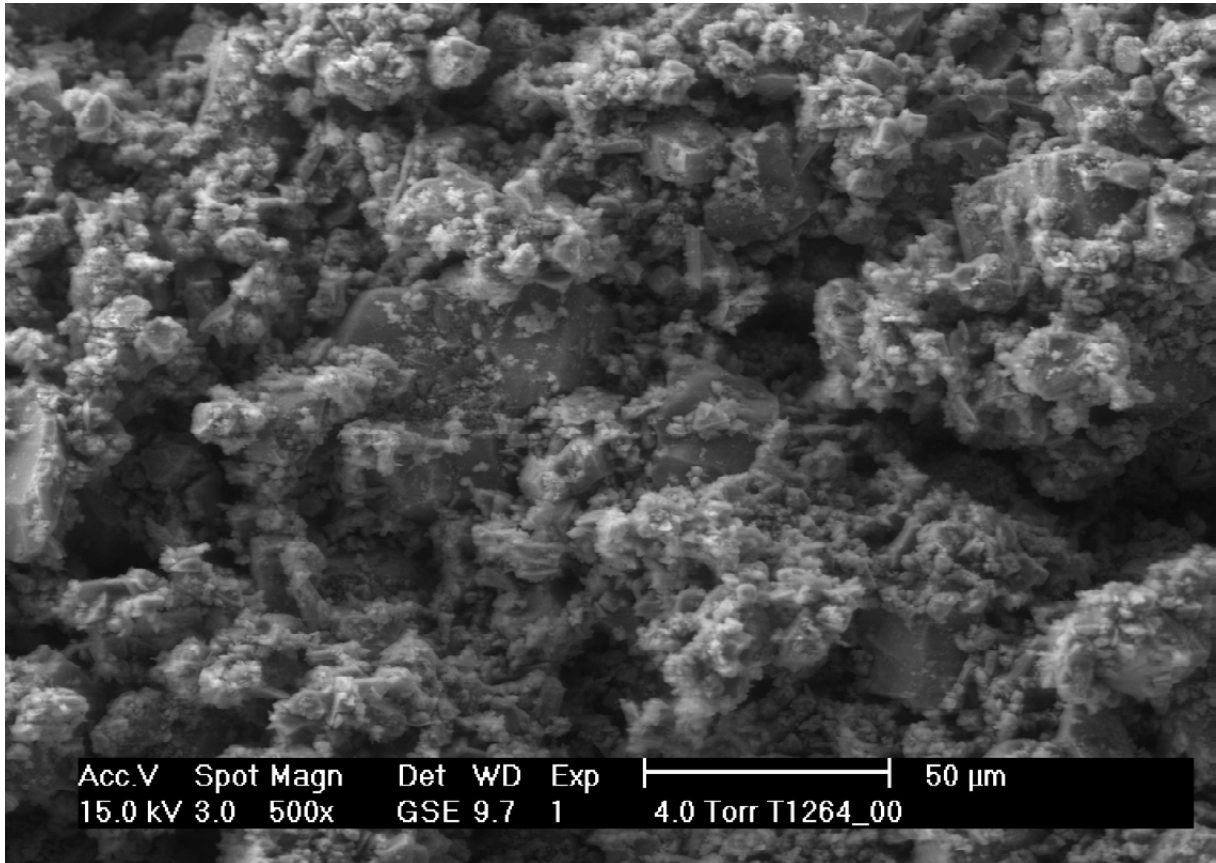


Fig. 5.48: Inhomogeneous texture of cement sample without CE 15 minutes after stirring.

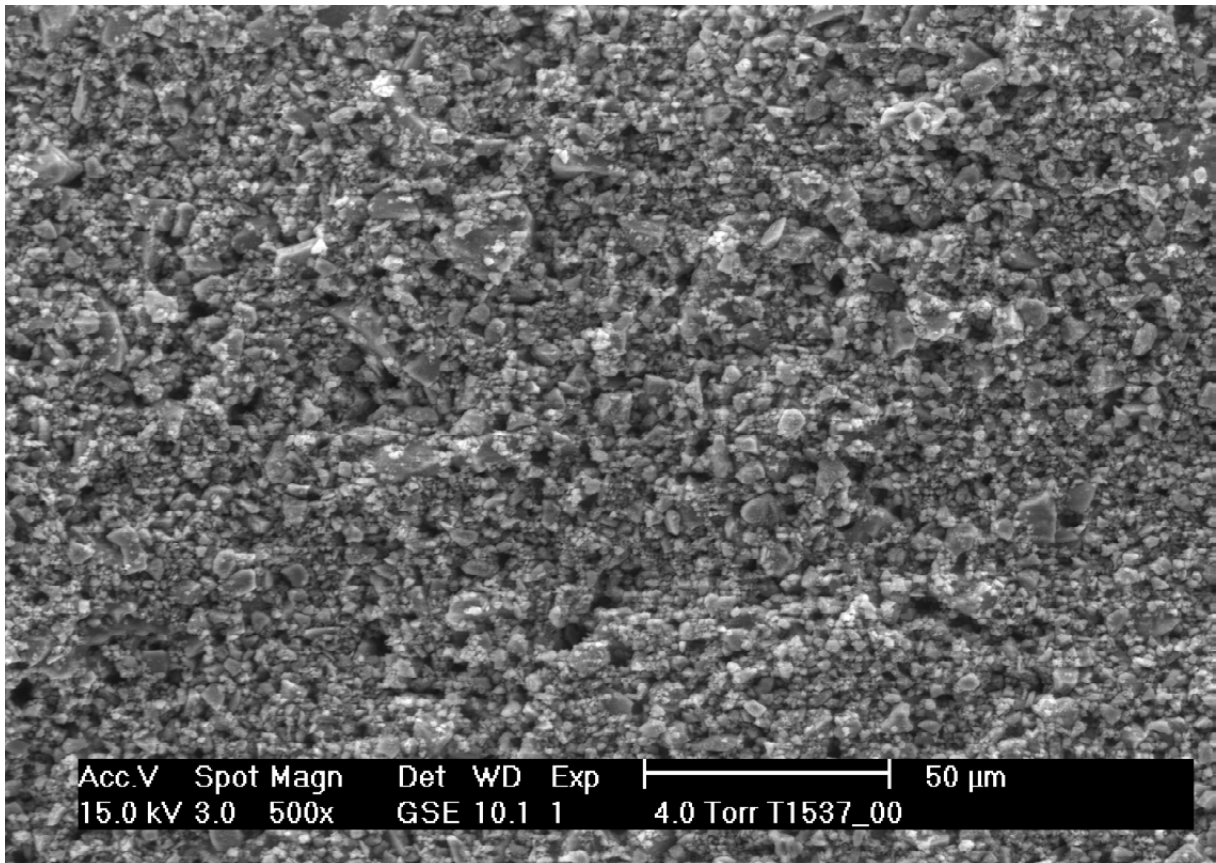
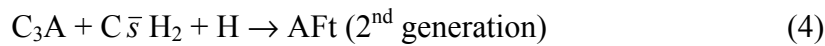


Fig. 5.47: Homogenous texture of a cement sample containing MHPC 1.7.

6. Summary

6.1 Portland Cement Hydration without Cellulose Ether

During the hydration of the investigated Portland cement the following phase reactions were observed within the first 24 hours:



In the reference sample without cellulose ethers these reactions took place as follows: The first ettringite crystallization started immediately after water contact and last for about 10 minutes (1). Probably the anhydrite hardly contributed to this reaction since it was significantly less reactive than the bassanite. After this process had stopped the supernatant primary sulphate carriers (both) hydrated to gypsum until 4 hours (2 and 3). The different activities of anhydrite and bassanite during reactions (1) to (3) is a conclusion from experiments with pure phase mixtures of C_3A , $C\bar{s}H_{0.5}$ and $C\bar{s}$ investigated by synchrotron XRD (fig. 5.29 – 5.31). Figure 5.29 shows clearly that bassanite is consumed in ettringite formation directly after water contact while anhydrite kept stable for a longer time. Anhydrite dissolves much slower (fig. 5.31) at a time when gypsum appears (fig. 5.30).

After about 4 hours renewed ettringite growth occurred in OPC (4) contemporary with portlandite precipitation (5). In the second ettringite formation gypsum is consumed. Portlandite is a side product of calcium silicate hydration. In this case it was C_3S that mostly contributed to portlandite formation because C_2S was much more stable within the first 24 hours of hydration (fig. 5.22). The formation of monosulphate and the hydration of $C_2(A,F)$ were not observed in the given time. So far they correlate with the studies of Scrivener ^[Scr1], Stark ^[Sta1, Sta2], and Rothstein ^[Rot1].

In experiments with pure phase mixtures in tap water and without silicates the reaction of C_3A with calcium sulphates turned out to be a continuous process, combining reactions (1) to (3) with only little gypsum formation (fig. 5.30). In calcium hydroxide saturated solution the ettringite formation was strongly inhibited. Instead, bassanite hydrated to gypsum while anhydrite kept stable (fig. 5.34, 5.35). Before gypsum formation no primary sulphate carrier was consumed. Transferring these results to the reactions observed in Portland cement hydration the author of the present study came to the conclusion that the ettringite formation

in cement was basically controlled by the level of Ca(OH)_2 -saturation in the pore water. Little ettringite was formed in reaction (1) until the dissolution of C_3S leads to Ca(OH)_2 -saturation. The level of saturation decreased as portlandite (solid Ca-hydroxide) precipitated (5), thus allowing ettringite to crystallize further (4). The question is if the high pH-level or the ion concentration of Ca^{2+} controlled the ettringite precipitation. The answer was given by Rothstein et al ^[Rot1]. Their studies showed that the pH-level was high at all times while the Ca^{2+} -concentration dropped down drastically with portlandite precipitation. Therefore the author of the present study assumes that the Ca^{2+} -concentration controls the ettringite crystallization. A concentrated ion-solution decreases the solubility of solids that contain the same ion components as the solution. Therefore the dissolution rates of Ca-sulphates or C_3A were decreased by high Ca^{2+} -concentration in the pore water leading to a lack of either sulphate- or aluminate-components for ettringite formation. Since the sulphates hydrated to gypsum, a dissolution-precipitation-process, it was rather the C_3A that was inhibited to dissolve and therefore there was probably not sufficient amount of the aluminate component dissolved in water for ettringite growth. Evidence for a lack of dissolved aluminium component to be responsible for the disturbed ettringite formation during the dormant period of Portland cement hydration is the fact that ettringite formation can be increased by the addition of Al(OH)_3 as described in chapter 5.2.3. The solubility of aluminium hydroxide, a further aluminium source for ettringite formation, did not seem to be affected by a high Ca(OH)_2 saturation level in the pore solution.

Conclusions

- Ettringite crystallization is controlled by the Ca(OH)_2 -saturation level.
- A high Ca(OH)_2 -concentration in the pore water inhibits the dissolution of C_3A , leading to a lack of dissolved aluminate component needed for ettringite crystallization.
- The lack of dissolved aluminate component can be compensated by adding Al(OH)_3 .

6.2 CE-caused Retardation

Cellulose ethers showed a retarding effect on cement hydration. As a result of this study one key parameter is the degree of substitution: the lower the DS the stronger the retardation. This result was confirmed by independent experimental methods such as ultrasonic and calorimetric measurements, laboratory and synchrotron X-ray diffraction as well as neutron diffractometry and environmental scanning electron microscopy. Those results were also confirmed by the studies of Pourchez^[Pou1] and Haecker^[Hae2]. The influence on single reactions during hydration was differentiated. The first ettringite formation in Portland cement was not affected at all by the presence of CE. This result correlates with those of Peschard^[Pes1]. Since only little ettringite was formed at this point of hydration the residual sulphates reacted with water to gypsum. This reaction was slightly retarded by CE depending on the degree of substitution. This is in agreement with the study by Brandt^[Bra2]. The renewed ettringite crystallization is strongly retarded by cellulose ethers as a function of DS. Generally, the lower the DS the stronger the retardation. MHPCs showed stronger effects than MHECs. The delay of second ettringite formation correlated with the strong CE-caused retardation of portlandite precipitation. Pure phase experiments using HFC confirmed the DS-specific strong retardation of C₃S hydration but showed only a weak and DS-unspecific effect on the hydration of C₃A in presence of sulphates and in absence of silicates. The latter effect is ascribed to an unspecific influence of increased viscosity of the pore solutions with reduced ion mobility. As discussed earlier, second ettringite formation takes always place contemporaneously with portlandite precipitation and a steep decline of the Ca²⁺-concentration in the pore water. It is assumed that by retarding the CH precipitation, together with a delay of CSH formation, the decline of the Ca²⁺-concentration in the pore solution was also delayed. Thus the second ettringite crystallization was indirectly retarded by CE in the presence of silicates. This would also explain that the retarding effect of CE on the reaction of calcium aluminate with sulphates in absence of silicates (chapter 5.2.2) is weak and unspecific.

Cellulose ethers retard the C₃S hydration significantly, in Portland cement as well as the pure phase. The lower the degree of substitution the stronger the retarding effect. MHPCs have a stronger retarding effect than MHECs at same DS. C₃A hydration is indirectly affected by CE in Portland cement, while the retarding effect on the hydration process in pure phase mixtures is weak and independent of the DS.

Conclusions

- The DS-specific retarding effect of cellulose ethers is confirmed by several independent investigation methods: ultrasonic, HFC, laboratory and synchrotron XRD, n-diffraction and ESEM-FEG imaging.
- CEs have a direct retarding effect on C_3S hydration: The lower their DS the stronger the retardation.
- The C_3A hydration in Portland cement is controlled by the $Ca(OH)_2$ -saturation level in the pore water with an indirect influence of CE.
- The $Ca(OH)_2$ -saturation level in the pore water is affected by the presence of CE depending on the degree of substitution. CE retards the portlandite precipitation DS-specifically. The delayed CH precipitation leads to delayed decrease of $Ca(OH)_2$ -concentration in the pore water. Thus the second ettringite formation is retarded, too.

6.3 CE-adsorption

The DS-specific retardation of Portland cement could be ascribed to the differentiated adsorption behaviour of cellulose ethers on the surfaces of cement phases. The highest amount of CE adsorbed was found on C_3S . The lower the DS the more CE was adsorbed. The C_3S hydration was mostly affected by the cellulose ether DS-specifically. High amounts of CE also adsorbed on portlandite but the adsorption was DS-independent. A DS-specific adsorption was found on gypsum but with significantly smaller amounts than on C_3S . Gypsum crystallization was moderately and DS-specifically retarded in OPC. No adsorption of CE at all was found on ettringite. CE did not effect the first ettringite crystallization, the second ettringite formation was indirectly affected as discussed earlier.

The conclusion suggests that the adsorbed cellulose ether on the surfaces of the cement phases retards the crystal growth of the hydration product. Strong adsorption was found on C_3S and portlandite and the C_3S hydration was strongly retarded. The DS-dependence of this retardation could not be explained by CE-adsorption on portlandite since it was DS-independent. But the strong adsorption on C_3S could be correlated with the degree of substitution. The adsorption behaviour of cellulose ethers on CSH-phases could not be determined. For gypsum and ettringite the relation between adsorption and retardation is obvious: moderate and DS-specific adsorption on and retardation of the gypsum, no adsorption and no direct effect on the ettringite. The CE-caused effects on the cement phases and their hydration processes are summarized in table 6.1.

The CE-adsorption on the surfaces of cement phases apparently increased with proceeding hydration time. Two different mechanisms might be responsible for this effect: 1. The steadily increasing total surface area with proceeding precipitation of tiny crystals of the hydration products. 2. Once a cellulose ether molecule was adsorbed on the surface of a growing crystal it could even be incorporated as inclusion as the crystal growth proceeded. The increasing amount of included molecules would then be falsely counted as "adsorbed on surface". The outward growing surface is covered by further molecules.

Comparison of the molecular weight distribution of CE dissolved in pore solution before and after adsorption experiments showed that smaller molecules adsorbed on portlandite preferentially, depending on the CE/portlandite ratio. The higher the ratio the more smaller molecules adsorbed on the mineral surface. The molecular weight distribution of the adsorbed polymers did not affect the total amount in mass per surface area of adsorbed CE.

Conclusions

- The DS- and phase-specific adsorption behaviour of cellulose ethers on cement phases is responsible for their retarding effect on Portland cement hydration.
- DS-dependence: The lower the DS the stronger the CE-adsorption and the stronger the retarding effect.
- Phase-dependence: The stronger the CE-adsorption on a specific cement phase, the stronger the retarding effect of CE on the hydration process in which this cement phase is involved.

phase admixture	CE-adsorption	observed process	CE-caused retardation	investigation method
OPC	strong, DS-specific	hydration	strong, DS-specific	ultrasonic
C ₃ S	very strong, DS-specific	dissolution	strong, DS-specific	synchrotron XRD
C ₃ S	very strong, DS-specific	hydration	strong, DS-specific	HFC
C ₃ A, no sulphates	strong, DS-specific		n.d.	
C ₃ A + sulphates	none	hydration	weak, unspecific	HFC
ettringite, 1 st generation	none	precipitation	none	synchrotron XRD
ettringite, 2 nd generation	none	precipitation	indirect, strong, DS-specific	synchrotron XRD
gypsum	moderate, DS-specific	precipitation	moderate, DS-specific	synchrotron XRD
gypsum	moderate, DS-specific	dissolution	indirect, strong, DS-specific	synchrotron XRD
portlandite	strong, unspecific	precipitation	strong, DS-specific	synchrotron XRD

Tab. 6.1: Phase-specific CE-adsorption and the CE-caused retardation of hydration processes.

7. Discussion

7.1 Stepwise Ettringite Formation

The mineral phase reactions of early cement hydration as monitored in the present study are generally in agreement with studies of Scrivener^[Scr1], Stark^[Sta1, Sta2], and Rothstein^[Rot1]. Cerulli^[Cer1] doubts the phase content of ettringite in an early stage of hydration as it was calculated by Rietveld analysis based on synchrotron X-ray diffraction data (Fig. 5.20). In his opinion about 80 % of all ettringite formed in the whole hydration process of OPC already precipitates within the first few minutes. The ettringite formed at this point of time is poorly crystalline and gives only a weak X-ray reflection. The so-called "second ettringite" crystallization is thereafter a recrystallization process forming a well-crystalline phase that results in stronger reflections. He argued that the existence of an X-ray amorphous ettringite phase is proven by ESEM-FEG images. Furthermore the results of quantitative phase analysis depend strongly on the sample preparation method. In-situ measurements always show weak reflections while samples quenched with acetone for laboratory X-ray diffraction show stronger signals. Indeed also in the present study the estimation of the ettringite content based on laboratory X-ray data of quenched samples suggests that approximately two thirds of all ettringite is formed within the first minutes (fig. 5.13), a figure that roughly correlates with Cerulli's estimation. An X-ray amorphous ettringite phase was also described by Eckart and Stark^[Eck1] based on ESEM-FEG images of hydrating pure phase admixtures of C₃A and Ca-sulphate. They reported a dependence of the ettringite morphology on the pH-value of the pore water. At a pH-level above 12 ettringite exists as very fine, X-ray amorphous crystals.

In the present study similar experiments with pure phase admixtures were done using synchrotron X-ray diffractometry instead of ESEM-FEG. The results show that the formation of crystalline ettringite was indeed strongly inhibited in Ca(OH)₂-saturated solution. But not only the ettringite reflections were weak, also the signals of the primary sulphate carriers kept stable until Ca-sulphate hemi-hydrate was consumed in gypsum precipitation (fig. 5.32-5.35). If significant amounts of X-ray amorphous ettringite were formed the consumption of primary sulphate carriers should had been indicated by a decrease of the intensity of their reflections. That was not the case.

A rough estimation of the sulphate consumption in Portland cement could be made based on Rietveld analyses of the synchrotron X-ray diffraction data. After 4 hours of hydration the cement paste of the control sample (without CE) consisted of 1.5 mass-% of gypsum (fig. 5.21) and 4 mass-% of (well crystalline) ettringite (fig. 5.20). The mass balance as given in chapter 5.2.4 indicates that ettringite has a Ca-sulphate (anhydrite) component of

approximately 38 mass-%. Gypsum has a Ca-sulphate component of 93 mass %. Therefore the mass content of Ca-sulphate bond in ettringite and gypsum after 4 hours of hydration was 2.9 mass-% in OPC which is fairly close to the 3 mass-% of primary sulphate carriers. This did not leave much sulphate for the formation of X-ray amorphous ettringite. The existence of an X-ray amorphous phase cannot be excluded. But if the formation of this phase does not consume sulphate, it is reasonable to doubt in a chemical composition of that of ettringite. Moeser ^[Moe1, Moe2] gave an explanation why ettringite and other cement phases occasionally occur as poorly crystalline phases in ESEM-FEG images. The tiny crystals were destroyed by the electron beam resulting in a change of the chemical composition and the loss of crystallinity.

Stark et al. ^[Sta3] explained the stepwise growth of ettringite by changing accessibility of C₃A during the hydration process. The present work shows that the ettringite crystallization could as well be controlled by the ion-concentration, especially the Ca²⁺-content in the pore water. Lothenbach et al. ^[Lot1] showed that the thermodynamic modelling of the temporal development of the equilibria between fluid and solid phases showed a good correlation with the actual phase development in Portland cement.

The author of the present thesis comes to the conclusion that: 1. ettringite formation in Portland cement is a process of two different crystal growth stages, 2. the crystal growth of ettringite is controlled by the ion-saturation in pore water and not necessarily by accessibilities of its educts, 3. X-ray amorphous ettringite does not exist in early hydration stage of undisturbed cement and the second ettringite generation is no recrystallization process since it would not correlate with the sulphate balance and therefore 4. the amount of ettringite formed during first generation correlates with the results of quantitative phase analysis based on in-situ synchrotron X-ray diffraction data.

7.2. Interactions of Cellulose Ethers with Cement.

It is generally accepted that cellulose ethers have a significant DS-specific retarding effect on cement hydration mechanism. But the nature of the CE-cement interaction is subject of controversial discussions. Some authors believe in alkaline degradation of CE in the pore water of cement and ascribe the retarding effect to degradation products. The chemical stability of CE against alkaline degradation is indeed a function of DS. The higher the DS the stronger the CE's resistance. Furthermore sugar acids as degradation products of polysaccharides are well-known for their strong retarding effects on cement hydration. Peschard et al ^[Pes1] followed this idea and found degradation products of dextrin and starch

ethers but not of cellulose ethers. This correlates with results achieved in this study where no degradation of CE in highly alkaline solution within 24 hours was found (chapter 5.1). Furthermore cellulose ethers are produced in high alkaline caustic soda for several hours at temperatures above 100 °C. There is no reason why a molecule that survived this treatment should give up within four hours at room temperature to let its degradation product retard the portlandite formation in time.

Whether a chemical reaction between CE and the mineral phase on the surface of the crystal take place as Coarna et al. ^[Coa1] assume based on electron spectroscopy data, could neither be confirmed nor denied in the present study. Nevertheless a DS-specific adsorption behaviour of cellulose ether is obvious since significant amounts of CE vanished from the fluid phase (fig. 5.01). Whether the nature of CE-adsorption is rather more a physisorption or chemisorption still remains unanswered.

Haecker ^[Hae2] agrees that both effects are DS-specific but in his opinion the CE-adsorption is not necessarily the reason for retardation. He argues that the CE-caused retardation of cement can still be enforced by increasing the CE/cement ratio above the maximum amount of CE that can be adsorbed. However, cement hydration is a dynamic process which involves neo-formation of hydrated phases. Therefore new surface area is generated continuously, which is suitable for CE-adsorption. Dynamic adsorption experiments showed that the amount of adsorbed CE increases with progressing hydration time. Figure 5.01 shows that 0.5 masspercent of HEC on Portland cement was completely adsorbed after 8 hours. That means that from this point on, the pore solution was CE-free. Further crystallization processes cannot be influenced by CE in solution anymore. A higher dosage level of CE would certainly have affected the ongoing hydration process. An adsorption analysis after 4 hours showed that 30 masspercent of the added HEC was not adsorbed (at this point of time). Nevertheless this 30 % and probably more would have had a retarding effect on further processes. The difficulty is to determine the maximum amount of CE that can be adsorbed in such a dynamic process.

8. Outlook

The degree of substitution was determined as a key parameter of cellulose ethers that controls the adsorption behaviour of the polymer. But no relation was found between DS and the properties of the surfaces of those mineral phases on which CE adsorbs. Further studies of CE-adsorption in batch-type experiments on a widened range of minerals are necessary to correlate CE-adsorption with surface characteristics of the mineral phase. Those minerals do not have to be phases of construction materials necessarily. It is worth to study the adsorption behaviour of cellulose ether on any suitable mineral phase. Minerals with perfect cleavage like talc, micas and carbonates seem to be the best objects to be investigated since those minerals are also suitable for atomic force microscopy (AFM). Especially the micas are very interesting due to the broad variety of the chemical composition. F. Brandt^[Bra1] investigated the crystal growth of gypsum in presence of CE by AFM and found a change in surface step growth at very low DS (HEC 1.1). Since cellulose ethers showed a stronger affinity to the Si₃N₄-tip of the AFM probe than to gypsum, the adsorbed CE molecules were removed from the crystal surface during the measurements. The development of an AFM tip on which CE does not adsorb will improve the results of AFM studies significantly.

New insights in cement hydration, especially at the very early stage of a few minutes, will be achieved by using synchrotron XRD in combination of the experimental set-up that was developed at the Swiss Light Source. The liquid injection method is a very powerful tool to investigate phase transitions in liquid-solid reactions of any kind, especially on a narrow time scale. Further improvements in respect of viscous fluids must be made to investigate CE-solutions.

Appendix

A.1 Figures

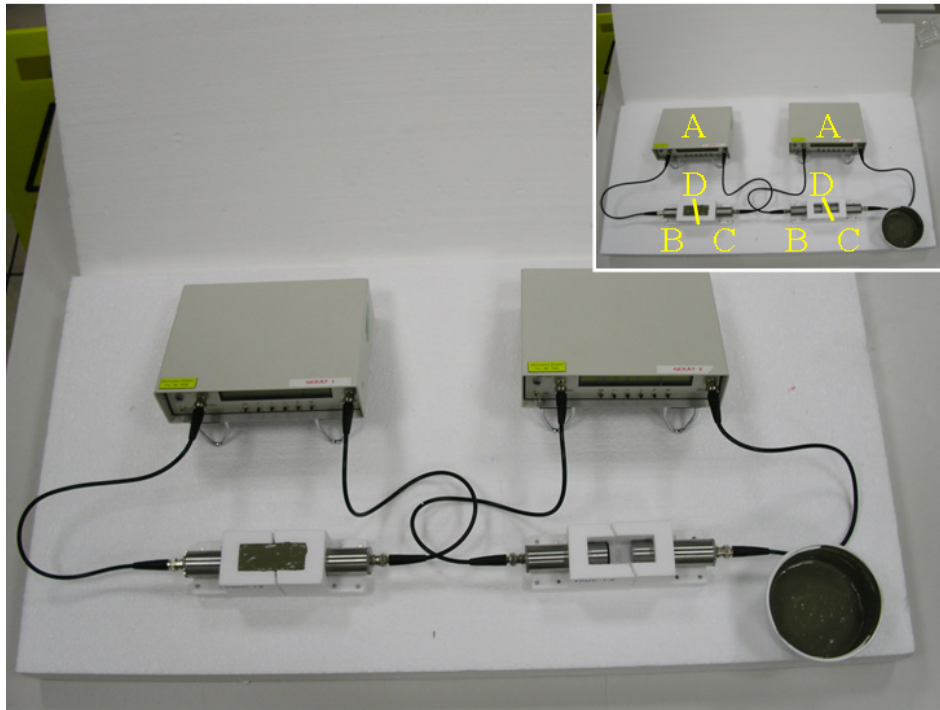


Fig. A.01: Steinkamp BP7 ultrasonic tester. A: BP7 field unit, B: 25 kHz sender, C: receiver, D: gap in the mould to decouple sender and receiver acoustically.

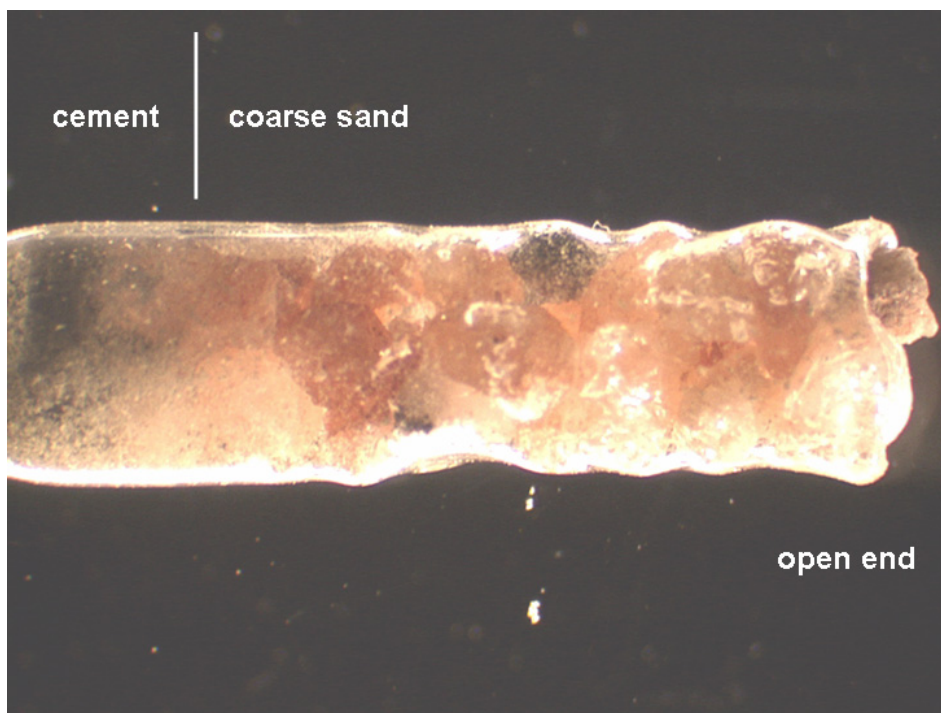


Fig. A.02: Open end of a glass capillary filled with cement (left) and sand (right). The glass wall is shrunk onto the sand grains.

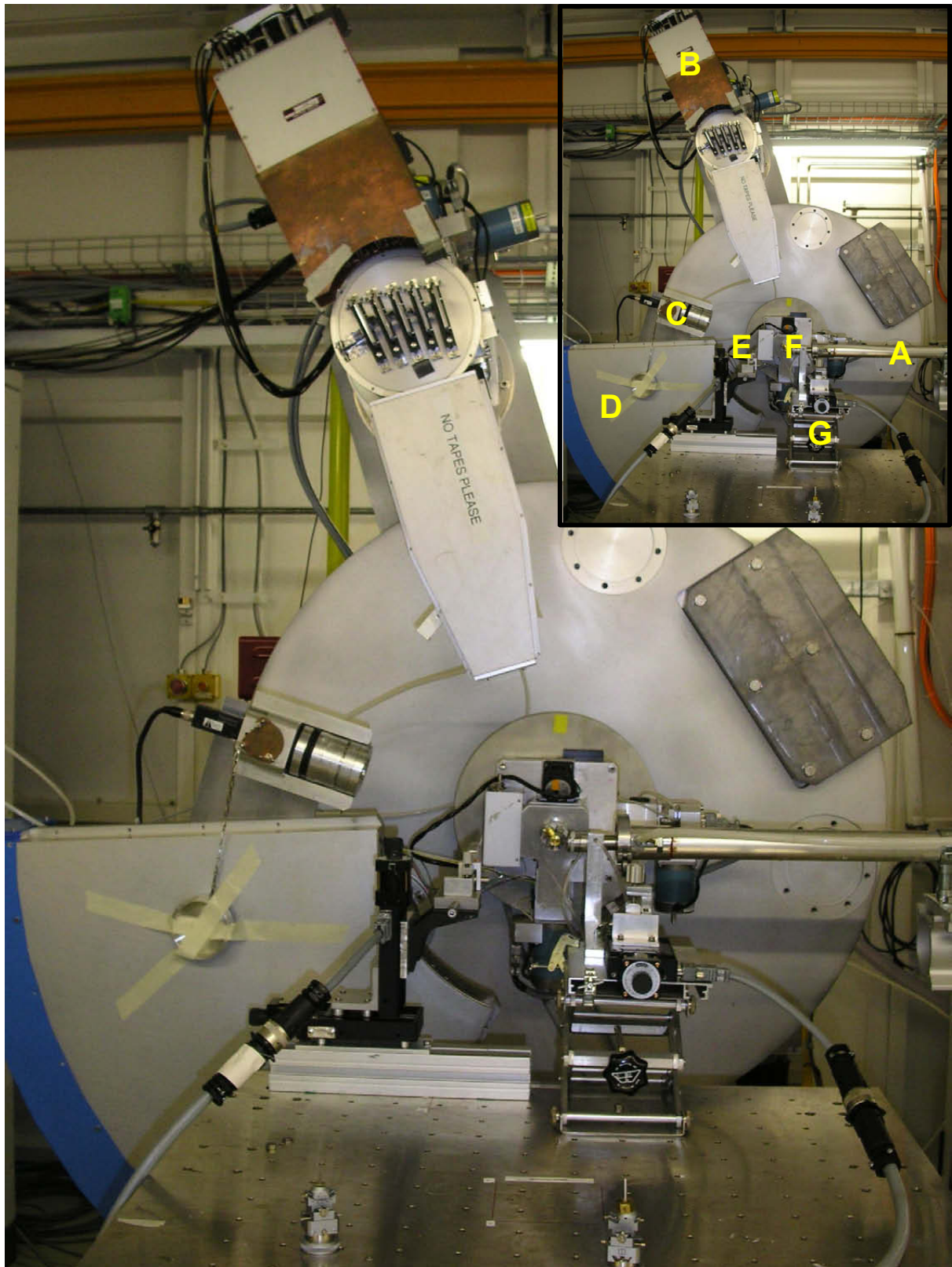


Fig. A.03: Diffractometer at the SLS Material Science Beamline.

A: beam pipe flooded with Helium
 B: detector with high spatial resolution
 C: X-ray camera
 D: Mythen multistrip detector

E: primary beam stopper
 F: sample
 G: remote controlled step motor
 and syringe

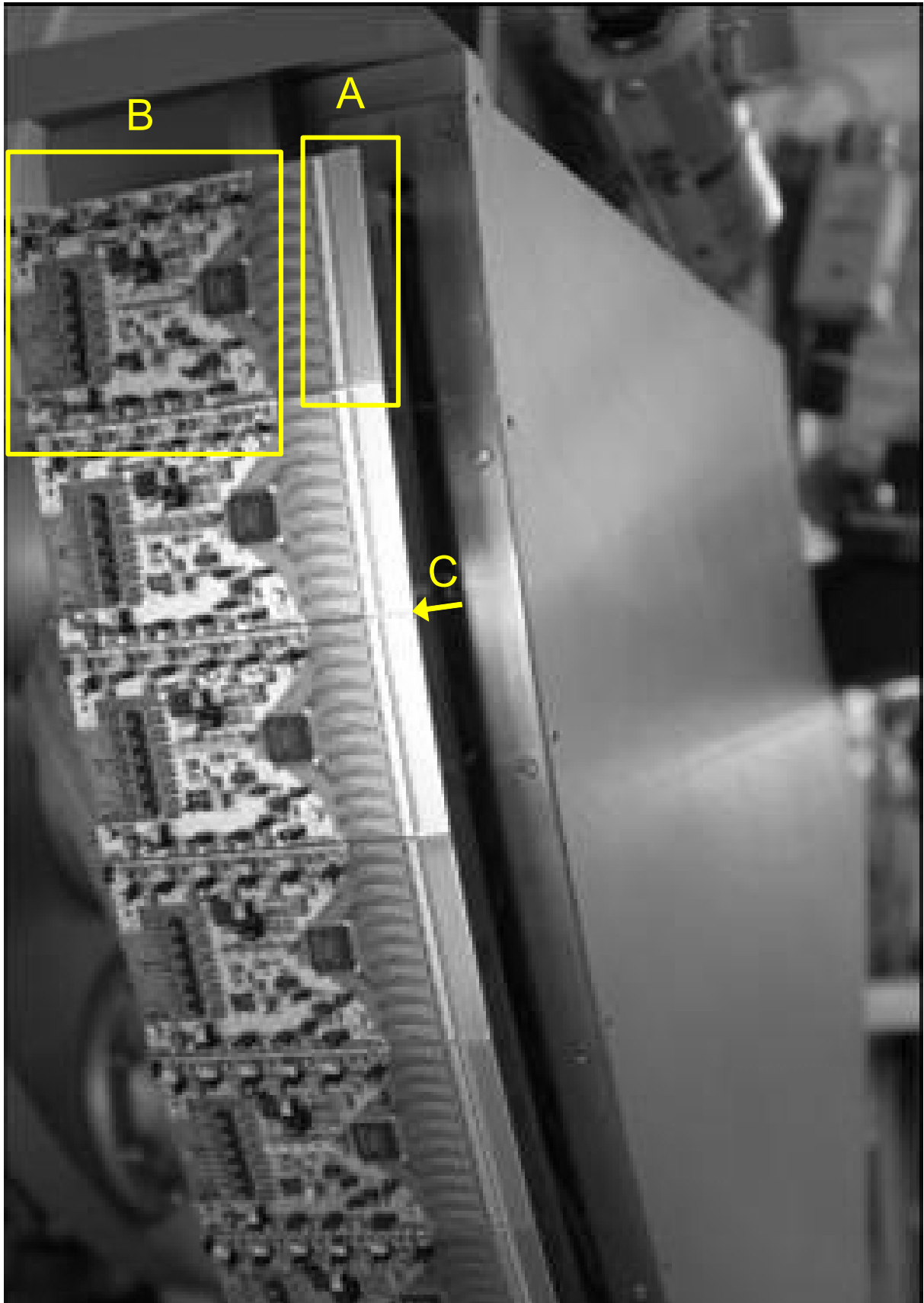


Fig. A.04: Mythen detector modules.
A: detector strips; B: read out electronic; C: gap between two modules

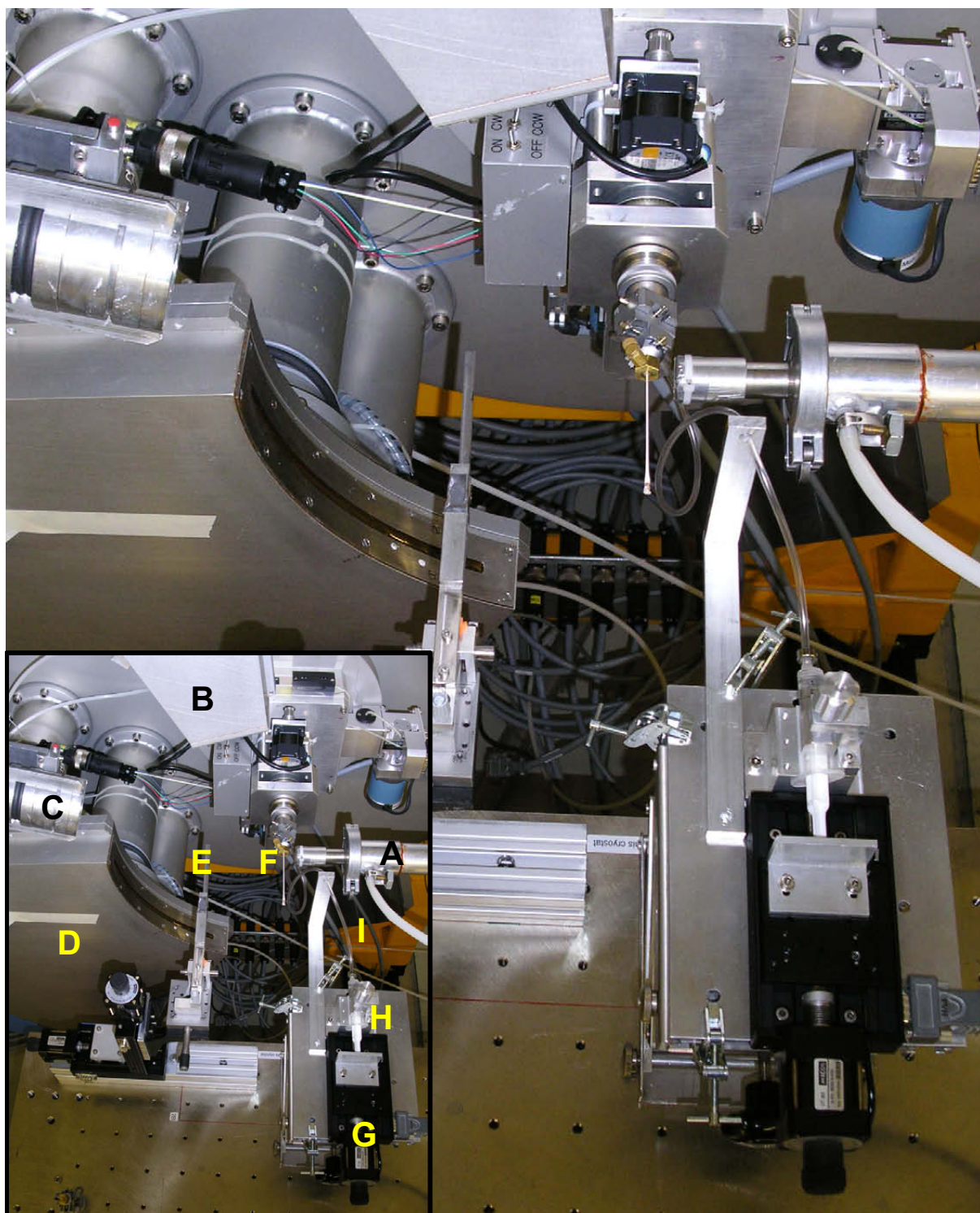


Fig. A.05: Experimental setup with water injection device

A: beam pipe flooded with Helium
 B: detector with high spatial resolution
 C: X-ray camera
 D: Mythen multistrip detector
 E: primary beam stopper

F: sample with goniometer head
 and hose adapter
 G: remote controlled step motor
 H: syringe
 I: flexible hose

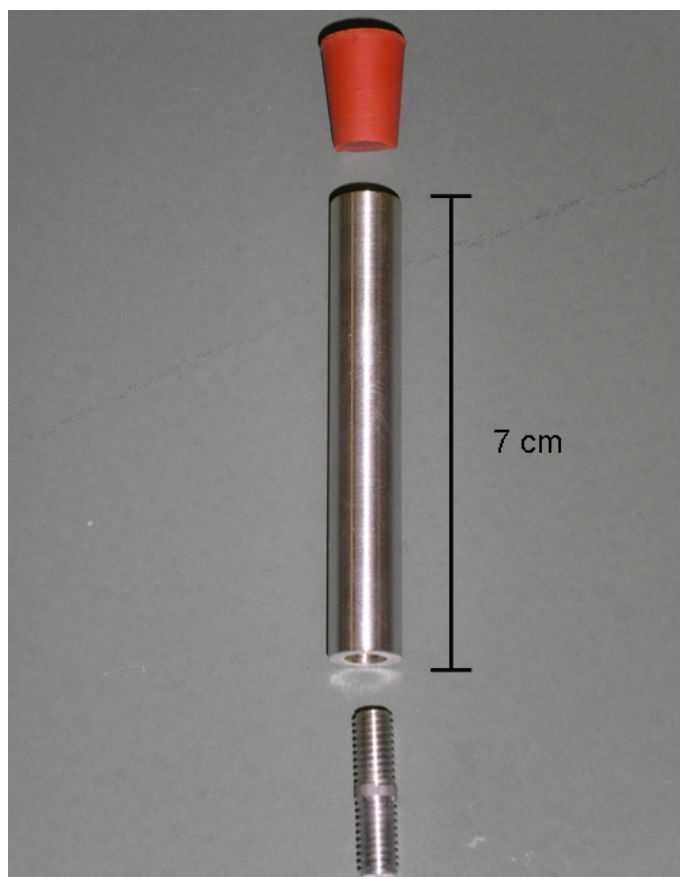


Fig. A.06: Sample carrier for neutron diffraction. The rubber stopper was replaced by a cadmium lid during the measurements.

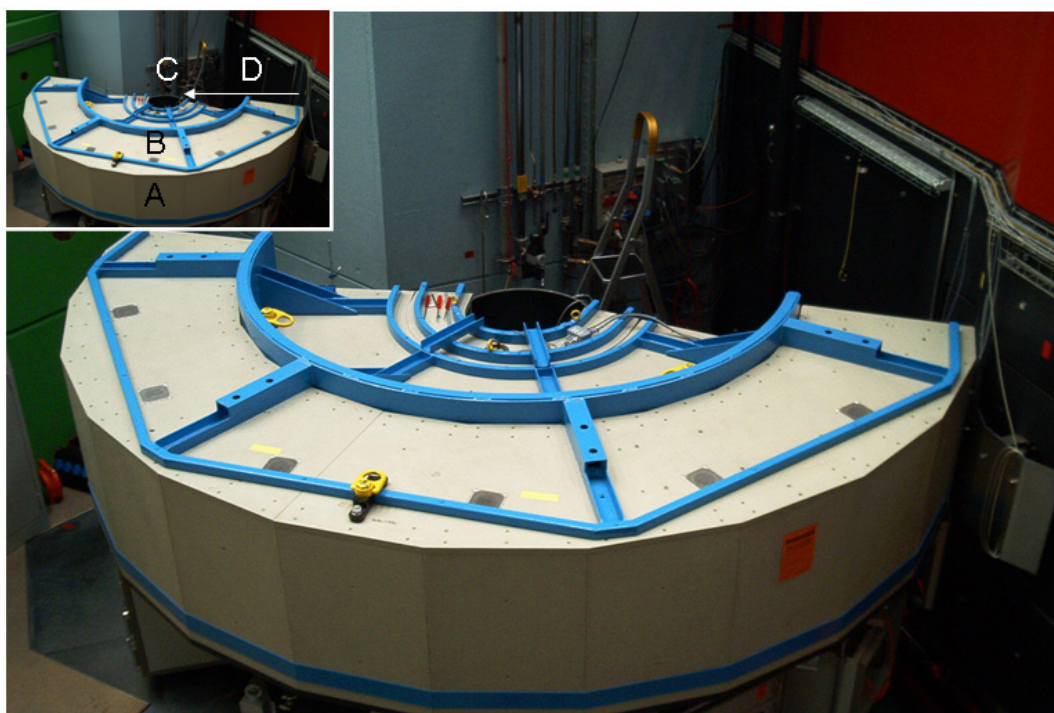


Fig. A.07: HRPT beamline at the SINQ neutron source of the PSI. A: detector, B: radial Soller slits, C: sample chamber, D: direction of primary neutron beam. Photograph taken by M. Zwanzig ^[Zwal].

A.2 Abbreviations

A	ceramic formula for Al_2O_3
AD	anno Domini
AFm	calcium aluminate ferrite monosulphate hydrate
AFM	atomic force microscopy
AFt	calcium aluminate ferrite tri-sulphate hydrate
approx.	approximately
aq.	aqueous
BC	before Christ
BET	Brunauer, Emmet and Teller
C	ceramic formula for CaO
C_3A	tri-calcium aluminate
$\text{C}_2(\text{A},\text{F})$	calcium aluminate ferrite
C_4AF	calcium aluminate ferrite
CAH	calcium aluminate hydrate
CE	cellulose ether
CEReM	Consortium d'études et de recherches des mortiers
conc.	concentration, concentrated
$\text{C}\bar{\text{s}}$	calcium sulphate
$\text{C}\bar{\text{s}}\text{H}_{0,5}$	calcium sulphate hemi-hydrate
$\text{C}\bar{\text{s}}\text{H}_2$	calcium sulphate di-hydrate
C_2S	di-calcium silicate
C_3S	tri-calcium silicate
CSH	calcium silicate hydrate
DIN	German standard
DMG	Deutsche Mineralogische Gesellschaft
DP	degree of polymerization
DS	degree of substitution
DTG	differential thermo-gravimetry
eg.	example given, for example
EMRS	European Material Research Society
EN	European standard
ESEM	environmental scanning electron microscopy
EU	European Union
F	ceramic formula for Fe_2O_3
FEG	field emission gun
fig.	figure
form.	formulation
FZK	Forschungszentrum Karlsruhe
g	standard gravity force, $g = 9.81 \text{ Nm}$
GDCh	Gesellschaft Deutscher Chemiker
H	water (ceramic formula)
HEC	hydroxy-ethylcellulose
HFC	heat flux calorimetry
HPLC	high pressure liquid chromatography
HRPT	high resolution powder diffraction of thermal neutrons
HS	highly substituted
ICDD	International Centre for Diffraction Data
i.e.	id est, that means
INE	Institut fuer Nukleare Entsorgung, FZK

K	ceramic formula for K ₂ O
lab	laboratory
l/s	liquid/solid ratio
M	ceramic formula for MgO
MC	methylcellulose
MHEC	methyl-hydroxy-ethylcellulose
MHPC	methyl-hydroxy-propylcellulose
MS	molar substitution
n.d.	not determined
no.	number
OPC	ordinary Portland cement
PSI	Paul Scherrer Institut
PSD	particle size distribution
p	page
pp	pages
PSI	Paul-Scherrer-Institut
rpm	rounds per minute
SEM	scanning electron microscopy
SEC	size exclusion chromatography
SI	saturation index
SINQ	neutron source of the PSI
SLS	Swiss Light Source
sol.	solution
SSP	Swiss Society of Physics
tab.	table
U.S.	United States (of America)
VDZ	Verein Deutscher Zementwerke
WR	water ratio
WRV	water retention value
w/s	water/solid ratio
XRD	X-ray diffraction
XRF	X-ray fluorescence

Other abbreviations used in the text are international standardized symbols such as SI-units or chemical elements.

A.3 References

- [Alw1] Al-Wakee, E.I., El-Deen, I.M.; El-Zayat, L.A. (2002); *Polymers Modifiers in Portland Cement Hydration*; Egypt. J. Chem., 45, No. 3; pp 463-482
- [Ama1] Amathieu, L.; Estienne, F. (2003); *Impact of the conditions of ettringite formation on the performance of products, based on CAC + C\$ + OPC*; 15. Internationale Baustofftagung; F.A. Finger-Institut f. Baustoffkunde; Tagungsbericht Bd. 1
- [Aza1] Azaroff, L. (1968); *Elements of X-ray Crystallography*, pp 365-367; McGraw-Hill Book Co.; Library of Congress Catalogue Card No. 68-11600
- [Bar1] Barnett, S.; *Database of Cement Mineral Synthesis*;
<http://www.abdn.ac.uk/chemistry/research/cement/dcc/dcms/data/ettringite.html>
- [Bay1] Bayer, R; Lutz, R; *Dry Mortars*; Ullmann's Encyclopaedia of Industrial Chemistry, Vol. 9
- [BGG1] (1995); *Gips-Datenbuch*; Bundesverband der Gips- und Gipsbauplattenindustrie e.V. (editor), Birkenweg 13, D-64295 Darmstadt
- [Bos1] Bosbach, D.; Hochella, M. F., Jr. (1996) Gypsum growth in the presence of growth inhibitors: a scanning force microscopy study; *Chemical Geology* 132 (1996), pp 227-236
- [Bra1] Bragg, W.L. (1943); *The Diffraction of Short Electromagnetic Waves by a Crystal*; Science in Britain, Institute of Physics, London
- [Bra2] Brandt, F. (2000); *Crystallisation of gypsum in presence of cellulose ethers*; diploma thesis, Inst. f. Min., Univ. Muenster, not published
- [Bru1] Brunauer, S.; Emmet, P.H.; Teller, E. (1938); *Adsorption of Gases in Multimolecular Layers*; J. Am. Chem. Soc. 60, pp 309-319
- [Cer1] Cerulli, T. (2005); private communication; Milan, Feb. 15th 2005
- [Chr1] Christensen, A.N.; Jensen, T.R.; Hanson, J.C. (2003); *Formation of ettringite, Ca₆Al₂(SO₄)₃(OH)₁₂·26H₂O, AFt and monosulphate, Ca₄Al₂O₆(SO₄)·14H₂O, in hydrothermal hydration of Portland cement and of calcium aluminium oxide-calcium sulphate dihydrate mixtures studied by in situ synchrotron X-ray powder diffraction*; Jour. Solid State Chem. 177, pp 1944-1951
- [Coa1] Coarna, M.; Georgescu, M.; Puri, A.; Diaconu, D. (2004); *ESCA, MIP and Mechanical Characterisation of Some Portland Cement - Methyl-Cellulose Composites*; Key Engineering Materials, Vols. 264-268, pp 2153-2156
- [Cro1] Croessmann, F.; Klaus, W. (1975); *Wasserloesliche Celluloseaether im Spiegel der Anwendungstechnik*; collection of publications by a group of authors of Kalle, branch of Hoechst AG, Wiesbaden-Biebrich
- [Dye1] Dyer, D.; Sicilia, D.B. (1990); *Labors of a modern Hercules, Evolution of a Chemical Company*; Harvard Business School Press; ISBN 0 87584 227 5
- [Eck1] Eckart, A.; Stark, J.; *Betrachtung der Hydratationsprodukte des Calciumaluminats und des Calciumferrits im ESEM-FEG*;
- [Irs1] Irsch, H.-P. (2000); *Die Entwicklung der Moertel-, Misch- und Verputztechnik unter Verwendung von Werk trockenmoertel*; 14. Internationale Baustofftagung; F.A. Finger-Institut f. Baustoffkunde; Tagungsbericht Bd. 2
- [Ger1] Gerthsen; Kneser; Vogel, H. (1986); *Physik*, 15th edition; chapter 11.3.2., p 554 and chapter 13.3.3, pp 659-663; Springer Verlag; ISBN 3 540 16155 4 (Berlin); ISBN 0 387 16155 4 (N.Y.)
- [Go1] Gozzo, F.; Schmitt, B.; Bortolamedi, T.; Giannini, G.; Guagliardi, A.; Lange, M.; Meister, D.; Maden, D.; Willmott; P.; Patterson, B.D. (2004); *First experiments at the Swiss Light Source Materials Science beamline powder diffractometer*; Journal of Alloys and Compounds 362, pp 206-217

- [Hae1] Haecker, C.-J.; Bentz, D. P. (2000); *Einfluss des Sulfattraegers (Menge und Modifikation) auf die Hydratation von Portlandzement: Experimentelle Untersuchungen und Computersimulationen*; 14. Internationale Baustofftagung; F.A. Finger-Institut f. Baustoffkunde; Tagungsbericht Bd. 1
- [Hae2] Haecker, C.-J.; private communication; Paris, March 11th 2005
- [Han1] Hansi, W. (1974); *Die wasselloeslichen Celluloseaether; Lehrbuch der Lacke und Beschichtungen*; Kittel, H. (editor); Vol. 1; Verlag W.A. Colomb, Oberschwandorf
- [Her1] Herb, A. T. (2003); *Indirekt Beobachtung des Erstarrens und Erhaertens von Zementleim, Moertel und Beton mittels Schallwellenausbreitung*; PhD-thesis, Universitaet Stuttgart, Institut fuer Werkstoffe im Bauwesen
- [Icd1] International Centre for Diffraction Data (2002); *Powder Diffraction File*; Release 2002, PDF-2
- [Kue1] Kuehn, H.; Oelschlaeger, P. (1976); *Technologie der Bindebaustoffe, Band 1, Eigenschaften, Rohstoffe, Erhaertung*; VEB Verlag fuer Bauwesen Berlin
- [Lec1] Lechner, M. D.; Gehrke, K.; Nordmeier (1996); *Makromolekulare Chemie*; Birkhaeuser Verlag, Basel; ISBN: 3 7643 5343 0
- [Lot1] Lothenbach, B.; Winnefeld, F.; Holzer, L. (2003); *Thermodynamische Modellierung der Hydratation von OPC*; 15. Internationale Baustofftagung; F.A. Finger-Institut f. Baustoffkunde; Tagungsbericht Bd. 1
- [Moe1] Moeser, B. (2003); *Nano-Charakterisierung von Hydratphasen mittels Rasterelektronenmikroskopie*; 15. Internationale Baustofftagung; F.A. Finger-Institut f. Baustoffkunde; Tagungsbericht Bd. 1
- [Moe2] Moeser, B.; Stark, J. (2003); *High Resolution Imaging of Wet Building Material Samples in their Natural State using Environmental Scanning Electron Microscope*; 11th International Congress On The Chemistry Of Cement; Durban, South Africa
- [Odl1] Odler, I. (2003); *The BET-specific area of hydrated Portland cement and related materials*; Cem. Concr. Res. 33, pp 2049-2056
- [Pat1] Patterson, P.D., Gozzo, F.; Kuhne, H.; Lange, M.; Maden, D.; Meister, D.; Schmitt, B.; Spielmann, M.; Stampanoni, M.; Wilmott, P.R. (2004); *The Material Science Beamline: recent developments*; PSI Scientific Report 2003 / Vol. VII, ISSN 1660-4709; pp 5-6
- [Pes1] Peschard, A.; Govin, A.; Fredon, E.; Grosseau, P.; Fantozzi, G. (2004); *Influence of Polysaccharides on Cement Hydration*; Key Engineering Materials, Vols. 264-268, pp.2141-2144
- [Pla1] Plank, J.; Hirsch, C.; Winter, C.; Chatziagorastou, P. (2003); *Neues zur Wirkungsweise von Polycarboxylat-basierten Fliessmitteln*; 15. Internationale Baustofftagung; F.A. Finger-Institut f. Baustoffkunde; Tagungsbericht Bd. 1
- [Pou1] Pourchez, J.; Peschard, A.; Grosseau, P.; Vallée, F. (2004); *Cellulose ethers influence on cement hydration*; CEReM Jour. 2004
- [Pou2] Pourchez, J.; Govin, A.; Grosseau, P.; Guyonnet, R.; Guilhot, B.; Ruot, B. (2005); *Alkaline stability of cellulose ethers and impact of their degradation products on cement hydration*; Cement Research; in press
- [Ran1] Ranke-Graves, R. (1936); *I, Claudius*; 9th edition; Arthur Barker (editor), London
- [Rid1] Ridi, F.; Fratini, E.; Mannelli, F.; Baglioni, P. (2005); *Hydration Process of Cement in Presence of a Cellulosic Additive. A Calorimetric Investigation*; J. Phys. Chem. B 2005, 109, pp 14727-14737
- [Rie1] Rietveld, H.M. (1967); *Line profiles of neutron powder-diffraction peaks for structure refinement*; Acta Cryst. 22, p 151
- [Roe1] Roessler, C.; Stark, J. (2003); *Der Einfluss von Fliessmitteln auf die Hydratation von Zement*; 15. Internationale Baustofftagung; F.A. Finger-Institut f. Baustoffkunde; Tagungsbericht Bd. 1

- [Rot1] Rothstein, D.; Thomas, J. J.; Christensen, B. J.; Jennings, H. M. (2002); *Solubility behaviour of Ca-, S-, Al- and Si-bearing solid phases in Portland cement pore solutions as a function of hydration time*; Cement and Concrete Research 32, pp 1663-1671
- [Sch1] Schoene, M. (1979); *Von der Leimabteilung zum groessten Klebstoffwerk Europas*; Henkel KGaA, Duesseldorf; Stabsstelle fuer Oeffentlichkeitsarbeit/Werksarchiv
- [Scr1] Scrivener, K.L. (1989); *The Microstructure of Concrete*; Materials Science of Concrete I; edited by Skalny, J.P.; American Ceramic Society, Westerville, OH
- [Sie1] (2002) *Siroquant Quantitative XRD Software*, Version 2.5 for Windows, Sietronics Pty Ltd
- [Sta1] Stark, J.; Moeser, B.; Eckart, A. (2000); *Neue Ansaetze zur Zementhydratation*; 14. Internationale Baustofftagung; F.A. Finger-Institut f. Baustoffkunde; Tagungsbericht Bd. 1
- [Sta2] Stark, J.; Moeser, B.; Eckart, A. (2001); *Zementhydratation - neue Ansaetze*; ZKG International 01/2001 und 02/2001
- [Sta3] Stark, J.; Moeser, B.; Bellmann, F. (2003); *Ein neues Modell der Zementhydratation*; 15. Internationale Baustofftagung; F.A. Finger-Institut f. Baustoffkunde; Tagungsbericht Bd. 1
- [Ste1] Steinkamp, G. (1996); *Messung des zeitlichen Verlaufs von Abbindevorgaengen mit dem micrcontroller-gesteuerten Ultraschallpruefgeraet BP-7*; Prof. Dr.-Ing. Georg Steinkamp Labor fuer Technische Physik; Steingraben 5, D-28259 Bremen
- [Str1] Struble, L.J. (1987); Proc. VIIIth International Congress on the Chemistry of Cement Vol. VI, pp 582-588
- [Tay1] Taylor, H.F.W (1997); *Cement Chemistry*, 2nd edition; Thomas Telford Publishing; ISBN 0 7277 2592 0
- [Tay2] Taylor, J.C.; Hinczak, I. (2001); *Rietveld made easy*; Sietronics Pty Ltd; ISBN 0 9750798 0 8
- [VDZ1] *Zement Taschenbuch 2002*; Verein Deutscher Zementwerke e.V. (editor); Verlag Bau+Technik; ISBN 3 7640 427 4
- [Vit1] Vitruv (1st century B.C.); *De architectura*
- [Wey1] Weyer, H.P.; Schmitt, B.; Mueller, I.; Bosbach, D.; Putnis, A. (2005); *Time-resolved monitoring of cement hydration: Influence of cellulose ethers on hydration kinetics*; Nuclear Instruments and Methods (in press)
- [Whi1] Whitfield, P.S.; Mitchell, L.D. (2003); *Quantitative Rietveld analysis of the amorphous content in cements and clinkers*; Jour. Mat. Sci. 38, pp 4415- 4421
- [Wil1] Williams, P.J.; Biernacki, J.J.; Bai, J.; Rawn, C.J. (2003); *Assessment of a synchrotron X-ray method for quantitative analysis of calcium hydroxide*; Cement and Concrete Research 33, pp1553-1559
- [Win1] Winnefeld, F. Lothenbach, B.; Holzer, L.; Ploetze, M.; Rytz, G. (2003); *Einfluss verschiedener Sulfatraeger auf die Hydratation von Portlandzement – eine praxisnahe Studie an Werkzementen*; 15. Internationale Baustofftagung; F.A. Finger-Institut f. Baustoffkunde; Tagungsbericht Bd. 1
- [Yos1] Yoshioka, K.; Tazawa, E.; Kawai, K.; Enohata, T. (2002); *Adsorption characteristics of superplasticizers on cement component minerals*; Cement and Concrete Research, Vol.32, pp 1507-1513
- [You1] Young, R.A. (1993); *The Rietveld Method*; IUCR Monographs on Crystallography Vol. 5, Oxford University Press
- [Zwa1] Zwanzig, M.; Blume, S.; Schwinning, B.; Stammen, C. (2003); *Einfluss von wasserloeslichen Polymeren am Beispiel von Celluloseethern auf die Kristallisationskinetik der Hydratphasen im Zement*; report of apprenticeship at the Heinrich-Hertz-Berufskolleg, Duesseldorf

A.4 Technical Equipment

Sample preparation - Sartorius laboratory scale 0 - 2000 g \pm 0.01 g, Sartorius microscale 0 - 500 g \pm 0.0001 g, Braun multimix 350 W electric kitchen stirrer (Hercules)

BET - Micromeritics Gemini with N₂-supply, Micromeritics SmartPrep (Hercules)

He-Pycnometry - Mycromeritics AccuPyc 1330 with He₂-supply (Hercules)

Laser-granulometry - Sympatec Gradis PFS (Hercules)

Ultrasonic - Steinkamp BP 7 with 25 kHz transmitter set (Hercules)

Size exclusion chromatography - Waters 2695 Separation Module, Waters 410 Differential Refractometer, Viscotec T 60 A Dual Detector (Hercules)

Heat flux calorimetry - custom-made heatflux calorimeter built by H. J. Kuzel, Inst. f. Min., Universitaet Erlangen-Nuernberg (Hercules)

Laboratory XRD - Panalytical (former Philips) X'pert PW3040 diffractometer (Inst. f. Min., Westfaelische Wilhelms-Universitaet Muenster)

Synchrotron XRD - Swiss Light Source, Material Science Beamline, Mythen multistrip detector (PSI)

Thermal neutron powder diffraction - SINQ neutron source, HRPT beamline (PSI)

Environmental Scanning Electron Microscopy - Philips ESEM XL30 FEG. (VDZ)

Photography - Minolta DiMAGE F200 (private)

Software - Microsoft (MS) Windows NT, MS Windows 2000, MS Windows XP, Linux Red Hat, MS Office 2000, MS Office 97, MS Office 2003, Panalytical X'Pert, Sietronics Siroquant 2.5, Nero Burning Rom 6.0, Dell Image Expert Standard Edition, DiMAGE Viewer, several device-specific software (private, Hercules, Universitaet Muenster, PSI)

A.5 Co-operations

Hercules Inc.
Aqualon Division
German Branch: Hercules GmbH
Paul-Thomas-Str. 56
D-40599 Duesseldorf

Westfaelische Wilhelms-Universitaet Muenster
Institut fuer Mineralogie
Corrensstr. 24
D-48149 Muenster

Forschungszentrum Karlsruhe (FZK)
Institut fuer Nukleare Entsorgung (INE)
Postfach 3640
D-76021 Karlsruhe

Paul Scherrer Institut (PSI)
Swiss Light Source (SLS) and SINQ
CH-5232 Villigen PSI

Heinrich-Hertz-Berufskolleg
Redinghovenstr. 16
D-40225 Duesseldorf

Forschungsinstitut des Vereins Deutscher Zementwerke (VDZ)
Tannenstr. 2
D-40476 Duesseldorf

Roentgenlabor Dr. Ermrich
Am Kandelborn 7
D-64354 Reinheim

**In der Reihe "Karlsruher Geochemische Hefte" (ISSN 0943-8599)
sind erschienen:**

Band 1: U. Kramar (1993)

Methoden zur Interpretation von Daten der geochemischen
Bachsedimentprospektion am Beispiel der Sierra de San Carlos/ Tamaulipas Mexiko

Band 2: Z. Berner (1993)

S-Isotopengeochemie in der KTB - Vorbohrung und Beziehungen zu den Spuren-
elementmustern der Pyrite

Band 3: J.-D. Eckhardt (1993)

Geochemische Untersuchungen an jungen Sedimenten von der Galapagos-
Mikroplatte:
Hydrothermale und stratigraphisch signifikante Signale

Band 4: B. Bergfeldt (1994)

Lösungs- und Austauschprozesse in der ungesättigten Bodenwasserzone und
Auswirkungen auf das Grundwasser

Band 5: M. Hodel (1994)

Untersuchungen zur Festlegung und Mobilisierung der Elemente As, Cd, Ni und Pb
an ausgewählten Festphasen unter besonderer Berücksichtigung des Einflusses von
Huminstoffen.

Band 6: T. Bergfeldt (1995)

Untersuchungen der Arsen- und Schwermetallmobilität in Bergbauhalden und
kontaminierten Böden im Gebiet des Mittleren Schwarzwaldes.

Band 7: M. Manz (1995)

Umweltbelastungen durch Arsen und Schwermetalle in Böden, Halden, Pflanzen und
Schlacken ehemaliger Bergbauggebiete des Mittleren und Südlichen Schwarzwaldes.

Band 8: J. Ritter (1995)

Genese der Mineralisation Herrmanngang im Albtalgranit (SE-Schwarzwald) und
Wechselwirkungen mit dem Nebengestein.

Band 9: J. Castro (1995)

Umweltauswirkungen des Bergbaus im semiariden Gebiet von Santa Maria de la
Paz, Mexiko.

Band 10: T. Rüde (1996)

Beiträge zur Geochemie des Arsens.

Band 11: J. Schäfer (1998)

Einträge und Kontaminationspfade Kfz-emittierter Platin-Gruppen-Elemente (PGE) in
verschiedenen Umweltkompartimenten.

Band 12: M. A. Leosson (1999)

A Contribution to the Sulphur Isotope Geochemistry of the Upper Continental Crust:
The KTB Main Hole - A Case Study

Band 13: B. A. Kappes (2000)

Mobilisierbarkeit von Schwermetallen und Arsen durch saure Grubenabwässer in Bergbaualtlasten der Ag-Pb-Zn-Lagerstätte in Wiesloch

Band 14: H. Philipp (2000)

The behaviour of platinum-group elements in petrogenetic processes:
A case study from the seaward-dipping reflector sequence (SDRS), Southeast Greenland volcanic rifted margin

Band 15: E. Walpersdorf (2000)

Nähr- und Spurenelementdynamik im Sediment/Wasser-Kontaktbereich nach einer Seekreideaufspülung - Pilotstudie Arendsee -

Band 16: R. H. Kölbl (2000)

Models of hydrothermal plumes by submarine diffuse venting in a coastal area: A case study for Milos, South Aegean Volcanic Arc, Greece

Band 17: U. Heiser (2000)

Calcium-rich Rhodochrosite layers in Sediments of the Gotland Deep, Baltic Sea, as Indicators for Seawater Inflow

In der Fortsetzungsreihe "Karlsruher Mineralogische und Geochemische Hefte" (ISSN 1618-2677) sind bisher erschienen:

Band 18: S. Norra (2001)

Umweltgeochemische Signale urbaner Systeme am Beispiel von Böden, Pflanzen, und Stäuben in Karlsruhe

Band 19: M. von Wagner, Alexander Salichow, Doris Stüben (2001)

Geochemische Reinigung kleiner Fließgewässer mit Mangankiesen, einem Abfallsprodukt aus Wasserwerken (GReiFMan)

Band 20: U. Berg (2002)

Die Kalzitapplikation als Restaurierungsmaßnahme für eutrophe Seen – ihre Optimierung und Bewertung

Band 21: Ch. Menzel (2002)

Bestimmung und Verteilung aquatischer PGE-Spezies in urbanen Systemen

Band 22: P. Graf (2002)

Meta-Kaolinit als latent-hydraulische Komponente in Kalkmörtel

Band 23: D. Buqezi-Ahmeti (2003)

Die Fluidgehalte der Mantel-Xenolithe des Alkaligesteins-Komplexes der Persani-Berge, Ostkarpaten, Rumänien: Untersuchungen an Fluid-Einschlüssen

Band 24: B. Scheibner (2003)

Das geochemische Verhalten der Platingruppenelemente bei der Entstehung und Differenzierung der Magmen der Kerguelen-Flutbasaltprovinz (Indischer Ozean)

Ab Band 25 erscheinen die Karlsruher Mineralogischen und Geochemischen Hefte im Karlsruher Universitätsverlag online unter der Internetadresse

<http://www.uvka.de/univerlag/institut.php?fakultaet=1>

Auf Wunsch sind beim Karlsruher Universitätsverlag gedruckte Exemplare erhältlich („print on demand“).

Band 25: A. Stögbauer (2005)

Schwefelisotopenfraktionierung in abwasserbelasteten Sedimenten -
Biogeochemische Umsetzungen und deren Auswirkung auf den
Schwermetallhaushalt

Band 26: X. Xie (2005)

Assessment of an ultramicroelectrode array (UMEA) sensor for the determination of
trace concentrations of heavy metals in water

Band 27: F. Friedrich (2005)

Spectroscopic investigations of delaminated and intercalated phyllosilicates

Band 28: L. Niemann (2005)

Die Reaktionskinetik des Gipsabbindens: Makroskopische Reaktionsraten und
Mechanismen in molekularem Maßstab

Band 29: F. Wagner (2005)

Prozessverständnis einer Naturkatastrophe: eine geo- und hydrochemische
Untersuchung der regionalen Arsen-Anreicherung im Grundwasser West-Bengalens
(Indien)

Band 30: F. Pujol

Chemostratigraphy of some key European Frasnian-Famennian boundary sections
(Germany, Poland, France)

Band 31: Y. Dikikh

Adsorption und Mobilisierung wasserlöslicher Kfz-emittierter Platingruppenelemente
(Pt, Pd, Rh) an verschiedenen bodentypischen Mineralen

Cellulose ethers (CEs) are important rheological regulators in dry mortar application. They control water retention, wet mortar consistency and the hydration kinetic of cement phases. The retarding effect can be traced to the adsorption behaviour of CE. Silicates and their hydration products show the highest adsorption values and longest retardation times. Less CE adsorbs on gypsum, so sulfate hydration is less affected. The influence on alluminate hydration in presence of sulfate is less specific: no CE adsorbs on ettringite but second ettringite formation is strongly inhibited. This is an indirect phenomenon caused by delayed development of ion-concentration in the pore water. This delay again is a consequence of CE-caused retardation of the silicate hydration. First ettringite formation is not affected by CE. Beside the mineral phase the type of polymer controls the hydration kinetic, too. In general the lower the degree of substitution (key parameter of CE characterization) the stronger the adsorption and the longer the retardation time.